


FINAL RESEARCH REPORT

Antiviral agents against herpes simplex and avian influenza viruses from Thai medicinal plants

By

Professor Dr. Kittisak Likhitwitayawuid and Co-workers

JULY, 2016

Research Contract Number: BRG 5580004

FINAL REPORT

Antiviral agents against herpes simplex and avian influenza viruses from Thai medicinal plants

Investigators

Professor Dr. Kittisak Likhitwitayawuid	Chulalongkorn University
Associate Professor Dr. Vimolmas Lipipun	Chulalongkorn University
Associate Professor Dr. Ruedeekorn Wiwattanapatapee	Prince of Songkla University
Associate Professor Dr. Boonchoo Sritularak	Chulalongkorn University
Dr. Poonsakdi Ploypradith	Chulabhorn Research Institute
Dr. Supakarn Chamni	Chulalongkorn University

Supported by
The Thailand Research Fund

คำนำ

โครงการวิจัยเรื่อง “Antiviral agents against herpes simplex and avian influenza viruses from Thai medicinal plants” ได้รับทุนสนับสนุนจากสำนักงานกองทุนสนับสนุนการวิจัย (BRG 5580004) มีจุดมุ่งหมายที่จะสร้างองค์ความรู้ใหม่ที่เป็นพื้นฐานและเป็นประโยชน์ต่อการพัฒนาประเทศ มีลักษณะเป็นแผนงานวิจัย หรือ ชุดโครงการ (research program) ที่นำเอาองค์ความรู้ทางเคมีและฤทธิ์ทางชีวภาพของสาร oxyresveratrol ซึ่งคณะผู้วิจัยได้สร้างและสะสมมา เป็นแนวคิดเพื่อสร้างงานวิจัยที่มีศักยภาพที่สามารถนำไปวิจัยต่อยอดเชิงประยุกต์ได้ในอนาคต แผนงานวิจัยนี้ประกอบด้วยโครงการวิจัย (research project) 3 โครงการ ได้แก่ (1) Development and evaluation of nanocarriers for oral delivery of oxyresveratrol (2) Structural modification of oxyresveratrol และ (3) Search for new antiviral agents from Thai medicinal plants

ในภาพรวมแผนงานวิจัยนี้ได้ผลิตนักวิจัยรุ่นใหม่ 7 คน แบ่งเป็นระดับปริญญาเอก 3 คน และระดับปริญญาโท 4 คน ได้ผลิตผลงานวิจัยซึ่งพิมพ์เผยแพร่ในวารสารวิชาการระดับนานาชาติจำนวน 12 เรื่อง องค์ความรู้ใหม่ที่สร้างขึ้นนั้น ส่วนหนึ่งคณะผู้วิจัยได้นำมาทำการวิจัยต่อยอด ซึ่งเป็นงานวิจัยกึ่งพื้นฐานกึ่งประยุกต์เพื่อการพัฒนาประเทศ คือได้นำระบบนำส่งยา oxyresveratrol ที่ได้พัฒนาขึ้นใหม่ไปใช้ในการวิจัยเพื่อศึกษาฤทธิ์ของ oxyresveratrol ในสัตว์ทดลองในการป้องกันพิษของ β-amyloid ซึ่งมีบทบาทสำคัญที่ทำให้เกิดโรคอัลไซเมอร์ (Alzheimer’s disease) ทั้งนี้ได้รับทุนวิจัยสนับสนุนเบื้องต้นจากคณะกรรมการวิจัยแห่งชาติปี พ.ศ. 2558 นอกจากนี้ยังมีองค์ความรู้ใหม่ส่วนอื่นๆ คณะผู้วิจัยกำลังพิจารณาหาทางดำเนินการทำวิจัยต่อยอดต่อไป

คณะผู้วิจัยขอขอบพระคุณสำนักงานกองทุนสนับสนุนการวิจัยที่ได้ให้การสนับสนุนทุนวิจัยที่ได้ให้ทุนวิจัยในคราวนี้ และหวังเป็นอย่างยิ่งว่าจะได้รับการสนับสนุนในโอกาสต่อไป นอกจากนี้คณะผู้วิจัยขอขอบพระคุณคณะเภสัชศาสตร์ จุฬาลงกรณ์มหาวิทยาลัย คณะเภสัชศาสตร์ มหาวิทยาลัยสงขลานครินทร์ และห้องปฏิบัติการเภสัชเคมี สถาบันวิจัยจุฬาภรณ์ ที่ได้ให้การสนับสนุนสถานที่ เครื่องมือ และอุปกรณ์วิทยาศาสตร์ จนงานวิจัยนี้สำเร็จลุล่วงเป็นอย่างดี

บทคัดย่อ

รหัสโครงการ: BRG5580004

ชื่อโครงการ: สารต้านไวรัสเริมและไข้หวัดนกจากพืชสมุนไพรไทย

ชื่อนักวิจัย: กิตติศักดิ์ ลิขิตวิทยาวุฒิ คณะเภสัชศาสตร์ จุฬาลงกรณ์มหาวิทยาลัย

E-mail Address : Kittisak.L@chula.ac.th

ระยะเวลาโครงการ: 31 กรกฎาคม พ.ศ. 2555 ถึง 30 กรกฎาคม พ.ศ. 2558

ที่มาของแผนงานวิจัย: ออกซิเรสเวอราทรอล (oxyresveratrol หรือ 2,4,3′,5′-tetrahydroxystilbene) เป็นสาร phytoalexin ซึ่งพบในปริมาณมากในแก่นต้นมะหาด (วงศ์ Moraceae) สารนี้จัดอยู่ในกลุ่มสารต้านไวรัสที่มีโครงสร้างที่เป็น *bis*-aryl ซึ่งคณะผู้วิจัยได้เคยเสนอแนวความคิดไว้ ผลการศึกษาพบว่า oxyresveratrol มีฤทธิ์ยับยั้งไวรัสเริม (HSV) ดังนั้นจึงคาดว่าสารนี้อาจมีศักยภาพที่จะนำมาใช้ป้องกันหรือรักษาโรคอัลไซเมอร์ (AD) ได้ เพราะมีรายงานว่าการติดเชื้อ HSV ที่สมองมีส่วนเกี่ยวข้องกับการก่อโรค AD อย่างไรก็ตามจากการทดลองในสัตว์พบว่า oxyresveratrol มีประสิทธิภาพในการฆ่า HSV ที่ผิวหนังเมื่อให้โดยการทาบริเวณที่ติดเชื้อ แต่ไม่ให้ผลในการรักษาหากให้ทางปาก นอกจากนี้มีผู้รายงานว่า oxyresveratrol มีฤทธิ์ยับยั้งเอนไซม์ neuraminidase ของไวรัสไข้หวัดนกอีกด้วย

วัตถุประสงค์แผนงานวิจัย: นำองค์ความรู้เกี่ยวกับ oxyresveratrol และฤทธิ์ทางชีวภาพ ที่คณะผู้วิจัยได้สะสมไว้ รวมทั้งสมมติฐานข้างต้น มาเป็นพื้นฐานในการดำเนินการวิจัยเพื่อค้นหาหรือพัฒนายา หรือระบบนำส่งยาที่มีประสิทธิผลต่อโรคที่มีความเกี่ยวข้องกับไวรัสเริมหรือไข้หวัดนก

วิธีดำเนินการ: จัดทำเป็นชุดโครงการวิจัย ประกอบด้วย 3 โครงการคือ (1) การพัฒนาและประเมินระบบนำส่ง oxyresveratrol ทางปากโดยใช้ตัวพาที่มีขนาดนาโน (2) การดัดแปลงโครงสร้างสาร oxyresveratrol และ (3) การค้นหาสารต้านไวรัสจากพืชสมุนไพรไทย

สรุปผลแผนงานวิจัยและข้อเสนอแนะ:

(1) ได้ระบบนำส่งยาในรูปแบบของยารับประทานซึ่งสามารถเพิ่มการดูดซึม oxyresveratrol จึงมีความเห็นว่าควรนำระบบนำส่งยาดังกล่าวมาประยุกต์ใช้ศึกษาในโรคที่เกี่ยวโยงการติดเชื้อไวรัสเริมในสมองเช่น โรคอัลไซเมอร์

(2) ได้สารอนุพันธ์ 2 ชนิดคาดว่าอาจมีศักยภาพสูงกว่า oxyresveratrol ในการนำมาใช้กับโรคติดเชื้อเริมที่สมองและโรคอัลไซเมอร์ สารอนุพันธ์ 1 ชนิดคาดว่าอาจนำมาพัฒนาเป็นยาช่วยควบคุมระดับน้ำตาลในเลือดได้ดีกว่าเพราะอัตราการถูกทำลายในร่างกายที่คาดว่าช้ากว่า สารอนุพันธ์ 1 ชนิดที่แสดงความเป็นพิษสูงต่อเซลล์มะเร็ง HeLa จึงมีความเห็นว่าควรนำสารอนุพันธ์ที่มีศักยภาพสูงกว่า oxyresveratrol เหล่านี้ไปศึกษาต่อในสัตว์ทดลอง

(3) ได้ข้อมูลโครงสร้างและฤทธิ์ต้านไวรัสเริมของสารที่มีโครงสร้าง *bis*-aryl เพิ่มเติม จึงเสนอว่าควรนำมารวบรวมและวิเคราะห์ความสัมพันธ์เปรียบเทียบกับข้อมูลจากแหล่งอื่นๆ เพื่อประโยชน์ในการออกแบบการสังเคราะห์สารต้านไวรัสในอนาคต

คำสำคัญ ออกซิเรสเวอราทรอล ไวรัส เริม ไข้หวัดนก โรคอัลไซเมอร์ โรคเบาหวาน มะเร็ง

โครงการวิจัยที่ 1

วัตถุประสงค์ พัฒนาสูตรตำรับที่เหมาะสมในการนำส่ง oxyresveratrol (OXYR) ทางปาก

วิธีการทดลอง พัฒนาระบบนำส่ง oxyresveratrol 3 ระบบ ได้แก่ (1) ระบบ solid lipid nanoparticles (SLN) (2) ระบบ nanostructured lipid carriers (NLC) และ (3) ระบบ self-microemulsifying drug delivery systems (SMEDDS) ทำการทดลองจนได้สูตรตำรับและวิธีการเตรียมที่เหมาะสมที่สุดของแต่ละระบบ นำไปศึกษาคุณสมบัติทางฟิสิกส์เคมี ความสามารถของ oxyresveratrol ในแต่ละตำรับในการซึมผ่านในเซลล์เพาะเลี้ยง Caco-2 และถูกดูดซึมในหนูทดลองเมื่อให้ยาทางปาก

ผลการทดลอง ตำรับ SMEDDS มีลักษณะเป็นของเหลวคล้ายน้ำมันสีเหลือง ส่วนตำรับ SLN และ NLC มีลักษณะเป็นยาแขวนตะกอนซึ่งมีความหนืดน้อย ได้ศึกษาเปรียบเทียบคุณสมบัติทางกายภาพ ความเป็นพิษต่อเซลล์ และความสามารถในการซึมผ่านชั้นเซลล์ Caco-2 ชั้นเดียวของตำรับเหล่านี้ พบว่าตำรับ SMEDDS มีความสามารถในการรองรับยา (drug loading) คิดเป็น 13 เท่าของตำรับ SLN และ NLC ตำรับ SMEDDS มีขนาดอนุภาค (26.94 ± 0.08 นาโนเมตร) ซึ่งเล็กกว่าตำรับ NLC และ SLN (p <0.05) ตำรับ SMEDDS มีการกระจายตัวของขนาดอนุภาค (PDI, 0.073 ± 0.010) ที่แคบกว่าตำรับ NLC และ SLN (PDI, 0.2–0.3) ในการศึกษาความเป็นพิษต่อเซลล์ Caco-2 ด้วยวิธี MTT พบว่าตำรับ SMEDDS ซึ่งบรรจุ oxyresveratrol (OXYR-SMEDDS) มีความเป็นพิษต่อเซลล์ Caco-2 เป็น 4 เท่าของตำรับ SLN และ NLC ที่บรรจุ oxyresveratrol เมื่อนำแต่ละตำรับมาศึกษาผลต่อการดูดซึม OXYR แบบ in vitro กับเซลล์ Caco-2 โดยใช้ขนาดบรรจุ OXYR 100 มิลลิโมลาร์ (mM) ซึ่งไม่เป็นพิษต่อเซลล์ พบว่าเมื่อเปรียบเทียบกับการให้ OXYR ซึ่งไม่อยู่ตำรับ ตำรับทั้งสามช่วยให้ OXYR ที่อยู่ในตำรับซึมเข้าสู่เซลล์ได้มากขึ้นคิดเป็น 2.5 – 3 เท่า และช่วยลดการผลัก OXYR ออกจากเซลล์ลงคิดเป็น 1.3 – 1.8 เท่า ผลการศึกษาดังกล่าวจึงแสดงให้เห็นว่าตำรับทั้งสามสามารถเพิ่มการดูดซึม OXYR เข้าสู่ร่างกาย เมื่อให้ยาทางปากได้ โดยเพิ่มการซึมผ่านเข้าและยับยั้งการผลัก OXYR ออกจากเซลล์ เมื่อทำการศึกษาทางเภสัชจลนศาสตร์ในหนู Wistar rat พบว่าตำรับ SLN และ NLC ช่วยเพิ่มค่าชีวปริมาณของ OXYR คิดเป็นร้อยละ 125 และ 177 เมื่อเปรียบเทียบกับการให้ OXYR ซึ่งไม่อยู่ในตำรับ ส่วนตำรับ SMEDDS ช่วยเพิ่มค่าชีวปริมาณได้ถึงร้อยละ 218 – 786 ขึ้นกับปริมาณและชนิดของสารลดแรงตึงผิวที่ใช้

สรุป ระบบนำส่งยาในรูปแบบของยารับประทานที่พัฒนาขึ้นสามารถเพิ่มการดูดซึม oxyresveratrol ซึ่งอาจนำมาใช้ประโยชน์ในโรคที่เกี่ยวข้องกับการติดเชื้อไวรัสเริมในสมองเช่น โรคอัลไซเมอร์

ข้อเสนอแนะ นำระบบนำส่งยาที่พัฒนาขึ้นมาศึกษาการใช้ประโยชน์ในโรคที่เกี่ยวข้องการติดเชื้อไวรัสเริมในสมองเช่น โรคอัลไซเมอร์

โครงการวิจัยที่ 2

วัตถุประสงค์ ดัดแปลงโครงสร้างของ oxyresveratrol ด้วยวิธีทางเคมี และตรวจสอบฤทธิ์ต้านไวรัสเริมและฤทธิ์ยับยั้งเอนไซม์ neuraminidase ของไวรัสหวัดนกของอนุพันธ์ที่เตรียมได้

วิธีการทดลอง เติมหมู่ฟังก์ชันลงในโครงสร้างของ oxyresveratrol โดยใช้ปฏิกริยาเคมีต่างๆ

ผลการทดลอง ได้คิดค้นวิธีบังคับปฏิกริยาแบบ electrophilic substitution ให้เกิดขึ้นเฉพาะที่วง aromatic วงใดวงหนึ่ง ด้วยการเลือกใช้ชนิดและจำนวนหมู่ปกป้องที่เหมาะสม สามารถเตรียมได้อนุพันธ์จำนวน 26 ชนิด เมื่อนำ oxyresveratrol และอนุพันธ์ที่เตรียมได้ทั้งหมดมาทดสอบฤทธิ์ต้านไวรัสเริม พบอนุพันธ์ 2 ชนิดซึ่งมีฤทธิ์ต้านไวรัสเริมสูงกว่า oxyresveratrol ประมาณ 3 – 4 เท่าคือ 3′,5′-dihydroxy-2,4-dimethoxystilbene และ 5′-hydroxy-2,3′,4-trimethoxystilbene ส่วน

การทดสอบฤทธิ์ยับยั้งเอนไซม์ neuraminidase นั้นไม่พบว่า oxyresverarol และอนุพันธ์มีฤทธิ์ เมื่อนำสารทั้งหมดไปทดสอบฤทธิ์ทางชีวภาพอื่นเพิ่มเติม ได้แก่ฤทธิ์ยับยั้งเอนไซม์ α-glucosidase พบว่า 5′-Hydroxy-2,3′,4,-triisopropoxy-stilbene มีฤทธิ์ยับยั้งเอนไซม์ α-glucosidase ใกล้เคียงกับ oxyresveratrol ซึ่งมีรายงานว่ามีฤทธิ์ยับยั้งเอนไซม์นี้สูงและสามารถลดระดับน้ำตาลในสัตว์ทดลองได้ นอกจากนี้ได้ทดสอบความเป็นพิษต่อเซลล์มะเร็งของสารทั้งหมด พบว่า 3′,5′-diacetoxy-2,4-diisopropoxystilbene มีความเป็นพิษสูงและจำเพาะต่อเซลล์มะเร็ง HeLa

สรุป สารอนุพันธ์ที่เตรียมได้ 2 ชนิดมีฤทธิ์ต้านไวรัสเริมสูงกว่า oxyresveratrol ซึ่งคาดว่าอาจมีศักยภาพสูงกว่า oxyresveratrol ในการนำมาใช้กับโรคติดเชื้อเริมที่สมองและโรคอัลไซเมอร์ เพราะคุณสมบัติการละลายในไขมันที่คาดว่าสูงกว่า oxyresveratrol การศึกษาไม่พบว่า oxyresveratrol หรืออนุพันธ์ใดๆ มีฤทธิ์ยับยั้ง AIV neuraminidase สารอนุพันธ์ 1 ชนิดมีฤทธิ์ยับยั้งเอนไซม์ α-glucosidase ใกล้เคียงกับ oxyresveratrol แต่คาดว่าอาจมีศักยภาพที่จะนำมาพัฒนาเป็นยาสูงกว่าเพราะอัตราการถูกทำลายในร่างกายที่คาดว่าช้ากว่า นอกจากนี้มีสารอนุพันธ์ 1 ชนิดที่แสดงความเป็นพิษสูงต่อเซลล์มะเร็ง HeLa

ข้อเสนอแนะ นำสารอนุพันธ์ที่มีศักยภาพสูงกว่า oxyresveratrol ไปศึกษาต่อในสัตว์ทดลอง

โครงการวิจัยที่ 3

วัตถุประสงค์ วิจัยต่อยอดจากข้อสังเกตที่คณะผู้วิจัยได้เสนอว่าสารเมทาบอไลต์ทุติยภูมิจากพืชหลายกลุ่มที่มีฤทธิ์ต้านไวรัส มีโครงสร้างจัดเป็น *bis*-aryl เช่น กลุ่มสารคู่ฟลอโรกลูซินอล กลุ่มสารสติลบิน กลุ่มเฟลโวนอยด์ และกลุ่มลิกแนน

วิธีการทดลอง นำตัวอย่างพืชจำนวนหนึ่งซึ่งได้แก่ *Artocarpus lakoocha* (Moraceae), *Miliusa mollis*, *M. fragrans*, *M. umpangensis* (Annonaceae), *Mallotus plicatus* (Euphorbiaceae), *Dendrobium venustum* และ *Dendroium williamsonii* (Orchidaceae) มาตรวจสอบฤทธิ์ต้านไวรัสเริมแล้วทำการศึกษาต่อเพื่อแยกเอาสารออกฤทธิ์โดยวิธีโครมาโทกราฟี

ผลการทดลอง ได้สารบริสุทธิ์จำนวน 60 ชนิด พบว่าเป็นสารใหม่จำนวน 17 ชนิด ซึ่งจัดเป็นสารในกลุ่มเฟลโวนอยด์ 1 ชนิด ในกลุ่มลิกแนน 1 ชนิด ในกลุ่มนีโอลิกแนน 13 ชนิด และในสารกลุ่มกรดกอลิกกลัยโคไซด์ 2 ชนิด เมื่อนำสารเหล่านี้มาทดสอบ พบว่ามีสาร 10 ชนิดที่มีฤทธิ์ต้านไวรัสเริม จัดเป็นสารกลุ่มเฟลโวนอยด์ 4 ชนิด สารกลุ่มนีโอลิกแนน 3 ชนิดและสารกลุ่มไดไฮโดรสติลบิน สารเหล่านี้ต่างมีโครงสร้างส่วนหนึ่งเป็น *bis*-aryl ซึ่งสอดคล้องกับข้อสังเกตที่คณะผู้วิจัยได้เสนอมาก่อน สารที่มีฤทธิ์สูงสุดคือ 5,7,2′,4′-tetrahydroxy-3-prenyl-6-geranylflavone แต่จัดว่ามีฤทธิ์ปานกลางเมื่อเทียบกับยาต้านไวรัสเริม acyclovir นอกจากนี้ได้นำสารที่แยกได้บางชนิดมาทดสอบฤทธิ์ต้าน neuraminidase ของไวรัสไข้หวัด แต่ไม่พบสารใดที่มีฤทธิ์

สรุป การศึกษาในสารสกัดที่เตรียมจากพืช 7 ชนิด แยกสารได้ 60 ชนิด จัดเป็นสารใหม่ 17 ชนิด พบว่าสารที่แยกได้ 10 ชนิดมีฤทธิ์ต้านไวรัสเริม โดยทั้งหมดมีโครงสร้าง *bis*-aryl ซึ่งเป็นไปตามข้อสังเกตที่ได้เคยเสนอไว้ ไม่พบสารที่มีฤทธิ์ยับยั้ง AIV neuraminidase

ข้อเสนอแนะ ประมวลข้อมูลโครงสร้างและฤทธิ์ต้านไวรัสเริมของสารที่มีโครงสร้าง *bis*-aryl เพื่อนำมาใช้ประกอบในการวิเคราะห์ความสัมพันธ์ สำหรับการออกแบบการสังเคราะห์สารต้านไวรัสในอนาคต

ABSTRACT

Project Code: BRG5580004

Project Title: Antiviral agents against herpes simplex and avian influenza viruses from Thai medicinal plants

Investigator : Kittisak Likhitwitayawuid, Faculty of Pharmaceutical Sciences, Chulalongkorn University

E-mail Address: Kittisak.L@chula.ac.th

Project Period : 31 July 2012 – 30 July 2015

Rationale of research program: Oxyresveratrol (2,4,3′,5′-tetrahydroxystilbene) is a phytoalexin present in large amounts in the heartwood of *Artocarpus lakoocha* Roxb. (Moraceae). It is a representative of antiviral compounds with a *bis*-aryl structure, which was earlier elaborated in our recently proposed hypothesis. Our previous studies have revealed its inhibitory activity against herpes simplex virus (HSV). Because cerebral HSV infection has been implicated in the pathogenesis of Alzheimer's disease (AD), oxyresveratrol may have a potential use for preventing or treating AD. Although oxyresveratrol, by topical application, has been shown to be effective against cutaneous HSV infection, the compound lacks this activity when orally administered. Recently, oxyresveratrol has been claimed to possess inhibitory activity against neuraminidase of avian influenza virus (AIV).

Objectives of research program: To find/develop medicinally useful compounds or drug delivery systems for application in HSV, based on our earlier accumulated data on oxyresveratrol and its medicinal potentials, as well as our earlier proposed hypothesis.

Methodology of research program: The research program consists of three separate projects: (1) Development and evaluation of nanocarriers for oral delivery of oxyresveratrol; (2) Structural modification of oxyresveratrol; and (3) Search for new antiviral agents from Thai medicinal plants.

Results of research program and suggestions:

(1) New drug delivery systems (DDS) for enhancing the oral absorption of oxyresveratrol were obtained. We suggest that these DDSs be applied in the study of HSV-related cerebral disorders such as Alzheimer's disease (AD).

(2) Two compounds derived from oxyresveratrol may have higher potential than the parent compound for treating cerebral HSV-infection and AD, due to their possibly higher lipophilicity. One derivative may be a better blood sugar controlling agent, a result of a theoretically slower rate of metabolism. Another derivative showed potent cytotoxicity against HeLa cancer cells. In vivo studies are recommended for these active analogs.

(3) Additional facts on the structures and antiherpetic activity of *bis*-aryl compounds were obtained. It is suggested that these data be digitally stored and analyzed in comparison with information from other sources for future designs of antiviral drugs.

Key words: oxyresveratrol, virus, herpes, avian influenza, Alzheimer's disease, diabetes, cancer

Project 1

Objectives: Develop pharmaceutical formulations for the oral delivery of oxyresveratrol (OXYR).

Methods: Three different delivery systems were investigated: (1) solid lipid nanoparticles (SLN), (2) nanostructured lipid carriers (NLC) and (3) self-microemulsifying drug delivery systems (SMEDDS). Each system was successfully formulated using different optimized compositions and methods. Comparative analysis was done on the physicochemical properties of these OXYR formulations, as well as the ability to increase the permeability of oxyresveratrol against cultured Caco-2 cells and oral absorption in rats.

Results: The obtained SMEDDS appeared as a yellow oily liquid, while the SLN and NLC as low viscous suspensions. The physical properties, cytotoxicity, and drug permeability across the Caco-2 monolayer of the different systems were compared. The non-aqueous SMEDDS had about a 13-fold higher drug loading than the lipid nanoparticles (SLN and NLC). The particle sizes (26.94 ± 0.08 nm) of OXYR-SMEDDS were significantly smaller than that of the NLC and SLN (p <0.05). Also, a narrow size distribution of the SMEDDS (PDI, 0.073 ± 0.010) was obtained compared to the lipid nanoparticles (PDI, 0.2–0.3). In the MTT assay, the OXYR-SMEDDS showed a 4-fold greater toxicity on the Caco-2 cells than the SLN and NLC containing OXYR. At the non-toxic concentration of 100 mM of OXYR, the SMEDDS and the lipid nanoparticles had 2.5 to 3-fold enhanced permeability and 1.3 to 1.8-fold reduced efflux transport, as compared to the unformulated OXYR (p <0.05). The improvement of the *in vitro* oral absorption of the lipid-based formulations resulted from the increased permeability and the efflux inhibition. The *in vivo* pharmacokinetic studies of these OXYR-loaded formulations in the Wistar rat revealed that the SLN and NLC increased the relative bioavailability of OXYR to 125% and 177%, respectively when compared with unformulated OXYR. The SMEDDS enhanced bioavailability of OXYR to 218 – 786 %, depending on the type and quantity of the surfactant.

Conclusion: These newly developed drug delivery systems have provided the possibility of oral administration of oxyresveratrol for the treatment/prevention of Alzheimer's disease.

Suggestion: Study the potential application of OXYR formulations in cerebral HSV-related diseases such as Alzheimer's disease.

Project 2

Objectives: To chemically modify the structure of oxyresveratrol and determine the antiherpetic activity of the obtained derivatives.

Methods: Several types of chemical reactions were studied.

Results: We found that electrophilic substitution on the two aromatic rings could be controlled by manipulating the type and the number of protecting groups placed on the phenolic groups**.** A total of twenty-six derivatives were prepared from oxyresveratrol through. This innovative strategy has provided a valuable tool for the future chemical modification of similarly oxygenated aromatic structures. Oxyresveratrol and all of its prepared analogs were evaluated for inhibitory activity against herpes simplex virus (HSV) and neuraminidase of avian influenza virus (AIV). The most attractive products are the partially etherified analogs, namely 3′,5′-dihydroxy-2,4-dimethoxystilbene and 5′-hydroxy-2,3′,4-trimethoxy-stilbene, which displayed 3- to 4-fold higher antiherpetic activity than the parent compound. Because of the ether functionalities, these two synthetic compounds are expected to have higher lipophilicity and thus may have greater potential use in cerebral HSV infection, as well as HSV-related Alzheimer's disease (AD). Neither oxyresveratrol nor its derivatives showed AIV neuraminidase inhibition. Additional bioassays for α-glucosidase inhibition and cytotoxicity against cancer cells were performed on the twenty-seven stilbenoids. Due to its strong α-glucosidase inhibitory activity, oxyresveratrol has been recently suggested as an adjunct treatment for diabetes. The compound 5′-Hydroxy-2,3′,4,-triisopropoxystilbene obtained in this study showed as strong anti- α-glucosidase activity as oxyresveratrol, and could be a better drug candidate, as judged from its likely slower rate of metabolism. 3′,5′-Diacetoxy-2,4-diisopropoxystilbene, another analog derived oxyresveratrol, displayed selective and pronounced *in vitro* cytotoxicity against HeLa cancer cells, and should be further investigated for anticancer activity in animals.

Conclusion: Two derivatives showed greater antiherpetic activity than oxyresveratrol and might have better potential for cerebral infection and AD, due to their possibly higher lipophilicity. Niether oxyresveratrol nor any derivatives displayed AIV neuraminidase inhibition. One derivative was approximately as strong as oxyresveratrol in inhibiting α-glucosidase, and might be a more preferable drug candidate, thanks to its hypothetically slower rate of metabolism. Another derivative exhibited potent cytotoxicity against HeLa cancer cells.

Suggestion: Derivatives with improved activity should be further studied in vivo.

Project 3

Objectives: To further accumulate data on naturally occurring antiviral compounds with a *bis*-aryl structure, focusing on flavonoids, lignoids and stilbenoids.

Methods: Selected plants were evaluated for antiherpetic activity, and then subjected to detailed investigation, including *Artocarpus lakoocha* (Moraceae), *Miliusa mollis*, *M. fragrans*, *M. umpangensis* (Annonaceae), *Mallotus plicatus* (Euphorbiaceae), *Dendrobium venustum* and *Dendroium williamsonii* (Orchidaceae). Constituents of these plants were isolated by repeated chromatography, structurally characterized by spectroscopic methods, and then evaluated for antiherpetic activity by the plaque reduction assay.

Results: A total of sixty secondary plant metabolites were obtained. Seventeen of these isolates were determined as new compounds, consisting of a prenylated flavonoid [named 5,7,2′,4′-tetrahydroxy-3-prenyl-6-geranylflavone], a tetrahydrofuran lignan [named (+)-3-hydroxy-veraguensin], five dihydrobenzofuran neolignans [named miliumollin, 3′-methoxymiliumollin, 4′-*O*-methylmiliumollin**,** 7-methoxymiliumollin and miliumollinone], eight 8-*O*-4′ neolignans [named miliusamollin, (+)-3-*O*-demethyl-eusiderin C, (+)-4-*O*-demethyleusiderin C, (−)-miliusfragrin, (−)-4-*O*-methyl-miliusfragrin, (+)-eusiderin A, (−)-miliusfragranol A and (−)-miliusfragranol B], and two glycosidic gallic acid derivatives [named bergenin-8-*O*-α-L-rhamnoside and *seco*-bergenin-8-*O*-α-L-rhamnoside]. When subjected to antiherpetic activity evaluation, only ten compounds were found to exhibit activity, including four flavonoids [i.e. 5,7,2′,4′-tetrahydroxy-3-prenyl-6-geranylflavone, cudraflavone C, quercetin 3,7-dimethyl ether and chrysosplenol-D], three neolignans [i.e. miliumollinone, 4-*O*-demethyleusiderin C and licarin A] and three dihydrostilbenes (or bibenzyls) [i.e. gigantol, batatasin III and 3,3′-dihydroxy-4, 5-dimethoxybibenzyl].

Conclusion: All of the antiherpetic molecules contained a *bis*-aryl structure, in accordance with our previous observations. The most potent compound was 5,7,2′,4′-tetrahydroxy-3-prenyl-6-geranylflavone, which showed moderate activity as compared with the antiherpetic drug acyclovir. Some of the isolates were evaluated for anti-neuraminidase, but were devoid of such activity.

Suggestion: Data on the structures and activity should be digitally stored for future antiviral drug design.

EXECUTIVE SUMMARY

Oxyresveratrol has been shown to possess inhibitory activity against herpes simplex virus (HSV). It is a representative of antiviral compounds with a *bis*-aryl structure, as previously described in our earlier hypothesis. Because cerebral HSV infection has been implicated in the pathogenesis of Alzheimer's disease (AD), the compound may have a potential use for preventing/treating AD. Oxyresveratrol, by topical application, has been shown to be effective against cutaneous HSV infection, but the compound loses this activity when orally administered. Recently, oxyresveratrol has been reported to have inhibitory activity against avian influenza neurominidase.

Our research initiatives have been designed to find/develop medicinally useful compounds/drug delivery systems from our accumulated data on oxyresveratrol and its medicinal potentials, as well as our proposed hypothesis. The research program consists of three separate projects, constructed from the afore-mentioned postulations: (1) Development and evaluation of nanocarriers for oral delivery of oxyresveratrol; (2) Structural modification of oxyresveratrol; and (3) Search for new antiviral agents from Thai medicinal plants.

Project 1: The project attempted to develop pharmaceutical formulations for the oral delivery of oxyresveratrol (OXYR). Three different delivery systems were investigated: (1) solid lipid nanoparticles (SLN), (2) nanostructured lipid carriers (NLC) and (3) self-microemulsifying drug delivery systems (SMEDDS). Each system was successfully formulated using different optimized compositions and methods. The obtained SMEDDS appeared as a yellow oily liquid, while the SLN and NLC as low viscous suspensions. The physical properties, cytotoxicity, and drug permeability across the Caco-2 monolayer of the different systems were compared. The non-aqueous SMEDDS had about a 13-fold higher drug loading than the lipid nanoparticles (SLN and NLC). The particle sizes of OXYR-SMEDDS were significantly smaller than that of the NLC and SLN. In addition, a narrow size distribution of the SMEDDS was obtained, as compared to the lipid nanoparticles. In the MTT assay, the OXYR-SMEDDS showed greater toxicity on the Caco-2 cells than the SLN and NLC containing OXYR. At the non-toxic concentration of OXYR, the SMEDDS and the lipid nanoparticles showed enhanced permeability and reduced efflux transport, as compared to the unformulated OXYR. The improvement of the *in vitro* oral absorption of the lipid-based formulations resulted from the increased permeability and the efflux inhibition. The *in vivo* pharmacokinetic studies of these OXYR-loaded formulations in the Wistar rat revealed that the SLN and NLC could increase the relative bioavailability of OXYR to 125% and 177%, respectively when compared with unformulated OXYR, whereas the SMEDDS could boost the bioavailability of OXYR to 218 – 786 %. These newly developed drug delivery systems have provided the possibility of the oral administration of oxyresveratrol for the treatment/prevention of Alzheimer's disease.

Project 2: The purpose of this project was to chemically modify the structure of oxyresveratrol and evaluate the antiherpetic activity of the obtained derivatives. A total of 26 derivatives were prepared through several types and steps of reactions. A new strategy (manipulating the type and the number of *O*-protecting groups) was devised to control the electrophilic aromatic substitution, and this has provided a valuable tool for the future chemical modification of similarly oxygenated aromatic structures. Oxyresveratrol and the prepared analogs were evaluated for inhibitory activity against herpes simplex virus (HSV) and neuraminidase of avian influenza virus (AIV). Neither oxyresveratrol nor any of its derivatives showed AIV neuraminidase inhibition. Regarding antiherpetic activity, two derivatives, i.e. 3′,5′-dihydroxy-2,4-dimethoxystilbene and 5′-hydroxy-2,3′,4-trimethoxy-stilbene displayed higher potency than the parent compound, and with possibly higher lipophilicity, they may have greater potential use in cerebral HSV infection, as well as HSV-related Alzheimer's disease. Additional bioassays for α-glucosidase inhibition and cytotoxicity against cancer cells were performed on oxyresveratrol and derivatives. 5′-Hydroxy-2,3′,4,-triisopropoxystilbene showed as strong anti- α-glucosidase activity as oxyresveratrol, which has been suggested as an adjunct treatment of diabetes; nevertheless, the derivative could be a better drug candidate than the parent compound, due to its likely slower rate of metabolism. 3′,5′-Diacetoxy-2,4-diisopropoxy-stilbene displayed increased and selective *in vitro* cytotoxicity against HeLa cancer cells, and should be further investigated in animals.

Project 3: We have earlier made a remark that several groups of plant secondary metabolites with antiviral activity possess a *bis*-aryl structure for example, dimeric phloroglucinols, stilbenoids (eg. oxyresveratrol), flavonoids and lignans,. As a continuing study of this hypothesis, a number of plants were evaluated for antiherpetic activity, and then subjected to detailed investigation, including *Artocarpus lakoocha* (Moraceae), *Miliusa mollis*, *M. fragrans*, *M. umpangensis* (Annonaceae), *Mallotus plicatus* (Euphorbiaceae), *Dendrobium venustum* and *Dendroium williamsonii* (Orchidaceae). After repeated chromatographic separation, a total of sixty secondary plant metabolites were isolated and structurally characterized. Among these isolates, seventeen were determined as new compounds, consisting of a prenylated flavonoid, a lignan, thirteen neolignans, and two glycosidic gallic acid derivatives. Antiherpetic activity evaluation revealed that ten of the isolates exhibited the activity, including four flavonoids, three neolignans and three dihydrostilbenes (bibenzyls). All of the antiherpetic molecules were found to be polyphenolic compounds with a *bis*-aryl scaffold, in agreement with our earlier observations. The most potent compound was the polyprenylated flavonoid named 5,7,2′,4′-tetrahydroxy-3-prenyl-6-geranyl-flavone, showing moderate activity, as compared with the antiherpetic drug acyclovir. Regarding the neuraminidase inhibitory potential, oxyresveratrol and some of the isolates evaluated in this study were devoid of such activity. The chemical and biological data obtained in this study have provided additional knowledge useful for future research on the chemistry and antiviral activity of Thai medicinal plants.

OUTPUTS

(1) ผลงานตีพิมพ์ในวารสารวิชาการนานาชาติ

จำนวน 12 เรื่อง ได้แก่

(1) Yaowaporn Sangsen, Kamonthip Wiwattanawongsa, Kittisak Likhitwitayawuid, Boonchoo Sritularak and Ruedeekorn Wiwattanapatapee. Modification of oral absorption of oxyresveratrol using lipid based nanoparticles. Colloids and Surfaces B: Biointerfaces **131**: 182–190 (2015). (Impact Facto = 3.902)

(2) Yaowaporn Sangsen, Kamonthip Wiwattanawongsa, Kittisak Likhitwitayawuid, Boonchoo Sritularak, Potchanapond Graidist and Ruedeekorn Wiwattanapatapee. Influence of surfactants in self-microemulsifying formulations on enhancing oral bioavailability of oxyresveratrol: Studies in Caco-2 cells and in vivo. International Journal of Pharmaceutics **498**: 294–303(2016). (IF = 3.994)

(3) Sangsen, Y., Wiwattanawongsa, K., Likhitwitayawuid, K., Sritularak, B. and Wiwattanapatapee, R. 2016. Comparison between oily system and lipid nanoparticles of oxyresveratrol on the physicochemical properties and Caco-2 cells oral absorption European Journal of Lipid Science and Technology (in press). 15 JUN 2016, DOI:10.1002/ejlt.201600053 (IF = 1.953)

(4) Yaowaporn Sangsen, K. Likhitwitayawuid, B. Sritularak, Kamonthip Wiwattanawongs and Ruedeekorn Wiwattanapatapee. Novel solid lipid nanoparticles for oral delivery of oxyresveratrol: effect of the formulation parameterson the physicochemical properties and in vitro release. International Journal of Medical Science and Engineering **7**: 873-880 (2013).

(5) Nutputsorn Chatsumpun, Taksina Chuanasa, Boonchoo Sritularak, Vimolmas Lipipun, Vichien Jongbunprasert, Somsak Ruchirawat, Poonsakdi Ploypradith, and Kittisak Likhitwitayawuid. Oxyresveratrol: Structural modification and evaluation of biological activities. Molecules **21**: 489; doi:10.3390/molecules21040489 (2016). (IF =2.465)

(6) Boonchoo Sritularak, Kullasap Tantrakarnsakul, Vimolmas Lipipun and Kittisak Likhitwitayawuid. Flavonoids with anti-HSV activity from the root bark of *Artocarpus lakoocha.* Natural Product Communications **8**: 1079-80 (2013). (IF = 0.884)

(7) Kanokporn Sawasdee, Tanawat Chaowasku, Vimolmas Lipipun, Thi-Hanh Dufat, Sylvie Michel and Kittisak Likhitwitayawuid. Neolignans from leaves of *Miliusa mollis*. Fitoterapia **85**: 49–56 (2013). (IF = 2.408)

(8) Kanokporn Sawasdee, Tanawat Chaowasku, Vimolmas Lipipun, Thi-Hanh Dufat, Sylvie Michel and Kittisak Likhitwitayawuid. New neolignans and a lignan from *Miliusa*

fragrans, and their anti-herpetic and cytotoxic activities. Tetrahedron Letters **54**: 4259–4263 (2013). (IF = 2.347)

(9) Kanokporn Sawasdee, Tanawat Chaowasku, Vimolmas Lipipun, Thi-Hanh Dufat, Sylvie Michel, Vichien Jongbunprasert and Kittisak Likhitwitayawuid. Geranylated homogentisic acid derivatives and flavonols from *Miliusa umpangensis*. Biochemical Systematics and Ecology **54**: 179–181 (2014). (IF = 0.988)

(10) Kongsin Luangruangrong, Boonchoo Sritularak, Vimolmas Lipipun and Kittisak Likhitwitayawuid. New gallic acid glycosides from *Mallotus plicatus*. Heterocycles **89**: 1237–1244 (2014). (IF = 1.107)

(11) Prapapun Sukphan, Boonchoo Sritularak, Wanwimon Mekboonsonglarp, Vimolmas Lipipun and Kittisak Likhitwitayawuid. Chemical constituents of *Dendrobium venustum* and their antimalarial and anti-herpetic properties. Natural Product Communications 9: 825-827 (2014). (IF = 0.884)

(12) Pathrapa Rungwichaniwat, Boonchoo Sritularak and Kittisak Likhitwitayawuid. Chemical Constituents of *Dendrobium williamsonii*. Pharmacognosy Journal **6**: 36-41 (2014).

(2) การผลิตนักวิจัยรุ่นใหม่

จำนวน 7 คน แบ่งเป็นระดับปริญญาเอก 3 คน และปริญญาโท 4 คน

(3) การนำผลวิจัยไปใช้ประโยชน์

คณะผู้วิจัยได้คัดเลือกระบบนำส่ง oxyresveratrol ที่ได้พัฒนาขึ้นในโครงการนี้ มาใช้ศึกษาศักยภาพของ oxyresveratrol ในการป้องกันหรือบรรเทาอาการของโรคอัลไซเมอร์ในสัตว์ทดลอง ทั้งนี้ในเบื้องต้นได้รับทุนสนับสนุนจากสำนักงานคณะกรรมการวิจัยแห่งชาติ งบประมาณแผ่นดิน ปีพ.ศ. 2558

CONTENTS

	Page
คำนำ	i
บทคัดย่อ	ii
ABSTRACT	v
EXECUTIVE SUMMARY	ix
OUTPUTS	xi
INTRODUCTION	1
CHAPTER I	
Development and Evaluation of Nanocarriers for Oral Delivery of Oxyresveratrol	5
CHAPTER II	
Structural modification of oxyresveratrol	44
CHAPTER III	
Search for new antiviral agents from Thai medicinal plants	70

INTRODUCTION

1. Research problems

Oxyresveratrol [**1**] is a polyoxygenated stilbene with potentially useful antiviral activity. In our previous investigations, oxyresveratrol was found to possess *in vitro* antiviral activity against several types of virus, (Likhitwitayawuid et al., 2005a; Sasivimolphan et al., 2009). When topically administered, oxyresveratrol showed therapeutic efficacy on mice cutaneously infected with herpes simplex type 1 (HSV-1) (Chuanasa et al., 2008). Our recent study in mice showed that a topical cream containing 10% oxyresveratrol was as effective against HSV-1 dermal infection as a commercial cream containing 5% acyclovir (Lipipun et al., 2011). Mounting evidence has indicated the link between cerebral HSV-1 infection and the pathogenesis of Alzheimer's disease (AD) (Hill et al, 2009), suggesting another medicinal potential for **1**. Oxyresveratrol, however, was less active by oral administration (Chuanasa et al., 2008), restricting its clinical application. Prior to this study, the intestinal absorptivity of the compound has never been investigated, although several other metabolic behaviors of oxyresveratrol, including its fate in the blood circulation, its blood-brain barrier (BBB) permeability and its excretion have been reported (Qiu et al., 1996; Breuer et al., 2006; Huang et al., 2009; Bertram et al., 2010). It is clear that information on the intestinal absorption and the oral delivery system of oxyresveratrol is necessary if the compound is to be developed into its full clinical potential. This issue has become the focus of **Project 1**.

A number of stilbenes, including resveratrol, a stilbene with structure closely-related to **1**, have been shown to possess inhibitory activity against various classes of virus (Li et al., 2006; Beyoda et al., 2006; Cardin et al., 1991). Recently, inhibition against several types of influenza virus has been observed in some stilbenoids (Kernan et al., 1997; Liu et al., 2010; Nguyen et al., 2010). These findings attracted our attention to explore the possibility of synthesizing stilbenoids with higher antiherpetic potential, and/or inhibitory activity against avian influenza virus by structural modification of **1**. This turned into the objective of **Project 2**.

In our earlier reports (Likhitwitayawuid et al., 2005a; 2005b), we made an observation that some antiviral compounds have a structure consisting of two aromatic rings connected by an alkyl bridge. This structural scaffold can be generally called "*bis*-aryl", represented by [**2**]. Examples of natural products with this structure are phloroglucinol dimers (C_6-C_1-C_6) [**3**], stilbenoids (C_6-C_2-C_6) [**4**], flavonoids (C_6-C_3-C_6) [**5**] and lignans/neolignans (C_6-C_4-C_6) [**6**] (Supudompol et al., 2004; Likhitwitayawuid et al., 2006; Srirularak et al., 2009; Swasdee et al., 2010). Thus, search for antiviral agents derived from these four groups of plant secondary metabolites was the main purpose of **Project 3**.

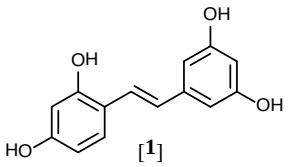

[**1**]

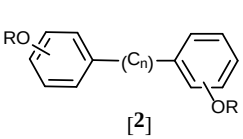

[**2**]

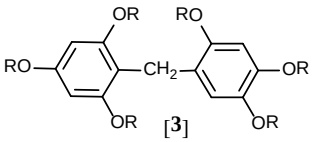

[**3**]

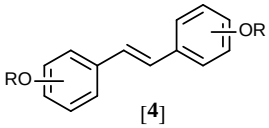

[**4**]

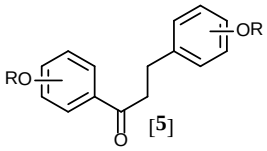

[**5**]

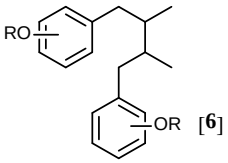

[**6**]

2. Research objectives

The overall objectives of this research program are:

(1) To develop nanocarriers for oral delivery of oxyresveratrol and to evaluate intestinal absorptivity of oxyresveratrol contained in the formulations.

(2) To modify the chemical structure of oxyresveratrol and evaluate the obtained derivatives for inhibitory activity against herpes simplex virus (HSV) and/or H5N1 neuraminidase of avian influenza virus (AIV)

(3) To search for naturally occurring compounds with *bis*-aryl structure that possess anti-HSV potential and/or inhibitory activity against AIV H5N1 neuraminidase.

To achieve these goals, the research work has been divided into three separate projects with corresponding objectives, as follows:

No.	Project Title	Objectives
1	Development and evaluation of nanocarriers for oral delivery of oxyresveratrol	1. To develop nanocarriers for oral delivery of oxyresveratrol. 2. To evaluate the physicochemical characteristics and *in vitro* release properties of developed oxyresveratrol formulations. 3. To determine the *in vitro* and *in vivo* oral absorption of developed oxyresveratrol formulations.
2	Structural modification of oxyresveratrol	1. To chemically modify the structure of oxyresveratrol. 2. To evaluate the prepared oxyresveratrol derivatives for inhibitory activity against herpes simplex virus or/and H5N1 neuraminidase.
3.	Search for new antiviral agents from Thai medicinal plants	1. To isolate antiviral compounds from selected plant extracts 2. To evaluate the isolated compounds for inhibitory activity against herpes simplex virus or/and H5N1 neuraminidase.

References

Bertram, R. M., Takemoto, J.K., Remsberg, C.M., Vega-Villa, K.R., Sablani, S. and Davies, N. M. High-performance liquid chromatographicanalysis: applications to nutraceutical content and urinary disposition of oxyresveratrol in rats Biomed. Chromatogr. 2010, 24, 516–521.

Beyoda, L.M., del Olmo, E., Sancho, R., Barboza, B., Beltrán, M., Garcia-Cadenas, A.E., Sánchez-Palomino, S., López-Pérez, J.L., Muñoz, E., Feliciano, A.S. and Alcamí, J. Anti-HIV activity of stilbene-related heterocyclic compounds. Bioorg. Med. Chem. Lett. 2006, 16, 4075–4079.

Breuer, C., Wolf, G., Andrabi, S. A., Lorenz, P. and Horn T.F.W. Blood–brain barrier permeability to the neuroprotectant oxyresveratrol. Neuro. Lett. 2006, 393, 113–118.

Cardin, A. D., Smith, P. L., Hyde, L., Blankenship, D. T., Bowlin, T. L., Schroeder, K., Stauderman, K. A., Taylor, D. L. and Tyms A. S. Stilbene disulfonic acids. J. Biol. Chem. 1991, 266, 13355–13363.

Chuanasa, T., Phromjai, J., Lipipun, V., Likhitwitayawuid K., Suzuki, M., Pramyothin, P., Hattori, M. and Shiraki, K. Anti-herpes simplex virus (HSV-1) activity of oxyresveratrol derived from Thai medicinal plant: mechanism of action and therapeutic efficacy on cutaneous HSV-1 infection in mice. Antiviral Res. 2008, 80, 62–70.

Hill, J.M., Zhao, Y., Clement, C., Neumann, D.M., Lukiw, W.J. HSV-1 infection of human brain cells induces miRNA-146a and Alzheimer-type inflammatory signaling. NeuroReport 2009, 20, 1500–5.

Huang, H., Chen, G., Lu, Z., Zhang, J. and Guo. D. Identification of seven metabolites of oxyresveratrol in rat urine and bile using liquid chromatography/tandem mass spectrometry Biomed. Chromatogr. 2010, 24, 426–432**.**

Kernan, M.R., Sendl A., Chen, J. L., Jolad, S. D., Blanc, P., Murphy, J. T., Stoddart, C. A., Nanakorn, W., Balick, M. J. and Rozhon, E. J. Two new lignans with activity against influenza virus from the medicinal plant *Rhinacanthus nasutus*. J. Nat. Prod. 1997, 60, 635–637.

Li, Y.-Q., Li, Z.-L., Zhao, W.-J., Wen, R.-X., Meng, Q.-W., Zeng, Y. Synthesis of stilbene derivatives with inhibition of SARS coronavirus replication. Eur. J. Med. Chem. 2006, 41, 1084–1089.

Likhitwitayawuid, K., Sritularak, B., Benchanak, K., Lipipun, V., Mathew, J., and Schinazi, R.F. Phenolics with antiviral activity from *Millettia erythrocalyx* and *Artocarpus lakoocha*. Nat. Prod. Res. 2005a, 19, 177–182.

Likhitwitayawuid, K., Supudompol, B., Sritularak, B., Lipipun, V., Rapp, K. and Schinazi, R.F. Phenolics with anti-HSV and anti-HIV activities from *Artocarpus gomezianus*, *Mallotus pallidus* and *Triphasia trifolia*. Pharm. Biol. 2005b, 43, 651–657.

Likhitwitayawuid, K., Chaiwiriya, S., Sritularak B. and Lipipun, V. Anti-HSV Flavones from the heartwood of *Artocarpus gomezianus* Chem. Biod. 2006, 3, 1138–1143.

Lipipun, V., Sasivimolphan, P., Yoshida, Y., Daikoku, T., Sritularak, B., Ritthidej, G., Likhitwitayawuid, K., Pramyothin, P., Hattori, M. and Shiraki, K. Topical cream-based oxyresveratrol in the treatment of cutaneous HSV-1 infection in mice. Antiviral Res. 2011, 91, 154–160.

Liu, A.-L., Yang, F., Zhu, M., Zhou, D., Lin, M., Lee, S. M-Y., Wang, Y.-T. and Du, G.-H. In vitro anti-influenza viral activities of stilbenoids from the Lianas of *Gnetum pendulum*. Planta Med. 2010, 76, 1874–1876.

Nguyen, P.-H., Na, M.-K., Dao, T.-T., Ndinteh, D. T., Mbafor, J. T., Park J.-Y., Cheong, H.-S. and Oh, W.-K. New stilbenoids with inhibitory activity on viral neuraminidases from *Erythrina addisoniae*. Bioorg. Med. Chem. Lett. 2010, 20, 6430–6434.

Qiu, F., Komatsu, K., Saito, K., Kawasaki, K., Yao, X. and Kano, Y. Pharmacological properties of traditional medicines. XII. Pharmacokinetic study of mulberroside A and its metabolites in rat. Biol. Pharm. Bull. 1996, 19, 1463–1467.

Sasivimolphan, P., Lipipuna, V., Likhitwitayawuid, K., Takemotoe, M., Pramyothin, P., Hattori, M. and Shiraki, K. Inhibitory activity of oxyresveratrol on wild-type and drug-resistant varicella-zoster virus replication in vitro. Antiviral Res. 2009, 84, 95–97.

Sritularak, B. and Likhitwitayawuid, K. New bisbibenzyls from *Dendrobium falconer*i Helv. Chim. Act. 2009, 92, 740–744.

Sawasdee, K., Chaowasku, T. and Likhitwitayawuid, K. New neolignans and a phenylpropanoid glycoside from twigs of *Miliusa mollis*. Molecules 2010, 15, 639–648.

Supudompol, B., Likhitwitayawuid, K., and Houghton, P.J. Phloroglucinol derivatives from *Mallotus pallidus*. Phytochemistry 2004, 65, 2589–-2594.

CHAPTER I

Project 1

Development and Evaluation of Nanocarriers for Oral Delivery of Oxyresveratrol

Principle Investigator: Associate Professor Dr. Ruedeekorn Wiwattanapatapee
Prince of Songkla University

Background

Oxyresveratrol (OXY) has been shown to possess inhibitory activity against herpes simplex virus (HSV-1 and HSV-2) (Likhitwitayawuid et al., 2005; Lipipun et al., 2011) and varicella zoster virus (VZV) (Sasivimolphan et al., 2009). In fact, a body of evidence has implicated HSV-1 infection in the brain as one of the key causative factors in the pathogenesis of Alzheimer's disease (AD) (Hill et al, 2009), and this has suggested another medicinal importance for oxyresveratrol. However, the oral absorption of OXY appears to be limited due to its high polarity that affects its intermediate permeability with involved efflux mediated mechanism (Mei et al, 2012). Once into the blood stream it is cleared by extensive hepatic metabolism and its rapid elimination results in a short half-life time (~0.96 h) in the body leading to a low oral bioavailability and largely restricts its clinical use (Lipipun et al., 2011; Charoenlarp et al., 1991; Huang et al., 2010; Tanunkat, 1990). In an effort to overcome this drawback, we attempted to develop different formulations that could modify the oral absorption of OXY and improve its bioavailability.

1. Objectives

1. To develop lipid-based delivery systems, including self-microemulsifying drug delivery systems (SMEDDS), solid lipid nanoparticles (SLNs) and nanostructured lipid carriers (NLCs) for oral delivery of OXY.
2. To evaluate the physicochemical characteristics and *in vitro* release properties of developed oxyresveratrol formulations.
3. To determine the *in vitro* and *in vivo* oral absorption of developed OXY formulations.

2. Methodology

Development of OXY-loaded lipid nanoparticle systems

Preparation of OXY-loaded SLN and NLC

The lipid nanoparticles including SLN and NLC were prepared by a high shear homogenization method (Sangsen *et al.*, 2015). The process was performed using a high speed

homogenizer (ULTRA-TURRAX®, IKA®, Germany) at 24,000 rpm for 15 min. Then the nanoemulsion was cooled to obtain lipid nanoparticles at room temperature (Figure 1.1).

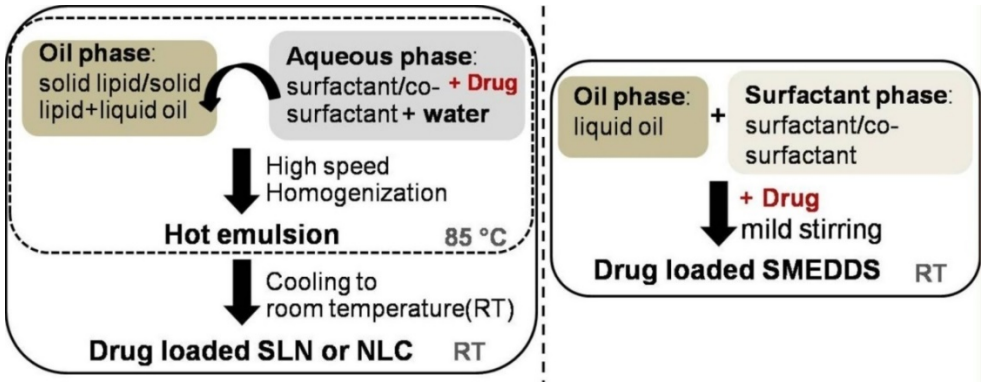

Figure 1.1 Diagram of production process for lipid nanoparticles compared to the preparation of SMEDDS

The OXY-loaded SLN (OXY-SLN) and OXY-loaded NLC (OXY-NLC) consisted of a lipid phase and an aqueous phase. The lipid phase contained only solid lipid (Compritol ATO 888®; Com888) for SLN while some parts of the lipid were replaced by liquid oil (Labrafac CC®; Lab CC) for the NLC. The aqueous phase of both systems consisted of OXY (0.3% w/w), surfactant (3.75% of Tween 80®), co-surfactant (1.875% of soy lecithin) and water. Blank SLN and NLC were prepared in the same way, without the drug. The formulation compositions are presented in Table 1.1.

Table 1.1 Composition of SLN and NLC formulations

Formulations	Compositions (% w/w)					
	Lipid phase		Aqueous phase			
	C888	Lab CC	Tween80	Soy lecithin	OXY	DI water
Blank SLN	5	-	3.75	1.875	-	89.375
Blank NLC1	4	1	3.75	1.875	-	89.375
Blank NLC2	3	2	3.75	1.875	-	89.375
Blank NLC3	2.5	2.5	3.75	1.875	-	89.375
SLN	5	-	3.75	1.875	0.3	89.075
NLC1	4	1	3.75	1.875	0.3	89.075
NLC2	3	2	3.75	1.875	0.3	89.075
NLC3	2.5	2.5	3.75	1.875	0.3	89.075

Physicochemical characterizations

Measurement of particle size, polydispersity index and zeta potential

The mean particle size (PS), the polydispersity index (PDI) and the zeta potential (ZP) of the developed SLN and NLC were measured at 25 °C using a zeta potential analyzer (Zetasizer Nano ZS®, Malvern Instruments, UK). Prior to the measurements, all samples were diluted with DI water. The PS and size distribution (PDI) were monitored by the dynamic light scattering (DLS) technique at an angle of 173 ºC. For the ZP, this was determined by measurement of the electrophoretic mobility. All measurements were performed in triplicate.

Determination of the total drug content

The total drug content (TDC) in the developed formulations was determined. Briefly, aliquots of 1mL of the OXY–loaded SLN or NLC dispersion were dissolved in methanol and the mixture was blended using a mixer (Vortex-gene 2, Becthai Bangkok Equipment & Chemical, Thailand) at a maximum speed for 15min in order to facilitate complete dissolution. Then, the obtained suspension was allowed to filter through a 0.45 µm membrane filter and diluted appropriately with the HPLC mobile phase. The resulting solution was analyzed by the HPLC method.

Drug entrapment efficiency and drug loading capacity

The encapsulation efficiency (EE) and loading capacity (LC) of OXY–loaded SLN or NLC were evaluated. The EE of the formulations was calculated by determining the amount of free drug that was not entrapped in the formulations. The drug loading content was the ratio of incorporated drug to lipid (w/w). One mL of the OXY-loaded SLN dispersion was placed in the dialysis bag (molecular weight cut off; MWCO 12–14 kDa). These bags were then placed in a centrifuge tube and the tube was filled with methanol and centrifuged at 13,500 rpm for 15min. The mixture of solvent containing the non-entrapped drug was

The total OXY (%) in the formulations, the EE (%) and LC (%) were calculated by the following equations where OXY_{exp} was the total content of OXY calculated from the experiment, OXY_{ther} was the theoretical OXY content, OXY_f was the amount of non-entrapped OXY, T_{lipid} was the total weight of the lipid phase in the formulation.

$$\text{TDC (\%)} = (OXY_{exp}/OXY_{ther}) \times 100$$

$$\text{EE (\%)} = [(OXY_{exp} - OXY_f)/OXY_{exp}] \times 100$$

$$\text{LC (\%)} = [(OXY_{exp} - OXY_f)/T_{lipid}] \times 100$$

Determination of morphology

The morphology of SLN and NLC formulations was observed by transmission electron microscopy (TEM; JEOL Ltd., Tokyo, Japan) at a 160 kV. The samples were placed on Formvar®

grids and stained with 2% w/v phosphotungstic acid for 10 min. Any excess fluid was then removed, and the grid surface was air dried at room temperature.

Analysis by differential scanning calorimetry (DSC) and powder X-ray diffraction (PXRD)

DSC and PXRD were used to identify the crystal form of the lipid and OXY dispersed in the lipid matrix. DSC analysis was performed using a DSC8000 differential scanning calorimeter (Perkin Elmer Inc., MA, USA). Accurately weighed samples were placed in aluminum pans and sealed with a lid. Al_2O_3 was used as the reference. In the scanning process, a heating rate of 5 °C/min was applied in the temperature range from 20 °C to 150 °C.

PXRD studies were performed using the Phillips X-ray diffractometer (X'Pert MPD, the Netherlands) and Cu-Kα radiation. The samples were scanned over a 2θ range of 0–90° at a scan rate of 0.05°/s. The freeze drying procedure was performed by freeze dryer (FTS systems, Tokyo, Japan) to practically determine of the OXY-SLN and OXY-NLC formulations.

In vitro release of OXY

The *in vitro* release studies of OXY were performed using the dialysis bag diffusion technique with some modifications (Tiwari and Pathak, 2011). Briefly, a suspension of OXY-SLN or OXY-NLC (equivalent to 10 mg OXY) was added into the dialysis bag (MWCO 12–14 kDa). The bag was immersed in 200 mL of release medium in a chamber of the USP30 dissolution apparatus 2 (Hanson Research Corporation, USA), stirred at 100 rpm and maintained at 37 ± 0.5 °C. The dissolution medium was simulated gastric fluid (SGF, pH 1.2) and simulated intestinal fluid (SIF, pH 6.8), respectively. 5 mL aliquots were withdrawn at various time intervals and replaced with fresh medium to maintain the sink condition. The samples were filtered and analyzed using the HPLC method. The cumulative percentage of the released drug from each formulation was calculated. Each determination was performed in triplicate.

The release kinetics of the drug in the matrix has been widely analyzed using the Ritger–Peppas model (Ritger and Peppas, 1987). The kinetic model was used according to the following equation where M_t/M_∞ was the fraction of drug released at time t, K was the constant incorporating structural and geometrical characteristics of the dosage form, and n was the release exponent that indicated the drug release mechanism. For the Fickian diffusion from the spheres, n = 0.43, while for the anomalous transport, n was between 0.43 and 0.85, and for a case II transport (zero-order release), n = 0.85.

$$M_t/M_\infty = Kt^n$$

Development of the OXY-loaded SMEDDS

Solubility studies and construction of ternary phase diagrams

The solubility of OXY in various vehicles, including oils (Capryol 90®, Labrafac CC®, Labrafac PG®, ethyl oleate, oleic acid, soybean oil and corn oil); surfactants (Cremophor EL®, Lauroglycol 90®, Labrafil M2125 CS® and Cremophor RH40®); co-surfactants (Lauroglycol FCC®, Tween80®, Labrasol® and Plurol oleique®); and co-solvents (PG and PEG 400) was determined. The shake flask method at room temperature was used and maintained until the OXY achieved an equilibrium solubilization (72 h). The selected vehicles from solubility studies were used to construct ternary phase diagrams using SigmaPlot 11.2.0 software (Systat Software Inc., CA, USA). A series of mixtures of the oil with a single surfactant or a combination of surfactant and co-surfactant were prepared in different vials and mixed using a vortex mixer. The concentration range of each component was 10–50% oil, 25–90% surfactant and 0–25% co-surfactant. In Table 1.2, the SMEDDS system was named as systems A, B, C and D for: Cremophor EL®, Lauroglycol 90®, Labrafil M2125CS®, Cremophor RH40® based system, respectively. One gram of each mixture was dispersed in 20 mL of deionized (DI) water. The self-microemulsification performance of the SMEDDS was assessed visually according to the published visual grading system (Singh *et al.*, 2009). After identification of their self-microemulsifying regions, the SMEDDS systems were selected at their optimum component ratios for developing OXY-SMEDDS formulations.

Table 1.2 The components of different SMEDDS

Formulation Components (Formulation system code)		
Oil	Surfactants	Co-surfactants
Capryol 90®	Cremophor EL® (A)	Lauroglycol FCC® (1)
	Lauroglycol 90® (B)	Tween 80® (2)
	Labrafil M2125CS® (C)	Labrasol® (3)
	Cremophor RH® (D)	PG (4)
		PEG 400 (5)

Preparation of OXY-loaded SMEDDS

According to the ternary phase diagram studies, the Cremophor RH40®-based system (system D) was chosen. Based on the co-surfactant/co-solvent used, these systems were coded as D1, D2, D3, D4 and D5 for Lauroglycol FCC®, Tween80®, Labrasol®, PG and PEG400, respectively (Table 2). To find the optimal loading amount of OXY, varied OXY amounts were added to the D2 formulations. To study the effects of the type and amount of surfactants in the SMEDDS on the oral bioavailability of OXY, four different SMEDDS formulations were

developed. Two sets of SMEDDS containing different types of co-surfactant, Tween80® (system D2) and Labrasol® (system D3), were compared. Each co-surfactant based system was divided into two groups that included a low amount of surfactant (LS) and a high amount of surfactant (HS) group. The formulations of the LS group, contained 50% of the surfactant phase (45% Cremophor RH40® and 5% co-surfactant) and 50% Capryol 90®, were coded as LT and LL for the SMEDDS containing Tween80® and Labrasol® respectively. For the HS group, the SMEDDS formulations contained 55% of the surfactant phase (40% Cremophor RH40® and 15% co-surfactant) and 45% Capryol 90®were coded as HT and HL for the SMEDDS containing Tween80® and Labrasol® respectively. Then, the mixtures were stirred continuously until a homogenous solution was achieved (Figure1). The formulations were then left for 48 h at room temperature. The self-microemulsification performance of the OXY-SMEDDS was assessed by the visual grading system (Singh *et al.,* 2009). The 900 mg of the SMEDDS containing a fixed amount of OXY were manually filled into hard gelatin capsules size 00 and the capsule shells were sealed with gelatin solution. The filled capsules were stored in glass containers and protected from light until used. The compositions of different OXY-SMEDDS are presented in Table 1.3

Table 1.3 Compositions of the different OXY-SMEDDS formulations

Formulation code	Composition (% w/w)				OXY amount (mg/1g SMEDDS)
	Co-surfactant		Cremophor RH40®	Capryol 90®	
	Type	Amount			
LT	Tween80®	5	45	50	40
HT		15	40	45	40
LL	Labrasol®	5	45	50	40
HL		15	40	45	40

Effect of the surfactant phase on the physical properties and morphology of the developed OXY-SMEDDS

Assessment of self-microemulsification performance

The effect of the surfactant phase on the self-microemulsification performance of the OXY-SMEDDS was assessed according to the visual grading system as described previously (Singh *et al.,* 2009). In this study, the formulations were subjected to various media, for example, DI water, simulated gastric fluid (SGF, pH1.2), transport medium (TM) pH6.5 and 7.4. Three replicates of each formulation were prepared.

Microemulsion droplet size and size distribution

The effect of the surfactant phase on the droplet size and polydispersity index (PDI) of the formulations was determined after dispersion in different media. After 24 h of dilution (at a ratio

of 1:20), the OXY-microemulsions were measured by the dynamic light scattering (DLS) technique using Zetasizer Nano ZS® (Malvern Instruments, UK). Light scattering was monitored at a 173º angle at room temperature. All measurements were performed in triplicate.

Total drug content

The total drug content (TDC) in different formulations was determined as follows: each OXY-SMEDDS was diluted with DI water (20-fold dilution) at room temperature. An aliquot of 1 mL of the microemulsion was dissolved by methanol and mixed for 10 min in order to facilitate complete dissolution. Then, the obtained dispersion was analyzed for OXY by the HPLC method. The TDC could be calculated by the following equation. Where OXY_c is the TDC of the OXY calculated from the experiment and OXY_t is the theoretical drug content.

$$TDC\ (\%) = (OXY_c/OXY_f) \times 100$$

Morphology as determined by transmission electron microscopy (TEM)

The morphology of the different OXY-SMEDDS was observed by TEM (JEOL Ltd., Tokyo, Japan). The OXY-SMEDDS were diluted with DI water at a ratio of 1:20. The microemulsion was stained in 2% w/v phosphotungstic acid for 10 min. TEM micrographs of the OXY-microemulsions were photographed.

Effect of the surfactant phase of the SMEDDS on the in vitro release of OXY

The release properties of the four different OXY-loaded SMEDDS were carried out according to two different published methods (Kang *et al.*, 2004; Sermkaew *et al.*, 2013). First, one capsule filled with 900 mg of the formulation (equivalent to 36 mg OXY) was subjected to release using dissolution by the USP 30 rotating paddle apparatus (Hanson Research Corporation, USA) (Sermkaew *et al.*, 2013) with 900 mL of SGF pH1.2 without pepsin at 100 rpm and a temperature of 37.0 ± 0.5 °C. Five milliliters of aliquot were withdrawn and replaced with fresh medium at 5, 10, 15, 30, 45, 60, 90 and 120 min. For determination of the release profile of the free drug, the release studies were carried out by the dialysis bag diffusion technique (Kang *et al.*, 2004). Unlike the first method mentioned above, the OXY-SMEDDS capsules were filled into the dialysis bag (molecular weight cut off; MWCO 12–14 kDa) to stop penetration of the drug contained in the microemulsion form and allow only the free drug to be dissolved in the medium. The samples were analyzed using the validated HPLC. Three separate replicate studies were conducted for each of the formulations.

Formulation stability

The stability tests of the SMEDDS were evaluated according to the ICH guidelines on the topic of Q1A (R2): stability testing of new drug substances and products. The hard gelatin capsules

containing liquid OXY-SMEDDS were stored in air-tight glass containers and protected from light. The samples were maintained in a stability chamber (Patron AH-80, Taiwan) under intermediate conditions [30 ± 2°C, 65 ± 5% relative humidity (RH)], and a stability chamber (Memmert® HPP 260, USA) under accelerated conditions [45 ± 2°C, 75 ± 5% RH]. Meanwhile, the stability of the two lipid nanoparticles (SLN and NLC) was studied at 4 ± 2 °C in a refrigerator. The samples were taken at 0, 1, 3, 6, 12 months. Appearance, mean size, size distribution (PDI) and TC were determined at each time point for all the developed formulations. Moreover, the self-microemulsifying properties of OXY-SMEDDS were additionally evaluated.

Quantification of OXY

The quantitative determination of OXY was performed using an Agilent HPLC system (HP 1100, Agilent, USA) with a C18 column (VertiSep™ pHendure 4.6 x 250mm, 5-µm, Ligand Scientific, Bangkok, Thailand), and a UV detector set at the wavelength of 320nm. Chromatographic conditions: the eluent was an isocratic solvent system at ambient temperature with a flow rate and injection volume of 1.0mL/min and 20 µL, respectively. The mobile phase consisted of acetonitrile and 0.5% v/v aqueous acetic acid in the ratio of 27:73 v/v. The retention time of OXY was about 7 min. The calibration curve for OXY was constructed by plotting the concentrations *versus* the corresponding mean peak areas that were calculated from three determinations**.** A good linearity was achieved with a correlation coefficient (r^2) of 0.9994 over the concentration range of 0.2-10 µg/mL. The intra-day precision was obtained by three repeated injections of each concentration of samples that showed the percent relative standard deviation (% RSD) of 0.14 to 0.86. The inter-day precision of the method gave a %RSD that ranged from 0.45 to 1.26. The recovery percentage of the method was between 95.50 ± 4.40 and 101.87 ± 1.61.

Caco-2 transport studies of OXY

Caco-2 cells culture experiment

The Caco-2 cell line (HTB-37, ATCC, Virginia, USA), derived from a human colorectal adenocarcinoma, were grown in Modified Eagle's Medium (MEM, Gibco®, USA) supplemented with 20% (v/v) fetal bovine serum and 1% (v/v) of penicillin (100 IU/mL)-streptomycin (100 mg/mL) (Gibco®, USA). The cells were maintained at 37 °C in a fully humidified atmosphere with 5% CO_2 in air, and passaged every 2-3 daysuntil, they reached an80-100 % confluency of a cell monolayer. The cells were then released from the culture flasks using a 0.25% trypsin-EDTA solution (Gibco®, Canada). Viable cell numbers were then determined prior to use by live-cell staining using 0.4% trypan blue and by counting viable cells with a standard haemocytometer.

Cytotoxicity test by MTT assay

As damage of the intestinal epithelium sometimes affects the intestinal permeability of the samples hence cell viability was assessed by the standard MTT test (Freshney, 2005) to optimize the non-toxic concentrations of the samples prior to the transport study. The stock solution of OXY

in DMSO (Amresco®, USA) was prepared and then diluted with transport medium (HBSS-HEPES) pH 7.4 to obtain OXY concentrations that ranged from of 0-800 µM. After evaluating the most suitable concentration range for the OXY, the OXY-formulations including SLN, NLC, and SMEDDS, were evaluated by comparison with blank formulations and unformulated OXY. The samples were diluted with the HBSS-HEPES medium to obtain equivalent concentrations of OXY of 25-400 µM for the lipid nanoparticles (SLN and NLC) and 25-200 µM for the SMEDDS. Briefly, the Caco-2 cells were seeded in 96-well cell culture plates at a density of 5×10^4 cells/well. After overnight incubation, the culture medium was removed, and the cells were washed with 100 µL of PBS pH 7.4. 100 µL of the samples were added to each well. 1 % sodium lauryl sulfate (SDS) and HBSS-HEPES medium were used as a negative control and positive control, respectively. After 24 h treatment, the samples were removed and the cells were washed with PBS pH 7.4. The cells were added with 50 µL of 0.5 mg/ml MTT solution and then incubated for 4h. After removing the MTT solution carefully, the formazan crystals formed by the viable cells were dissolved by adding DMSO. Duplicates were performed for each sample. The absorbance was measured at 570 nm by the microplate reader (DTX 880 Multimode Detector, Beckman Coulter Inc., Austria). The positive control (HBSS-HEPES medium) was presented as the 100% cell viability control. The percentage cell viability of the samples was calculated relative to the measured absorbance of the positive control. The ABS_{sample} and $ABS_{control}$ represented the measured absorbance of the sample and the positive control, respectively.

$$\% \text{ Cell viability} = (ABS_{sample}/ABS_{control}) \times 100$$

Preparation of the samples

The samples (OXY solution in DMSO and each OXY-formulation) were diluted with transport medium pH 6.5 and pH 7.4 for apical (AP) side loading and basolateral (BL) side loading, respectively, to obtain the desired concentration of OXY. The transport medium was composed of HBSS containing 20 mM of MES or HEPES and adjusted to pH 6.5 (for apical compartment) and pH 7.4 (for basolateral compartment) by 1N HCl or 1N KOH.

Caco-2 transport study of the samples

A caco-2 cell permeability study, commonly used as an *in vitro* method to predict *in vivo* absorption of the compound, was performed to help to predict the ability to transport different SMEDDS formulations of OXY across the intestinal epithelium (Yee, 1997). The *in vitro* permeability studies of each OXY-formulation were carried out according to a previous report (Sermkaew *et al.*, 2013). The Caco-2 cells (passage number 25-29) were used in this study. The cells were seeded on Transwell® 6-well plates (Costar®, USA) at a density of 60,000 cells per cm^2 of Transwell® insert (area: 4.67 cm^2, Corning®, USA), and cultured until the cells had completely

differentiation (about 21-23 days). The culture medium was changed every two days for both the donor compartment and the receiver compartment. Before the transport study, the transepithelial electrical resistance (TEER) value was measured using a Millicell®-ERS Voltmeter (Millipore Corp., Bedford, MA, USA) to evaluate the integrity of the cell monolayer. The caco-2 cell monolayers with an average TEER values > 300 Ωcm^2 indicated the cells were intact that were used in this study.

In the bidirectional experiment, the absorptive transport (AP-BL) experiment and the secretive transport (BL-AP) experiment the effectiveness of the formulations to inhibit the active efflux transporter(s) of the monolayer were determined. For the absorptive transport experiment, 1.5 mL of samples in HBSS/MES medium pH 6.5 and 2.6 mL of HBSS/HEPES medium pH 7.4 were added to the apical side (donor compartment) and the basolateral side (receiver compartment), respectively. For the secretive transport (BL→AP) experiments, 2.6 mL of samples in HBSS/HEPES medium pH 7.4 and a 1.5 mL of blank HBSS/MES medium pH 6.5 were added to the basolateral side (donor compartment) and the apical side (receiver compartment), respectively. The transport studies were performed on a shaking incubator (HandyLAB® system, N-BIOTEK Co., Ltd, Korea) maintained at 37±0.5 ºC with a shaking rate of 100 rpm. At various times, sample volumes of 400 µL and 100 µL were removed from the receiver compartment and donor compartment, respectively, in the bidirectional experiments. Meanwhile, the volumes withdrawn from the receiver compartment in both experiments were immediately replaced with warmed fresh transport medium at various times (5, 15, 30, 45, 60, 90, 120, 150 and 180 min). To determine the accumulation of the drug in the Caco-2 cells, the cells were washed with PBS pH 7.4 and then scrapped from the insert filters at the end of experiments. After that, the cells were lysed and centrifuged to collect the supernatant. The amounts of OXY were quantified by the validated HPLC method. The amount of the cumulative drug that permeated through the Caco-2 monolayer as measured in the receiver compartment was plotted against the sampling time to obtain a linear slope. Then, the apparent permeability coefficient (*P*app) and the efflux ratio (ER) (Hubatsch *et al.*, 2007) were calculated following equations and compared between each of the formulations.

$$P\text{app} = (dQ/dt)/ (AC_0)$$

Where dQ/dt is the cumulative transport rate (µg/s) defined as the slope obtained by linear regression of the cumulative transported amount (µg) as a function of time (s). A is the surface area of the filter (4.67 cm^2 in 6-wells insert). C_0 is the initial concentration of OXY on the donor compartment (µg/mL).

$$ER = P\text{app(BL-AP)}/ P\text{app(AP-BL)}$$

Where *P*app (AP-BL) is the apparent permeability coefficient for the absorptive transport and *P*app (BL-AP) is the apparent permeability coefficient for the secretory transport.

Quantitative determination of OXY in cell culture experiment

The quantitative determination of OXY in the transport medium was by the HPLC method using resveratrol (RES) as an internal standard. The system consisted of an Agilent HPLC system (HP 1100, Agilent, USA) with a UV detector set at 320 nm. A reverse phase column: a Vertisep pHendure C18 4.6 x 250 mm, 5 µm column and guard column (Ligand Scientific, Bangkok, Thailand) were used. Chromatographic conditions: the isocratic solvent system consisted of acetonitrile and 0.5% v/v aqueous acetic acid (27:73 v/v) with a flow rate of 1.0 mL/min and an injection volume of 50 µL. The OXY and RES exhibited a well-defined chromatographic peak with a retention time of about 7 and 12 min, respectively (data not shown). The calibration curve for OXY was constructed by plotting concentrations *versus* the ratios of the peak areas of OXY and RES from three determinations. A good linearity was achieved with a correlation coefficient (r^2) of 0.9999 over the concentration range of 0.1-10 µg/mL. The intra-day and inter-day precision studies were obtained by three daily injections for each concentration of the spiked medium samples over a 3 day period. The intra-day precision gave the percentage relative standard deviations (%RSD) of 0.97%-2.90%, whereas the %RSD of inter-day precisions ranged from 7.67% to 12.55%, respectively. The recovery percentage of the method ranged from 90.18±2.38-102.46±3.99. The limit of detection (LOD) and the lower limit of quantification (LLOQ) was 0.01 and 0.1 µg/mL respectively. The results of the validation of the *in vitro* HPLC method showed that the determination of OXY could be performed by this validated HPLC method with an acceptable accuracy and precision.

In vivo absorption studies

Male Wistar-strain rats (250-300 g) were provided by the Animal House, Faculty of Science, Prince of Songkla University. All animals received human care and laboratory experiments were approved according to the guidelines of the Animal Care and Use Committee of Prince of Songkla University (MOE 0521.11/063). They were housed and maintained under standard rodent conditions (at 24 °C, 55% RH, 12 h light-dark cycle controls). The rats had unlimited access to water but were excluded from food for 12 h before the experiment. Each group was administered orally with the OXY aqueous suspension (control group) or OXY formulated as SLN, NLC, SMEDDS, at an equivalent OXY dose of 180 mg/kg body weight (Huang *et al.*, 2008; Sangsen *et al.*, 2015). Blood samples (250 µL) were collected via the rat tail clipping method (Clark et al., 1991) at various times (5, 10, 15, 20, 30, 45, 60, 90, 120, 180, 240, 360, 480, and 600 min) after oral dosing, into heparinized centrifuge tubes. The samples were centrifuged at 13,000 rpm 20 °C

for 5 min and the plasma samples were selected for assay. The internal standard (RES) was spiked into the plasma. Then, an equal volume of acetronitrile (1:1 v/v) was added to the plasma sample, vortexed, sonicated and allowed to stand for 5 min to precipitate the protein. The samples were centrifuged at 13,000 rpm 20 °C for 5 min. The supernatant was filtered and injected to the validated HPLC analysis. Data from these samples (n=7) were used to plot the profiles of the OXY absorption with time.

Pharmacokinetic parameters

The main pharmacokinetic parameters of the unformulated OXY and OXY in different lipid formulations were carried out using the Microsoft Excel 2007 Software (Microsoft Corporation, USA). The maximum concentration (C_{max}) and time to reach maximum concentration (T_{max}) were obtained directly from the plasma concentration-time curves. The area under the concentration-time curve ($AUC_{0\text{-}10h}$) was determined using the trapezoidal rule. The relative bioavailability over 10 h ($F_{r,\ 0\text{-}10h}$) at the same dose of OXY formulated as lipid formulations compared to the OXY suspension, was calculated as:

$$F_{\mathrm{r},0-10\mathrm{h}} = \frac{\mathrm{AUC}_{(0-10\mathrm{h})\mathrm{oral,formulation}}}{\mathrm{AUC}_{(0-10\mathrm{h})\mathrm{oral,suspension}}} x\ 100$$

HPLC analysis of plasma samples

For the determination of the quantity of OXY absorbed *in vivo*, the same HPLC system as that for the *in vitro* studies was used. The spiking technique was used for validation of the HPLC method. The internal standard method was used for analysis of OXY in the plasma samples. The retention time of OXY and resveratrol (an internal standard), were approximately 7 and 12 min, respectively. The calibration curve for OXY was constructed by plotting concentrations *versus* the average peak area ratio of OXY to the internal standard, calculated from three determinations. A linear relationship was demonstrated with a correlation coefficient (r^2) of 0.9994 over the concentration range of 0.2-10 µg/mL of OXY. The intra-day and inter-day precisions were obtained by three daily injections per each concentration of these spiked plasma samples over a 3 day period. The intra-day repeatability gave relative standard deviations (%RSD) of 1.00% - 2.32%, whereas the % RSD of the inter-day precision ranged from 2.23% to 10.26%, respectively. The recovery percentage of the method ranged from 88.96 ± 2.20 to 100.02 ± 2.34. The limit of detection (LOD) and the lower limit of determination (LLOQ) was 0.02 and 0.1 µg/mL respectively.

Statistical analysis

Data were expressed as mean values ± SD. Statistical comparisons were performed by one-way ANOVA using Graphpad Prism® software (Graphpad software Inc.). Statistical probability (*p*)

values of less than 0.05 were considered to be significantly different. *In vitro* study and cell culture experiments were performed in triplicate, while *in vivo* studies were evaluated in seven replicates.

3. Results and Discussion

Development of OXY-loaded lipid nanoparticles including SLN and NLC

Preparation and optimization of OXY-loaded SLN

The hot high speed homogenization method was used to produce lipid nanoparticles due to it being simple and quick for laboratory production. The good characteristics of SLN which were nano-sized (< 200 nm), had a narrow size distribution (PDI~0.2-0.4), high entrapment efficacy, high loading capacity and sustained release properties were optimized. Thus, many factors influenced on these properties were investigated. The speed rate of 24,000 rpm and a time of 15 min which produced homogeneous suspension were selected as the standard homogenization step for all tested formulations. Using the optimized conditions, the effects of formulation compositions on physicochemical properties of developed SLN were also determined. For the proportions of solid lipid, the formulation containing a highest weight proportion of solid lipid (5% w/w) provided the acceptance particle sizes and size distribution. For the types of the solid lipid, glyceryl monostearate (GMS) were compared to the glyceryl behenate (Com888). After incorporation of OXY, the Com888-based showed better properties than GMS-based. The Com888 was thus chosen as the solid lipid matrix in this study. This related to its having an amphiphilic characteristic with a high chemical stability that resulted in a good ability to encapsulate a lipophilic and/or hydrophilic drug (Kipp, 2004). In addition, a larger size and a greater PDI of the nanoparticles was obtained by increasing the incorporated OXY in the SLN formulations. This result was due to an insufficient amount of the lipid to encapsulate the drug. Therefore, the 0.3% w/w of OXY was the optimum OXY loaded in the SLN formulation. Soy lecithin, selected as a co-surfactant, was an important factor for drug-loaded SLNs (Luo *et al.*, 2006; Hu *et al.*, 2010). In this study, the soy lecithin (HLB of 5) was added to the system to adjust the HLB of other surfactants so as to enhance the ability to emulsify the lipid and stabilize the system. Seven different types of surfactant at the equal concentration were used to form the OXY-SLNs. The formulations, S1, S2, and S5 containing poloxamer® 188 (P188; HLB of 29), Tween80® (HLB of 15), and 1:1 of P188:Tween80®, respectively, had a good appearance and did not flocculate. The mean particle sizes obtained from these formulations was < 200 nm and they also had a narrow size distribution (PDI 0.22-0.27). On the basis of similar total drug content (about 100% TDC), the entrapment efficiency of the S1, S2, and S5 formulations was satisfactorily high. The non-toxic and non-ionic P188 and Tween80® have been used as surfactants for the Com888-based formulations due to their compatibility.

In order to develop a controlled release system, the conventional dialysis bag diffusion technique is widely used for measuring the release of drugs from colloidal solutions. The OXY suspension

presented a cumulative release of OXY of 30% within 4 h in the SGF pH 1.2 and 80% within 48 h in the SIF pH 6.8, respectively. Meanwhile, the release curves of the three SLN formulations (S1, S2, S5) showed no initial burst release and slowed down considerably in both media. From the experimental data, the slowest release rate of S2 formulated using Tween80® was observed during the study times. The retarded release profile could be explained by the retardant property of Com888 for a sustained release dosage form and the stronger solubilization of P188 compared to Tween80 (Souto *et al.*, 2006; Wu and Lee, 2009; Hu *et al.*, 2010). Moreover, the S2 exhibited the highest %EE and %LC of 90.55 ± 0.28% and 5.54 ± 0.02% among the three SLN formulations. From all data, the S2 formulation comprising 5% w/w Compritol® 888 ATO with Tween80® (3.75 %) combined with soy lecithin (1.875 %) had an ability to entrap the 0.3% w/w OXY (Table 1.4). Based on these finding, the formulation S2 was judged to be the optimum SLN formulation, and will be utilized as the starting formulation for further NLC production.

Table 1.4 Summary of homogenization conditions, compositions and properties of the optimum S2 formulation

Formulation	Homogenization conditions		Compositions (% w/w)			Physicochemical properties					
	Speed (rpm)	Time (min)	Solid lipid (5%)	Surfactant (3.75%)	Co-surfactant (1.875%)	Appearance	PS (nm)	PDI	TDC (%)	EE (%)	LC (%)
S2	24,000	15	C888	Tween80®	Soy lecithin	Milky suspension	134.40 ±0.57	0.25 ±0.00	102.05 ±1.97	90.55 ±0.28	5.54 ±0.02

Preparation and formulations of OXY-loaded NLC

The NLC were prepared by hot/high speed homogenization method using a high speed homogenizer 18G-25N (ULTRA-TURRAX®, IKA®, Germany). According to SLN production, the NLC were formulated by taking the SLN compositions as the starting formulation and differently lipid phase consisted of varied ratios of Com888 and liquid lipid (Labrafac CC; Lab CC) including 4:1 (NLC1), 3:2 (NLC2) and 2.5:2.5 (NLC3). The same concentration of OXY (0.3% w/w) was added in each formulation. The result revealed that the Com888 and Lab CC of the three NLC formulations exhibited good miscibility in the nanoparticulate state.

Both blank formulation and SLN containing drug had a well milky appearance with low viscosity and non-flocculation (Figure 1.2). The small particle sizes (< 110 nm) with a uniform size distribution and high ZP values (about -50 mV) were obtained. This indicated that the incorporated OXY did not change the physical properties of the SLN. In case of NLC, all the blank NLC and the OXY-NLC presented similarly a high ZP of above -30 mV. Compared with the SLN, the PS of NLC in all formulations was significantly smaller than those of the SLN ($p < 0.05$) (Table 1.5). Therefore, addition of the Lab CC oil to the system did affect the particle sizes due to reducing the melting point of the solid lipid and allowing a rapid distribution of the heat energy by liquid oils in the emulsification process (Zhuang *et al.*, 2010).

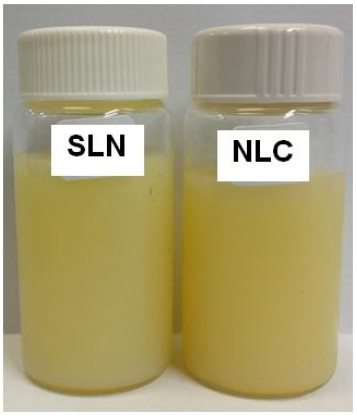

Figure 1.2 Picture of the appearance of OXY-loaded lipid nanoparticles (SLN and NLC3)

All the developed SLN and NLC had 100% (w/w) of the incorporated OXY in the formulations indicating no drug loss occurred during the preparation process. After preparation (0 month), the %EE of the NLC including NLC1 and NLC3 was significantly higher than for the SLN ($p < 0.05$) while, no significant difference of LC of the SLN and NLC (~5% w/w, of solid lipid) ($p > 0.05$). Thus, the NLC1 and NLC3 were selected to evaluate in the next step compared to the SLN.

Table 1.5 Physicochemical characteristics and stability data at 4 ± 2°C of the blank formulations, OXY-SLN and OXY-NLC

Code	PS (nm) ± SD	PDI ± SD	ZP (mV) ± SD	TC (%)	EE (%)	LC (%)
0 month						
Blank SLN	97.7 ± 0.1	0.302 ± 0.003	-52.7 ± 1.2			
Blank NLC1	98.2 ± 0.5	0.302 ± 0.003	-49.8 ± 0.6			
Blank NLC2	97.9 ± 0.7	0.278 ± 0.011	-45.6 ± 0.1			
Blank NLC3	90.7 ± 0.4	0.278 ± 0.009	-41.7 ± 2.4			
SLN	107.5 ± 0.3	0.245 ± 0.004	-51.1 ± 1.0	100.7 ± 0.9	85.5 ± 0.8	5.2 ± 0.1
NLC1	99.3 ± 0.2	0.246 ± 0.005	-45.5 ± 0.6	101.3 ± 0.3	87.7 ± 0.4	5.3 ± 0.1
NLC2	99.8 ± 0.1	0.231 ± 0.006	-46.4 ± 0.4	102.1 ± 1.7	83.5 ± 1.1	5.1 ± 0.1
NLC3	96.0 ± 0.9	0.259 ± 0.006	-42.3 ± 0.9	101.1 ± 3.6	88.5 ± 0.1	5.4 ± 0.4
3 months						
SLN	111.0 ± 0.9	0.243 ± 0.012	-38.3 ± 1.1	102.9 ± 4.8	83.7 ± 0.1	5.2 ± 0.1
NLC1	101.8 ± 0.4	0.244 ± 0.001	-38.4 ± 1.3	99.7 ± 1.9	83.7 ± 0.5	5.0 ± 0.1
NLC3	97.6 ± 1.3	0.249 ± 0.008	-33.2 ± 2.2	101.7 ± 3.8	87.8 ± 0.3	5.2 ± 0.1
6 months						
SLN	122.4 ± 1.0	0.249 ± 0.010	-34.9 ± 1.0	97.7 ± 6.2	84.0 ± 0.5	5.1 ± 0.1
NLC1	101.9 ± 0.6	0.272 ± 0.003	-39.8 ± 0.3	96.0 ± 7.4	84.7 ± 0.5	5.1 ± 0.1
NLC3	97.4 ± 0.8	0.251 ± 0.009	-41.5 ± 2.6	103.2 ± 1.1	87.7 ± 0.2	5.4 ± 0.1
9 months						
SLN	122.4 ± 1.3	0.259 ± 0.003	-30.0 ± 2.2	102.2 ± 1.3	83.2 ± 0.2	4.9 ± 0.1
NLC1	102.0 ± 1.3	0.256 ± 0.004	-37.4 ± 1.1	100.3 ± 2.7	84.3± 0.5	5.1 ± 0.0
NLC3	97.84 ± 0.5	0.278 ± 0.014	-39.5 ± 2.8	101.3 ± 1.0	84.7±0.1	5.2 ± 0.1
12 months						
SLN	159.2 ± 0.6	0.259 ± 0.015	-27.7 ± 0.5	98.4 ± 2.1	78.0± 0.3	4.6 ± 0.0
NLC1	104.2 ± 0.4	0.229 ± 0.005	-37.0 ± 1.6	103.0 ± 3.7	83.0 ± 0.0	5.0 ± 0.0
NLC3	106.2 ± 0.5	0.295 ± 0.005	-41.0 ± 0.4	100.7 ± 0.5	84.5 ± 0.3	5.1 ± 0.0

The observation by TEM, both the NLC formulations had spherical uniform shapes with smooth surfaces, and did not aggregate. The mean diameter of the SLN and NLC containing the OXY from the TEM was in agreement with the results obtained by the PCS. Meanwhile, the morphology of SLN changed from spheres at 0 month (Figure 1.3A) to two-layered particles with irregular surfaces (Figure 1.3B) after storage for 3 months. These results indicated less stability of SLN than NLC (Üner, 2006).

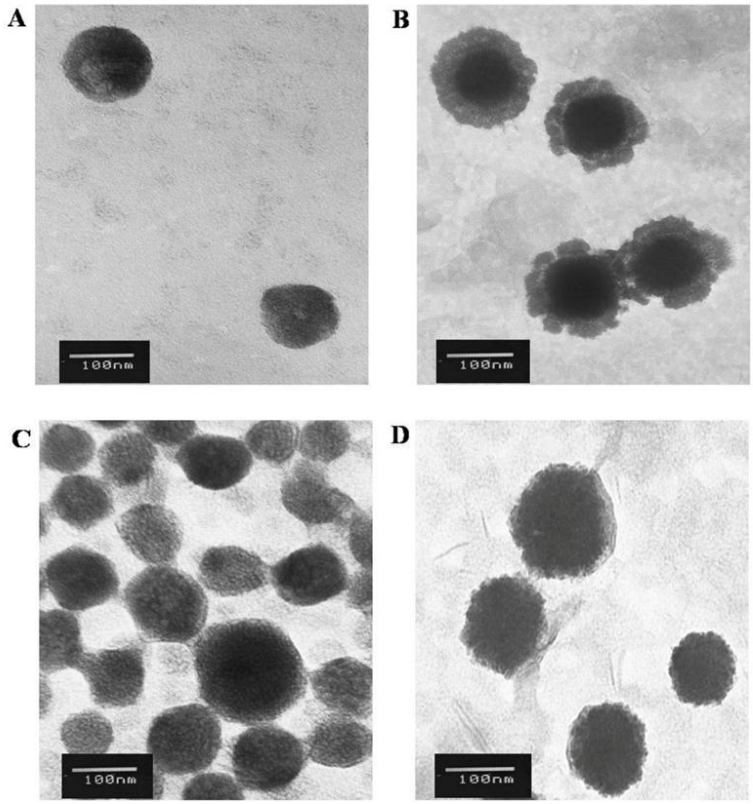

Figure 1.3 TEM images at ×100 K of SLN (A) at 0 month; SLN (B), NLC1 (C), and NLC3 (D) after 3-months storage.

For the DSC thermogram of physical mixture, the melting peak appeared at 109 °C and 71 °C representing the peaks of the OXY and Com888. The loss of the endothermic peak of OXY in the developed SLN and NLC indicated that the OXY in the lipid phase was in an amorphous state and formed a solid solution within the matrix of nanoparticles (Figure 1.4). The results related to the oil in the NLC systems that depressed the melting point of the lipid matrix in a concentration-dependent manner (Jenning *et al.*, 2000; Gokce *et al.*, 2012). This confirmed that NLC had a less ordered crystalline structure than SLN. The physical state of such systems was confirmed by the PXRD (Figure 1.5). The PXRD diagram of the physical mixture showed two characteristic wide peaks of C888 and a peak intensity of pure OXY. It indicated that the bulk matrix (Com888) and OXY were crystalline. In contrast, there was no characteristic peak of crystalline OXY observed in

the patterns of the three formulations indicating the molecular dispersion in an amorphous state of the incorporated OXY.

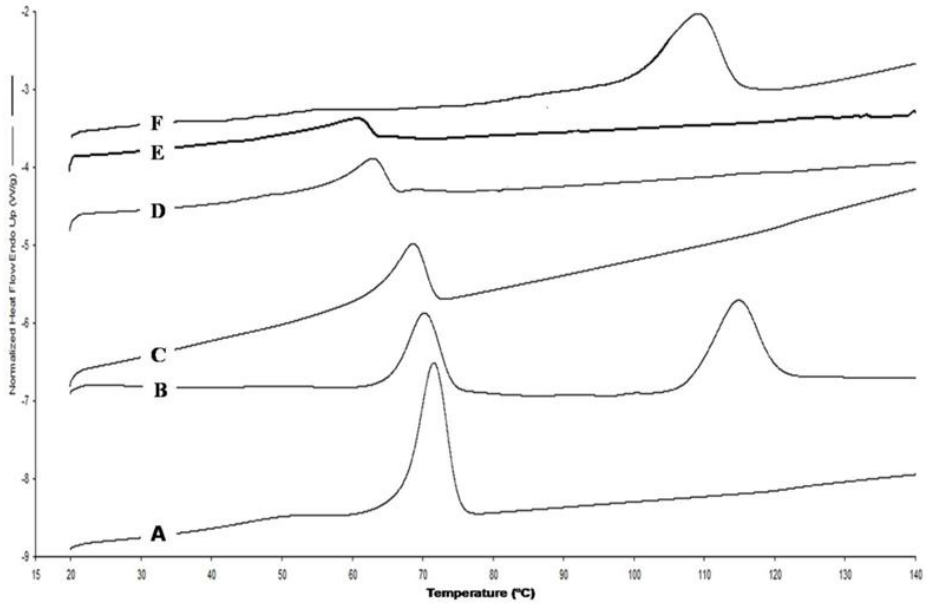

Figure 1.4 DSC thermograms of OXY (A); freeze dried powders of NLC3 (B); NLC1 (C); SLN (D); physical mixtures of Com888 and OXY (E); and C888 (F).

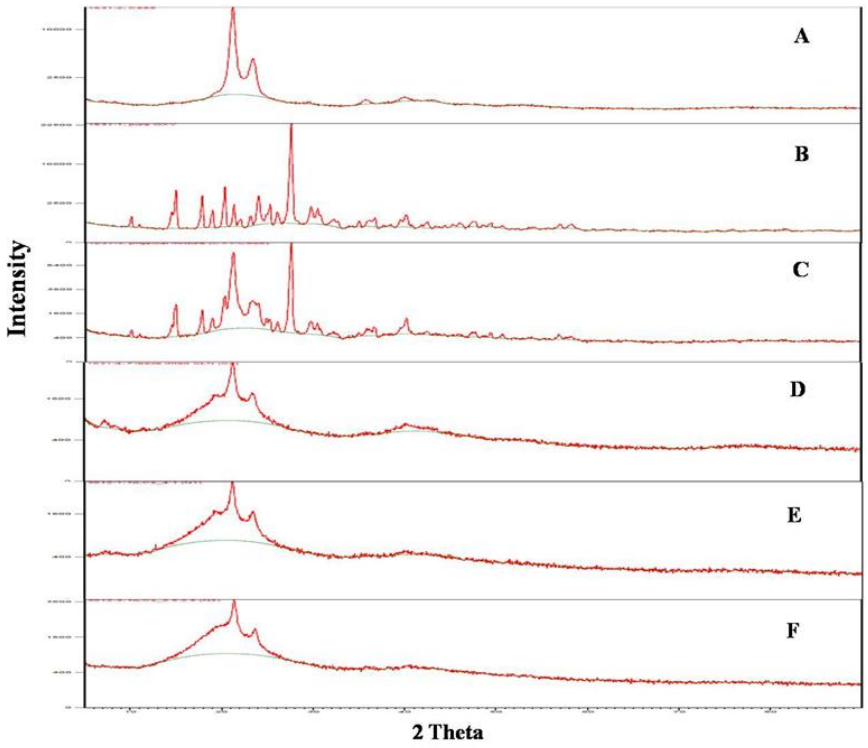

Figure 1.5 Powder X-ray images of Com888 (A); OXY (B); physical mixtures of Com888 and OXY (C), and freeze dried powders of SLN (D); NLC1 (E) and NLC3 (F).

From *in vitro* release data, the OXY suspension tended to release a high amount of OXY in both medium. On the other hand, the release of OXY from the SLN and NLC formulations slowed down considerably in the SGF pH1.2 and exhibited a sustained release up to 48 h in the SIF pH 6.8. Comparing each of the SLN and NLC formulations at pH 6.8, the slowest OXY release profile was observed in the NLC1 (Figure 1.6). The results indicated that the release rate of OXY might depend on the crystallinity of the lipid matrix. These results demonstrated that the OXY entrapped in SLN and NLC was protected from the strong acidic environment of the stomach and therefore subsequently reached the small intestinal. Moreover, the OXY release data from all developed SLN and NLC were best fitted to a Ritger-Peppas kinetic model as the R^2 was close to 1. Based on the model, the n values of the SLN and NLC were in the range of $0.43 < n < 0.85$ indicating that the release from the lipid nanoparticles contributing to a combination of drug diffusion and erosion from the lipid matrix. Furthermore, the n values of the three formulations (SLN, NLC1, and NLC3) were close to 0.85 indicated that the erosion was the predominant release mechanism. So that the major amount of drug was enriched in the matrix of the nanoparticles and only small drug amount in the shell can diffuse into the medium.

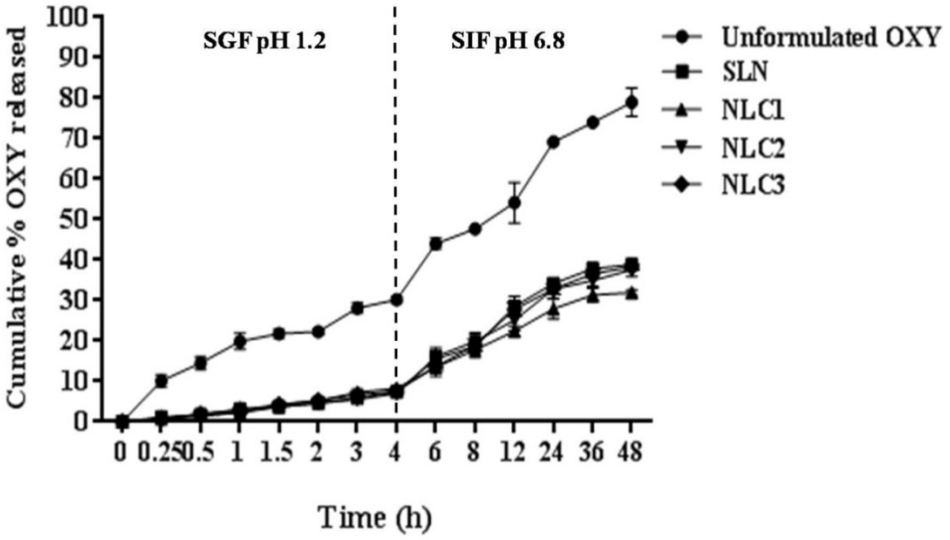

Figure 1.6 *In vitro* OXY release profiles of SLN and NLC formulations with different lipid to oil ratios (NLC1, NLC2, NLC3) compared with the unformulated OXY in SGF (pH1.2) and SIF (pH 6.8). Data represents the mean ± SD (n = 3).

There were no changes in the appearance and PDI up to 12 months for the OXY-SLN and OXY-NLC under storage conditions (4 ± 2◦C). The increase of PS and reduction of the ZP was remarkably observed during storage conditions for the SLN (Table 1.5). Meanwhile, the ZP of the NLC formulations remained in the high negative values (above 30 mV). Furthermore, the %EE and %LC of both the NLC were significantly higher than those of the SLN after 12 months of storage

($p < 0.05$). These results demonstrate the reduced stability of the SLN compared to the NLC which also agrees with the TEM analysis. Therefore, the NLC3 was selected to compare with the SLN in further *in vitro* permeability, and *in vivo* absorption studies to ensure it was a potential carrier for the oral delivery of OXY.

To obtain an optimal OXY concentration for the permeability study, the non-toxic concentration of solubilized OXY determined by MTT assay was not more than 400 µM. Similar to the lipid nanoparticle system, either blank formulations or formulations containing drug were compatible to the cells up to 400 µM of OXY (Figure 1.7). At 400 µM of OXY, the efflux ratio (ER) of the unformulated OXY was found 2.55 indicating a substrate for the efflux transporters of OXY. Moreover, the SLN and NLC reduced 2.8 folds and 3.3 folds, respectively, in the secretory permeability of OXY, whereas only enhanced absorptive permeability of NLC compared to those of unformulated OXY (Figure 1.8). Thus, the lipid nanoparticles system was significantly alleviated efflux transport of OXY with ER (≤ 1) of 0.59 and 1.01 for NLC and SLN, respectively.

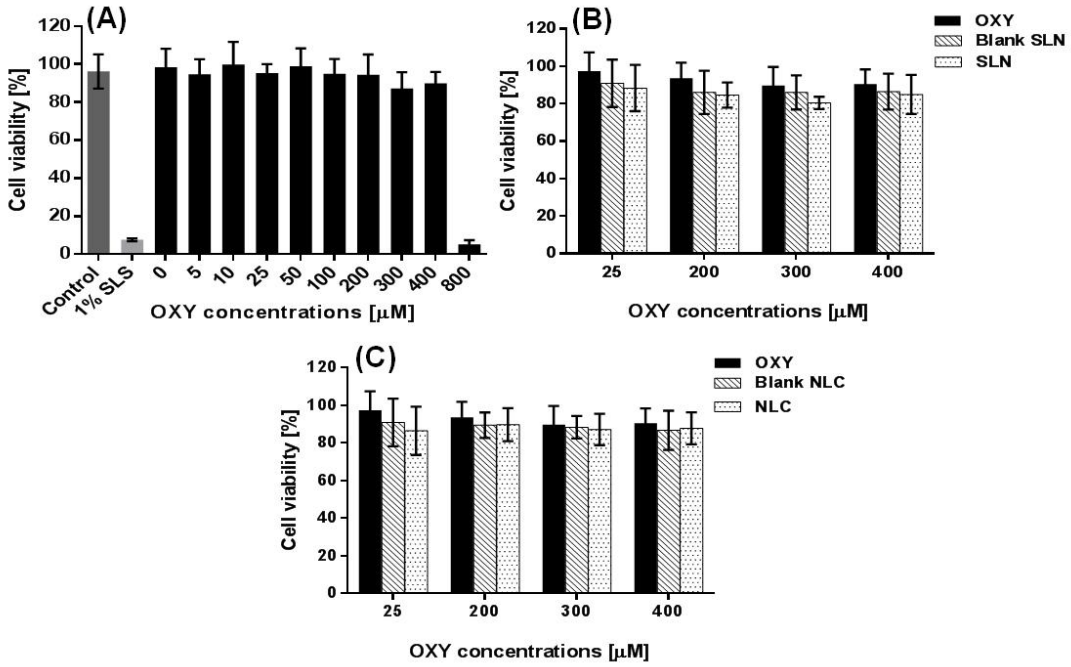

Figure 1.7 The percentage of Caco-2 cell viability to different concentrations of OXY (A), blank formulations and OXY-formulations of SLN (A) and NLC (B) (n = 8), duplications.

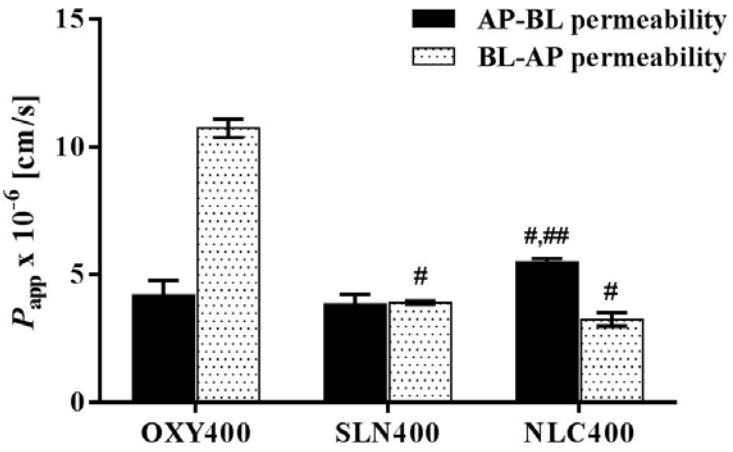

Figure 1.8 Bidirectional transport across the Caco-2 monolayers of OXY and developed OXY-formulations. The data are presented as the apparent permeability coefficient (*P*app) in the absorptive (AP-BL) and the secretory directions (BL-AP). $^{\#}p < 0.05$, comparison with OXY400; $^{\#\#}p < 0.05$, comparison with SLN400.

The pharmacokinetic parameters in rats after oral administration of OXY in either the aqueous suspension or SLN or NLC at an equimolar dose are summarized in Figure 1.8 and Table 1.6. In comparison to the OXY suspension, the *C*max of OXY administered as SLN was significantly decreased, while those from the NLC only slightly decreased. This data was consistent with the *in vitro* dissolution data. A greater AUC_{0-10} h ($p < 0.05$) was obtained from the NLC (177%) and the SLN (125%), than from the unformulated OXY (100%) and indicated that there was a significantly improved systemic exposure to OXY. The *in vivo* results were in agreement with the *in vitro* permeability data. Possible mechanisms for improving the OXY bioavailability from NLC over SLN after oral administration have been speculated. Firstly, the significantly smaller particle sizes of the NLC ($p < 0.05$) occupied a larger surface area than larger particles (i.e. SLN), a higher dispersibility, and prolonged residence time to adhere at the absorptive site of the intestinal epithelium (How *et al.*, 2011). Secondly, the Lab CC oil used in the NLC had a greater solubilization capability for drugs (Pouton and Porter, 2008). Furthermore, the oil itself had a permeation enhancing property which improved oral drug absorption by many of ways, for example, mucoadhesive properties of the vehicle and altering epithelial absorption (Lundin *et al.*, 1997). Furthermore, the medium chain triglyceride (MCT) oil and lipid were structurally similar to the fat in daily food. They could entrap the polar OXY and stimulate bile secretion, and thus enhance the uptake of intact particles by the gut wall and promote its draining into the lymphatic system. The absorption via the lymphatic system would also minimize rapid elimination of OXY. Finally, the sustained OXY release in the systemic circulation would achieve a longer availability of the drug in the body (Souto and Müller, 2010; Zhuang *et al.*, 2010; Tiwari and Pathak, 2011).

Moreover, the surfactant used in the formulation might enhance intestinal permeability by several means i.e. inhibiting the efflux transporters of P-gp, the MRPs family (Lo *et al.*, 2003; Shono *et al.*, 2004; How *et al.*, 2011). Furthermore, NLC entrapment could bypass the extensive first pass metabolism. Hence NLC is a promising carrier for improvements to the oral bioavailability of OXY. It was of interest that the multiple peaks of the plasma concentration of OXY observed in all the formulation tested would suggest enterohepatic recycling (EHC) of the absorbed OXY. Nevertheless, the time for the second mean peak (45 min) noted for each profile of formulation tested was the same (Figure 1.9). The consistency of the observation implied the altered absorption process of OXY, while disposition process could be minimally affected by the lipid nanoparticles.

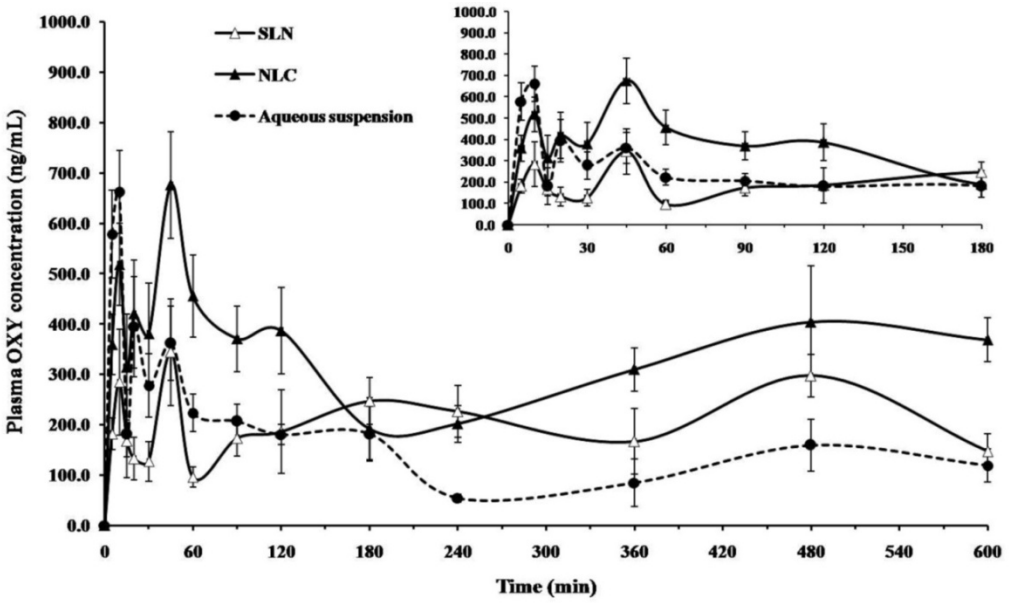

Figure 1.9 Plasma concentrations of OXY vs. time profiles after oral administration of OXY formulated as SLN and NLC, compared with the unformulated OXY (180 mg/kg of OXY). Data represents the mean ± SD (n = 7).

Table 1.6 Pharmacokinetics data of OXY after oral administration of different formulations including SLN, NLC and an aqueous suspension of OXY (equivalent to 180 mg/kg of OXY).

Parameters	OXY aqueous suspension	SLN	NLC
*C*max (µg/mL)	0.66±0.08	0.28±0.11*	0.52±0.08$^{*,\#}$
*T*max (min)	10	10	10
$AUC_{0\text{-}10h}$ (ng h/mL)	1,897.34±220.13	2,369.91±268.84*	3,365.78±64.94$^{*,\#}$
$F_{r,\,0\text{-}10h}$ (%)	100	125	177

$^{*}p < 0.05$, comparison with aqueous suspension; $^{\#}p < 0.05$, comparison with SLN

Development of OXY-loaded SMEDDS

In the self-microemulsifying system, the solubility of OXY in various vehicles was firstly determined to select the excipients for construction of ternary phase diagrams. In this study, all the selected excipients exhibited higher solubilization capacities for OXY than OXY solubility in water (0.993 ± 0.012 mg/mL) at room temperature. Capryol 90® was used as the oily phase with highest solubility for OXY (115.420 ± 4.475 mg/ml) and Cremophor RH40® was selected as the main surfactant. Based on co-surfactant, the ternary phase diagrams of the Tween80®-(D2) and Labrasol®-(D3) based systems, provided large self-microemulsion region (Figure 1.10). A fixed amount of OXY (40 mg/1g SMEDDS) was added into each system to find the most suitable surfactant concentration. The results demonstrated that only concentrations of Cremophor RH40® (40-45%) and co-surfactants (5-15%) in the formulations produced transparent microemulsions and no drug precipitation after 24 h. Therefore, two different concentration groups including a low (LS; 5% co-surfactant + 45% Cremophor RH40®) and high surfactant phase (HS; 15% co-surfactant + 40% Cremophor RH40®) of both types of SMEDDS were formulated. The four formulations including low and high of Tween80® (LT and HT), and low and high of Labrasol® (LL and HL) of the OXY-SMEDDS were compared.

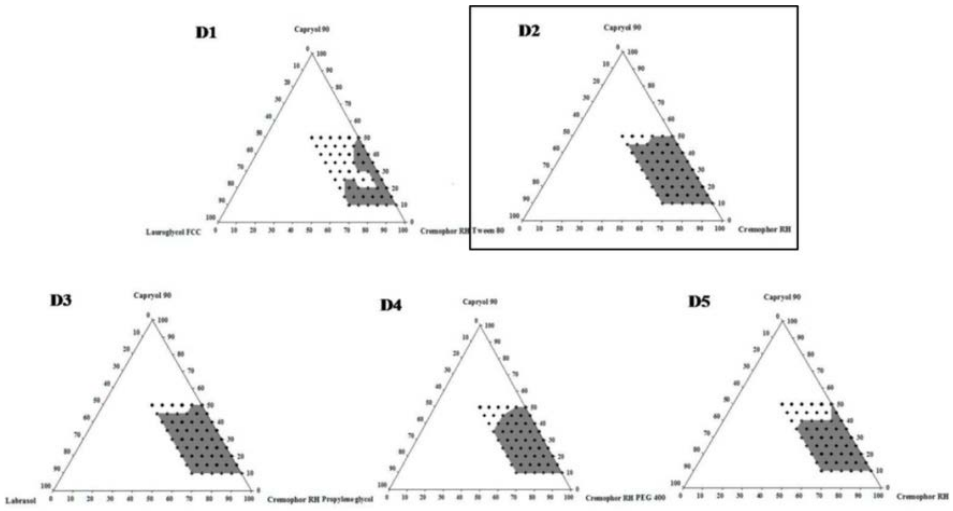

Figure 1.10 Ternary phase diagram of Cremophor RH40®-based SMEDDS (system D) containing different co-surfactants including Lauroglycol FCC® (D1), Tween80® (D2), Labrasol® (D3), PG® (D4) and PEG400 (D5). Gray areas represent the region of efficient self-microemulsification (Grade I), and the dots represent the compositions that were evaluated.

Four different formulations produced transparent microemulsion (visual grade I) after dilution with all of the dispersed media and the droplet size obtained < 50 nm (Figure 1.11). However, the Tween80®-based system (LT and HT) had a significantly smaller droplet size (~26

to 36 nm) than the Labrasol®-based system (LL and HL; ~34 to 45 nm) (Table 1.7). For the Tween80®-based system, the droplet sizes obtained from the HS formulation (HT) were significantly smaller ($p<0.05$) than from the LS formulation (LT) in all diluents. This finding indicated that the surfactant phase including the type and quantity did affect the microemulsion droplet size of the SMEDDS formulations. Meanwhile, there was no remarkable change in the total OXY content (~100% w/w) of the four SMEDDS formulations. The TEM micrographs (Figure 1.11) revealed that all microemulsions had a uniform spherical shape with no aggregation.

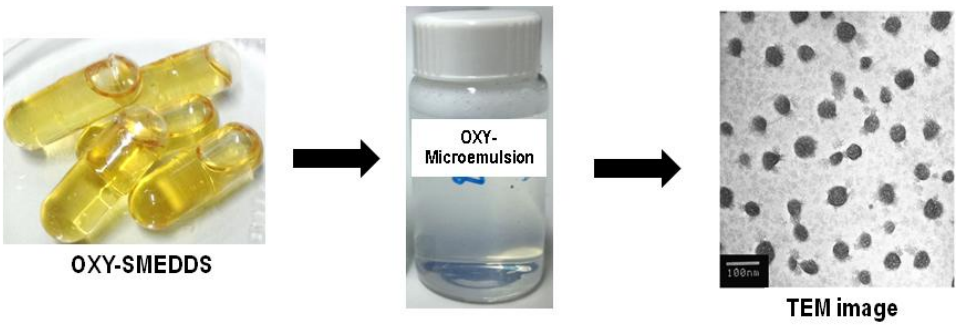

Figure 1.11 Example of capsule filled with OXY-SMEDDS formulation which produced transparent microemulsion and its morphology observed by TEM.

By the capsule method, all formulations showed a rapid release of OXY and reached 80% w/w within 10 min in the SGF pH1.2 without pepsin at 37 ºC (Figure 1.12). By the dialysis bag method, the microemulsion entrapping OXY was trapped in the bag and allowed only free OXY (< 6% of the cumulative % released) to be released into the dissolution medium up to 2h. These results implied that the major released content of OXY was in the microemulsion form.

After 24h-incubation of MTT test, the formulations of both Tween80®-(LT and HT) and Labrasol®-(LL and HL) based systems were compatible to Caco-2 intestinal cells up to the same OXY concentration of 100 µM. However, the four SMEDDS were more toxic than the unformulated OXY according to no toxicity of pure OXY up to 400 µM (Figure 1.13). Therefore, the OXY concentration in the SMEDDS should be not more than 100 µM, to be considered as a nontoxic concentration for the transport study.

Table 1.7 Effect of the surfactant phase on the droplet size, size distribution and the total drug content of the different OXY-SMEDDS. All values are presented as mean values ± SD (n = 3). $p<0.05$, in comparison with the LT (*) and HT (**) in the same diluent.

Code	Droplet size (nm ± SD)				PDI ± SD				Total drug content (%)
	Water	SGF pH1.2	TM pH6.5	TM pH7.4	Water	SGF pH1.2	TM pH6.5	TM pH7.4	
LT	31.7±0.6**	34.7±0.1**	36.1±0.1**	36.2±0.1**	0.07±0.01	0.06±0.01	0.07±0.01	0.06±0.00	100.2±1.0
HT	26.6±0.1*	31.4±0.2*	32.2±0.1*	32.4±0.2*	0.07±0.00	0.08±0.01	0.09±0.01	0.08±0.01	101.4±1.2
LL	36.6±0.4*,**	40.6±0.2*,**	41.0±0.1*,**	41.5±0.0*,**	0.08±0.02	0.07±0.01	0.08±0.00	0.09±0.01	101.4±1.7
HL	34.1±0.2*,**	42.1±0.2*,**	43.8±0.4*,**	44.9±0.2*,**	0.10±0.01	0.10±0.01	0.11±0.01	0.13±0.00	102.3±0.5

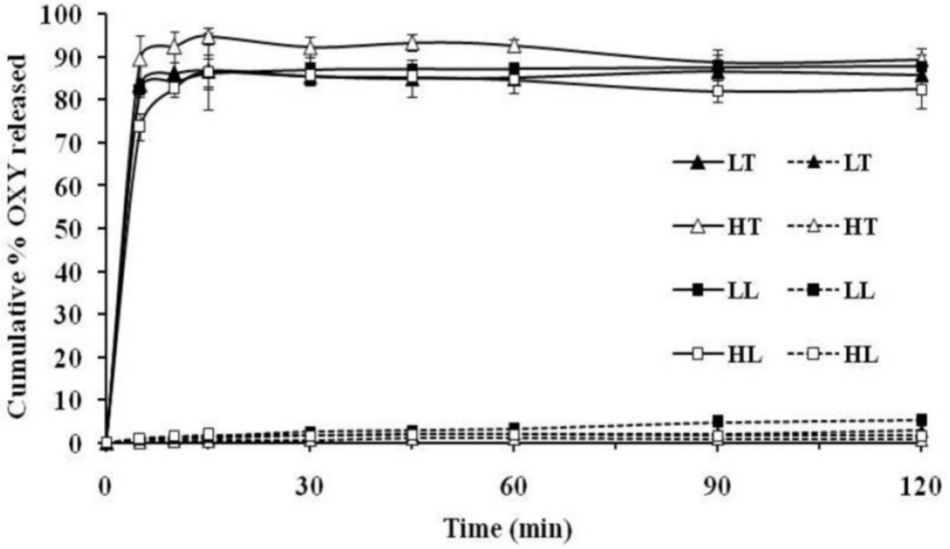

Figure 1.12 The dissolution profiles of OXY from the capsule (dark lines) and the dialysis bag (dot line) filled with the SMEDDS formulations in simulated gastric fluid (SGF, pH1.2) without pepsin. Data are represented by a mean ± SD (n = 3).

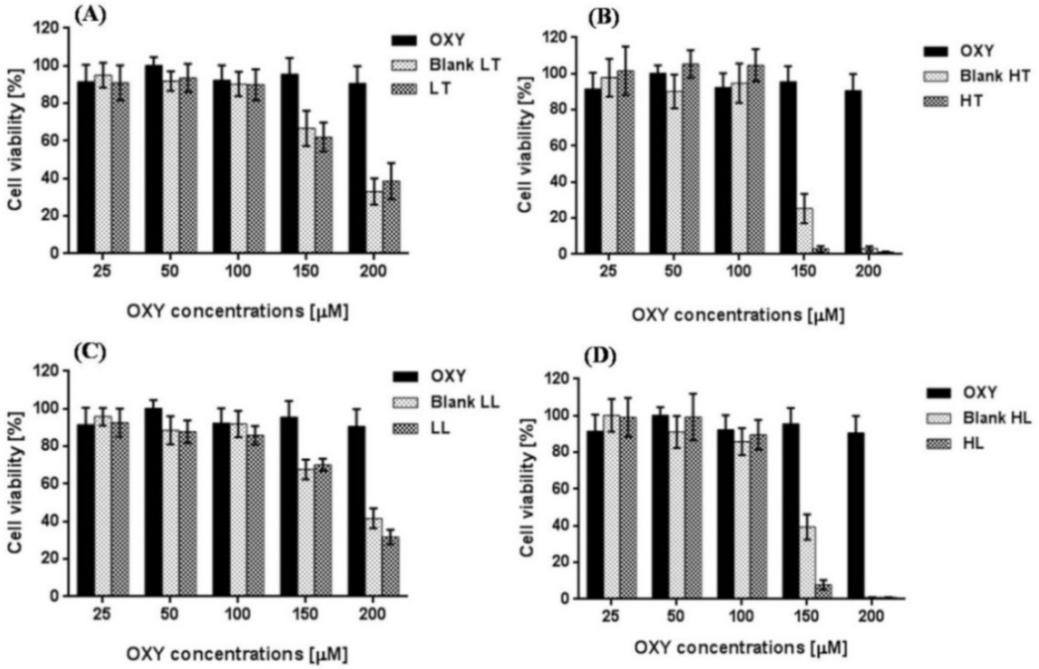

Figure 1.13 The percentage of Caco-2 cell viability to different concentrations of OXY, blank SMEDDS and OXY-SMEDDS; A) LT, B) HT, C) LL, D) HL, (n = 8), duplications.

From the bidirectional studies, the ER of the solubilized OXY was 5.02 at 100 μM. The significant increase *of* absorptive *P*app (1.2-2.0 folds) and significant decrease of secretory *P*app of for the OXY-SMEDDS formulations was consequence to a 5-fold reduction of the efflux ratio

(ER 0.94-1.14). This could imply that the SMEDDS formulated OXY enhanced the membrane permeability of OXY and inhibited the efflux pump. Moreover, the OXY-SMEDDS of the HS group (HT and HL) exhibited a better permeation across the Caco-2 monolayers (1.4-1.7 folds) than for the LS group (LT and LL) ($p < 0.05$). However, a similar absorptive and secretory permeability was obtained from either the Tween80®-based or the Labrasol®-based systems, at the same concentrations (Figure 1.14). This investigation indicated that the *in vitro* intestinal permeability of OXY was clearly improved by the developed SMEDDS.

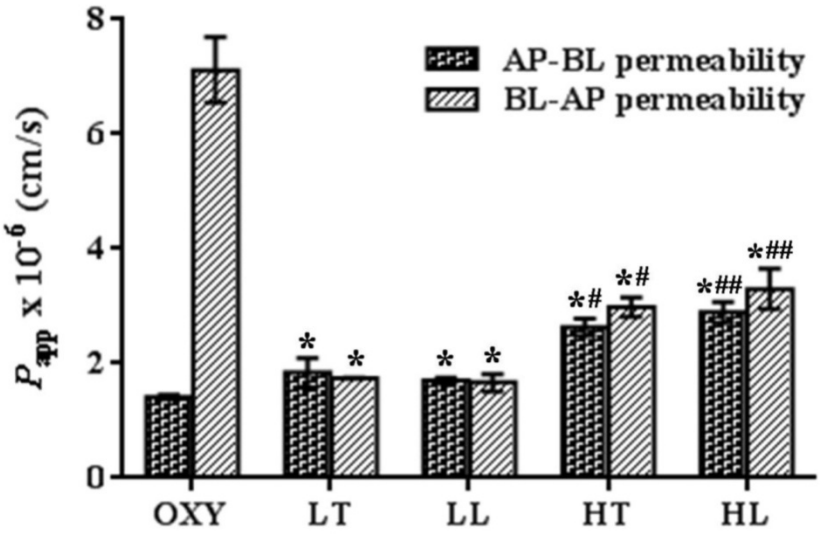

Figure 1.14 Bidirectional transport across the Caco-2 monolayers of OXY and different OXY-SMEDDS. The data are presented as the apparent permeability coefficients (*P*app) in the absorptive (AP-BL) and the secretory directions (BL-AP). $p < 0.05$, comparison with OXY (*); LT (#); LL (##) at the equivalent dose of OXY (100 µM).

The pharmacokinetic parameters in rats receiving 180 mg/kg OXY either in aqueous suspensions or various SMEDDS formulations, are summarized in Figure 1.15 and Table 1.8. All SMEDDS showed a significantly higher AUC_{0-10h} for OXY than for the unformulated OXY ($p < 0.05$), however, only the Tween80®-based formulations (LT and HT) showed a significantly ($p < 0.05$) higher *C*max than the unformulated OXY (*C*max 0.66 ± 0.08 µg/mL). Furthermore, the *T*max of the OXY from the SMEDDS formulations was comparable to those from the unformulated OXY (10 min). For the Labrasol®-based system, the HS formulation (HL; F_r 218.32%) had a significantly higher AUC_{0-10h} ($p < 0.05$) than the LS formulation (LL; F_r 137.98%) (Figure 1.15B and Table 1.8). Likewise, the HT formulation of Tween80®-based system was significantly greater ($p < 0.05$) *C*max (2.5 folds) and AUC_{0-10h} (4.3 folds) of OXY than those of the LT (Figure 1.15A and Table 1.8). The part of results correlated with the enhanced Caco-2 cell permeability data of these SMEDDS formulations.

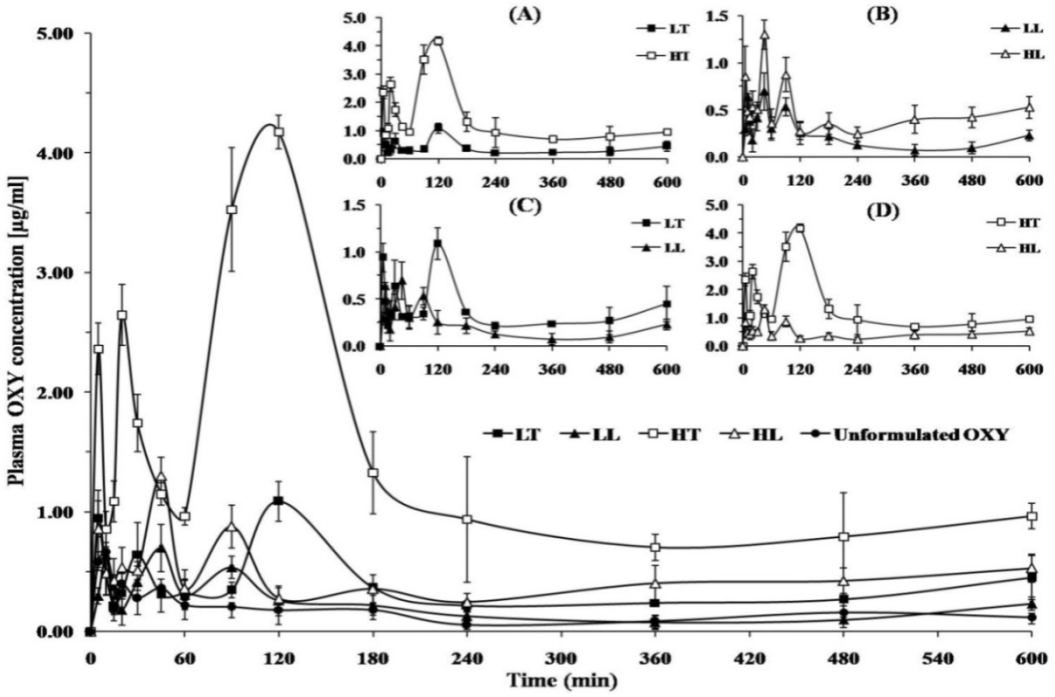

Figure 1.15 Plasma concentrations *vs.* time profiles after the oral administration of OXY formulated as SMEDDS and unformulated OXY after dosing with OXY of 180 mg/kg. Comparison of different surfactant concentrations of SMEDDS; low LT and high HT (A), and low LL and high HL (B), for Tween80®-based (T) and Labrasol®-based (L) systems, respectively. Comparison of different surfactant types of SMEDDS; Labrasol®-based LT and LL (C), and Tween80®-based HT and HL (D), for low (L) and high (H) concentrations, respectively. All values reported are mean values ± SD (n = 7).

As in Table 1.8, at the same concentrations, Tween80®-based system (both LT and HT) yielded a significantly greater *C*max (1.5-2.7 folds) ($p < 0.05$) and $AUC_{0–10h}$ (1.3-3.6 folds) for OXY than those of the Labrasol®-based system (LL and HL) (Figure 1.15C and 1.15D). On the contrary, there were no differences found between the *in vitro* permeability data of the OXY from such different systems in this study. Sometimes *in vitro* data could not predict *in vivo* data. Among other formulations and unformulated OXY, the HT formulation that contained the highest amount of Tween80® yielded the greatest improved in the oral bioavailability of OXY (F_r 786.32%). The superior enhancement of oral OXY absorption by the Tween80®-based system could be explained by the increased drug solubilization, effective stabilized and significantly reduced droplet size of microemulsion. Moreover, the high dispersibility and endocytotic internalization of the microemulsion followed by intracellular release of the drug and increased transcellular pathway (Sha *et al.*, 2005; Lin *et al.*, 2007; Kogan *et al.*, 2008). In addition, the restraining of the efflux transport by Tween80®, and tight junction opening to move the intact microemulsion droplets through paracellular pathway (Zhang *et al.*, 2003; Rege *et al.*, 2002; Ujhelyi *et al.*, 2012). Then, it

could bypass the first pass hepatic metabolism via increased lymphatic absorption by the Tween80® (Seeballuck *et al.*, 2004; Lind *et al.*, 2008). Furthermore, the rapid elimination of OXY might be minimized by inhibitory activity of Tween80® that resulted in maintaining a longer resident time for the drug in the blood circulation (Ellis *et al.*, 1996). Surprisingly, the similarity of enterohepatic recycling (EHC) pattern of the SMEDDS containing the same co-surfactant was observed. The persistence of the EHC prolonged the exposure time of the OXY in the body (Gao *et al.*, 2014). These findings have indicated the advantages of the SMEDDS formulation to enhance the bioavailability of the orally delivered OXY.

Table 1.8 Pharmacokinetics data of OXY after the oral administration of different SMEDDS formulations and an unformulated OXY (equivalent to 180 mg/kg of OXY). The values are presented as mean values ± SD (n = 7). $p < 0.05$, in comparison with the unformulated OXY (*); LT (**); LL (***); HL (#).

Parameters	*C*max (µg/mL)	*T*max (min)	$AUC_{0\text{-}10h}$ (ng h/mL)	$F_{r,\ 0\text{-}10h}$ (%)
Unformulated OXY	0.66±0.08	10	1,897.34±220.13	100
LT	0.94±0.15*,***	5	3,460.37±188.39*,***	182.38
LL	0.64±0.04	10	2,617.86±360.25*	137.98
HT	2.36±0.22$^{*,**,\#}$	5	14,919.16±522.00$^{*,**,\#}$	786.32
HL	0.86±0.32	5	4,142.33±45.32*,***	218.32

Comparison between lipid nanoparticles and SMEDDS for oral delivery of OXY

In this study, the developed lipid formulations of OXY could be divided into two main groups based on the lipid phase of the formulations. First, lipid nanoparticle systems include SLN and NLC. The other was an oily SMEDDS formulation. The lipid nanoparticles were prepared by mechanical techniques using the high shear homogenization while, the SMEDDS was simply produced by optimized concentrations of compositions (Figure 1.16). The liquid oil proportion in each formulation could be order as SMEDDS (45%) > NLC (2.5%) >SLN (0%). For surfactant phase, all formulations contain different Tween80® concentration of 10% (SMEDDS) > 3.75% (NLC = SLN). For drug loading, the SMEDDS containing 4% w/w of OXY was more than such of the SLN and NLC (0.3% w/w).

The dissimilarity on selected storage temperatures for SMEDDS (30 ± 2°C and 45 ± 2 °C) and lipid nanoparticles (4 ± 2 °C) could be explained by the difference of the composition in both systems. The temperature of refrigerator (4 ± 2 °C) was not suitable for SMEDDS system containing liquid oil (Capryol 90®) due to the oil would be wax at the lower melting point temperature. The conditions of room temperature (RT) or higher temperature were not proper for

the lipid nanoparticles which comprised of the solid lipid and most of water. At the RT, the contamination of the microorganism to the aqueous formulations was possible if no preservative adding. Moreover, too high temperature might be the reason of the solid lipid melted. The appearance of SMEDDS under accelerated conditions was changed to dark oily solution after storage for three months. Moreover, only the mean particle size of SLN significantly increased after three months of storage. Importantly, the total content of OXY in both lipid nanoparticles was almost 100% at various time points (0, 1, 3 months) whereas the OXY content in the SMEDDS was gradually decreased against the time (Figure 1.16). This result implied the instability of the oily SMEDDS according to the loss or degradation of drug. From the stability data, it might be concluded that the lipid nanoparticles were more stable than the oily formulations because of efficiency of the solid lipid to protect the entrapped drug in the system.

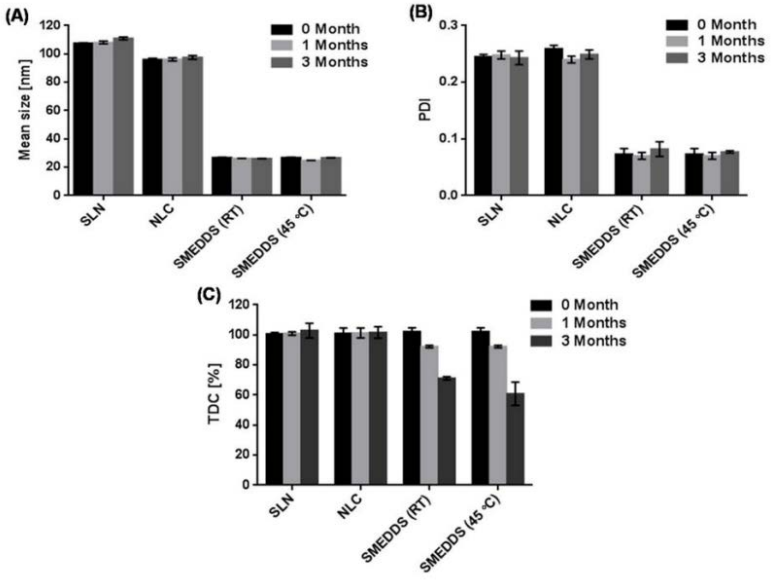

Figure 1.16 Physical characteristics and stability data (0, 1, 3 months) of the OXY formulated as SLN, NLC and SMEDDS; (A) Mean size, (B) PDI and (C) %Total drug content (TDC). Data represents the mean ± S.D. (n = 3).

In cytotoxicity test, the 4-folds higher in toxicity of SMEDDS (at 100 µM) than lipid nanoparticles (at 400 µM) might be related to the different compositions of the systems. As in previous report, the surfactants seem to be the major factor in cytotoxicity (Buyukozturk *et al.*, 2010; Ujhelyi *et al.*, 2012). In this study, the % surfactant phase (55 %w/w) of the SMEDDS was about 10 times greater than such of the lipid nanoparticles system (5.625 %w/w). Especially, the more % of Tween80® in SMEDDS (10 %w/w) than the nanoparticles systems (3.75 %w/w) indicates the more toxic of the former system due to a concentration-dependent manner of cytotoxic properties of the surfactants (Ujhelyi *et al.*, 2012). In addition, the Capryol 90® oil of the SMEDDS

which contained propylene glycol esters group implied the cytotoxicity on the Caco-2 cells at high concentration (Ujhelyi *et al.*, 2012; Thakkar and Desai, 2015). Meanwhile, the Com888 solid lipid, long chain glyceride, and Lab CC oil, medium chain triglyceride, commonly used in NLC was compatible to the intestinal cells because of its structure similar to physiological lipids of the body.

It is known that the low oral bioavailability of OXY was sequel from the low intestinal permeability which involved the efflux transporter mechanism (Mei *et al.*, 2012; Sangsen *et al.*, 2015). From bidirection experiment of transport studies, the only 1.5 times and 3 times increase in *P*app of the secretory direction and the absorptive direction, respectively, consequence to the decrease in the ER of the drug from 5.02 to 2.55 when increasing the OXY concentration from 100 µM to 400 µM. This can be explained by the saturation of activity of the efflux transporters at Caco-2 cell monolayer. From the impact of the bioactive content, both formulations of the nanaoparticles were compared to the SMEDDS system at the 100 µM of OXY. At this level, the NLC, SLN and SMEDDS were significantly improved 3, 2.8, and 2.5 folds in *P*app (AP-BL) value, respectively, compared to unformulated OXY. Meanwhile, the *P*app value of secretory direction (BL-AP) of the NLC, SLN, and SMEDDS was found 1.3, 1.8, and 1.5 folds decrease, respectively, comparing to unformulated OXY (Figure 1.17). The data continued to the efflux ratio of the three formulations was not different. Although the mechanisms of transport across the intestinal epithelium of different lipid-based systems were diversified but the effective of the mechanisms could be comparable. The lipid nanoparticles have been preferential uptake by specialized Peyer's patches (M cells) and the isolated follicles of the gut-associated lymphoid tissue located at the intestinal epithelium (Bilia *et al.*, 2014). Meanwhile, the microemulsion droplets of SMEDDS were mainly generated to be mixed micelles and then pass through chylomicron uptake mechanism by enterocytes. Finally, the compound formulated as solid lipid and oily formulations was further reached to systemic circulation (Bilia *et al.*, 2014; Porter *et al.*, 2008). Moreover, the inhibition activities on the efflux mediated transporter (s) and tight junction modulation of the surfactants in the lipid formulations promote thereby the oral absorption (Buyukozturk *et al.*, 2010; Thakkar and Desai, 2015; Ujhelyi *et al.*, 2012). These have been the potential mechanism of the lipid-based formulations implemented for the oral delivery.

Nevertheless, the data from the absorption study alone may not be able to predict explicitly oral drug bioavailability (Lasa-Saracíbar *et al.*, 2014; Mekjaruskul *et al.*, 2013). In particular of OXY, the three lipid formulations including SLN, NLC, and SMEDDS, were successfully improved *in vitro* absorption and oral bioavailability compared to unformulated OXY. Although, the difference of *in vitro* permeability of OXY from each formulation is not empirical as that observed in *in vivo* studies (Sangsen *et al.*, 2015; Sangsen *et al.*, 2016).

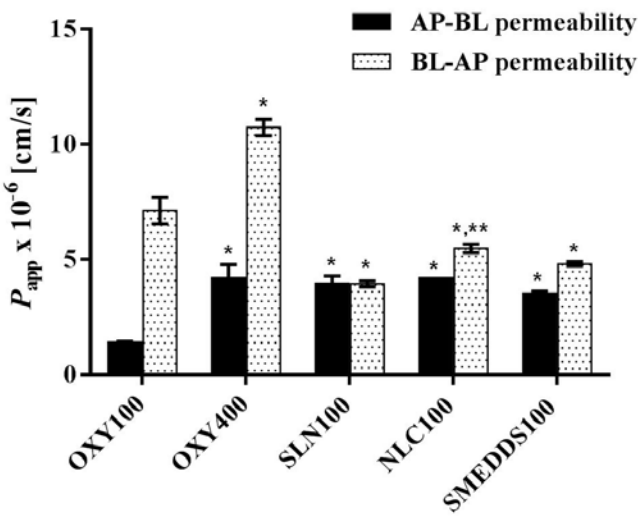

Figure 1.17 Bidirectional transport across the Caco-2 monolayers of OXY and developed OXY-formulations. The data are presented as the apparent permeability coefficient (*P*app) in the absorptive (AP-BL) and the secretory directions (BL-AP). *p < 0.05, comparison with OXY100; **p < 0.05, comparison with SLN100.

4. Conclusion

In this study, the different lipid-based drug delivery systems including lipid nanoparticles systems (SLN and NLC) and the SMEDDS have been developed for improved oral bioavailability of OXY. The OXY-loaded SLN were prepared by mechanical technique of the high speed homogenization. The OXY-loaded SLN formulation comprising Compritol® 888 ATO, Tween80® combined with soy-lecithin had a good appearance, high entrapment efficiency and the most favorable physicochemical properties. The optimized SLN could retard OXY release in SGF pH 1.2 and SIF pH 6.8. The optimum amounts of miscible components of SLN with efficient preparation procedure were chosen to use as the starting conditions for NLC production. The NLC were formulated by replacing some quantity of Compritol® 888 ATO with liquid lipid (Labrafac® CC). Compared with OXY-loaded SLN, the OXY-loaded NLC showed a smaller and more uniform nanoparticle size, higher entrapment efficiency, and a satisfactory loading capacity. Moreover, the OXY-loaded NLC was more stable than the OXY-loaded SLN after a 12-months storage period. A sustained release of OXY without an initial burst effect was also achieved from the NLC. The lipid nanoparticles loaded with OXY were not toxic to the Caco-2 cells up to 400 µM of OXY. Interestingly, the NLC was greater in decrease of the *P*app of the secretory permeability of OXY compared to that of SLN and unformulated OXY. Consequently, the NLC (ER, 0.59) significantly reduced the efflux transport of OXY compared with SLN (ER, 1.01) and unformulated OXY (ER, 2.55). Furthermore, an enhanced oral bioavailability of OXY in rats was obtained using NLC compared to both OXY-SLN and an OXY suspension.

The OXY-loaded SMEDDS were successfully developed by simple optimization of chemical compositions in the system. Although, the SMEDDS formulations presented a rapid OXY release (> 80% w/w) within 10 min in the SGF pH 1.2, the major released content of OXY was found to be in the microemulsion form. The co-surfactant types of SMEDDS influenced the droplet size according to the Tween80®-based SMEDDS provided the smaller droplet sizes than Labrasol®-based SMEDDS. Moreover, the high concentration of surfactant used in the system also affectively reduced the microemulsion size in different media. All SMEDDS formulation was compatible to Caco-2 intestinal cells up to 100 µM. For the transport study, the ER of the solubilized OXY was 5.02 at 100 µM. The OXY-loaded SMEDDS enhanced the membrane permeability of OXY and inhibited the efflux pump mechanisms which were consequence to a 5-fold reduction of the efflux ratio (ER 0.94-1.14). Furthermore, the OXY-SMEDDS of the high surfactant group exhibited a better permeation across the Caco-2 monolayers (1.4-1.7 folds) than for the low surfactant group ($p<0.05$).All developed SMEDDS increased the pharmacokinetics of OXY while retaining the intact enterohepatic pattern of the OXY in Wistar rats. The highest improvement of oral bioavailability of OXY *in vivo* ($F_{r,0\text{-}10h}$ 786.32%) was achieved from the SMEDDS containing high proportions of Tween80®.

This research noticeably indicates the benefits of SMEDDS in the enhancement of OXY oral absorption which may result from the increased permeability and inhibited efflux mediated mechanisms. Moreover, the SMEDDS presented the remarkable improvement of the oral bioavailability of OXY. This approach has raised the possibility of using this active compound in treating and preventing some importance diseases in future. However, to be use as a commercial product, it is necessary to improve the storage stability of this system. In addition, SMEDDS could also be used as a potential carrier for oral delivery of other compounds which are substrates for efflux transporters.

Outputs

1. Sangsen, Y., Wiwattanawongsa, K., Likhitwitayawuid, K., Sritularak, B. and Wiwattanapatapee, R. 2015. Modification of oral absorption of oxyresveratrol using lipid based nanoparticles. Colloids Surf., B. 131: 182-190. (IF = 3.902)

2. Sangsen, Y., Wiwattanawongsa, K., Likhitwitayawuid, K., Sritularak, B., Graidist, P. and Wiwattanapatapee, R. 2016. Influence of surfactants in self-microemulsifying formulations on enhancing oral bioavailability of oxyresveratrol: studies in Caco-2 cells and *in vivo*. Int. J. Pharm. 498(1-2): 294-303. (IF = 3.994)

3. Sangsen, Y., Wiwattanawongsa, K., Likhitwitayawuid, K., Sritularak, B. and Wiwattanapatapee, R. 2016. Comparison between oily system and lipid nanoparticles of

oxyresveratrol on the physicochemical properties and Caco-2 cells oral absorption Eur. J. Lipid Sci. Tech. (in press). 15 JUN 2016, DOI:10.1002/ejlt.201600053 (IF = 1.953)

4. Sangsen, Y., Likhitwitayawuid, K., Sritularak, B., Wiwattanawongsa, K. and Wiwattanapatapee, R. 2013. Novel Solid Lipid Nanoparticles for Oral Delivery of Oxyresveratrol: Effect of the Formulation Parameters on the Physicochemical Properties and in vitro Release. International Journal of Medical, Pharmaceutical Science and Engineering, 7 (12): 873-880.

References

Bilia AR, Isacchi B, Righeschi C, Guccione C, Bergonzi MC. Flavonoids loaded in nanocarriers: an opportunity to increase oral bioavailability and bioefficacy. Food Nutr Sci. 2014;5:1212-27.

Buyukozturk F, Benneyan JC, Carrier RL. Impact of emulsion-based drug delivery systems on intestinal permeability and drug release kinetics. J Control Release. 2010;142(1):22-30.

Charoenlarp P, Shaipanich C, Subhanka S, Lakkantinaporn P, Tanunkat A. Pharmacokinetics of the active constituent of Puag-haad in man, in: Symposium on Mahidol University Research and Development, ASEAN Institute Health Development, 25–29 February, Salaya, Nakhon Pathom, 1991.

Ellis AG, Crinis NA, Webster LK. Inhibition of etoposide elimination in the isolated perfused rat liver by Cremophor EL and Tween 80. Cancer Chemother Pharmacol. 1996;38(1):81-7.

Freshney RI. Culture of animal cells: A manual of basic technique. 5thed. New Jersey: Wiley & Sons; 2005.

Gao Y, Shao J, Jiang Z, Chen J, Gu S, Yu S, Zheng K, Jia L. Drug enterohepatic circulation and disposition: constituents of systems pharmacokinetics. Drug Discov Today. 2014;19:326-40.

Gokce EH, Korkmaz E, Dellera E, Sandri G, Bonferoni MC, Ozer O. Resveratrol-loaded solid lipid nanoparticles versus nanostructured lipid carriers: evaluation of antioxidant potential for dermal applications. Int J Nanomedicine. 2012;7:1841.

Hill JM, Zhao Y, Clement C, Neumann DM, Lukiw WJ. HSV-1 infection of human brain cells induces miRNA-146a and Alzheimer-type inflammatory signaling. Hill JM, Zhao Y, Clement C, Neumann DM, Lukiw WJ. HSV-1 infection of human brain cells induces miRNA-146a and Alzheimer-type inflammatory signaling. NeuroReport. 2009; 20: 1500-5.

How CW, Abdullah R, Abbasalipourkabir R. Physicochemical properties of nanostructured lipid carriers as colloidal carrier system stabilized with polysorbate 20 and polysorbate 80. Afr J Biotechnol. 2011;10(9):1684-9.

Hu L, Xing Q, Meng J, Shang C. Preparation and enhanced oral bioavailability of cryptotanshinone-loaded solid lipid nanoparticles. AAPS PharmSciTech. 2010;11(2):582-7.

Huang H, Zhang J, Chen G, Lu Z, Wang X, Sha N, et al. High performance liquid chromatographic method for the determination and pharmacokinetic studies of oxyresveratrol and resveratrol in rat plasma after oral administration of *Smilax china* extract. Biomed Chrom. 2008;22(4):421-7.

Huang H, Chen G, Lu Z, Zhang J, Guo D. Identification of seven metabolites of oxyresveratrol in rat urine and bile using liquid chromatography/tandem mass spectrometry. Biomed Chrom. 2010;24(4):426-32.

Hubatsch I, Ragnarsson EG, Artursson P. Determination of drug permeability and prediction of drug absorption in Caco-2 monolayers. Nat Protoc. 2007;2(9):2111-9.

Jenning V, Thünemann AF, Gohla SH. Characterisation of a novel solid lipid nanoparticle carrier system based on binary mixtures of liquid and solid lipids. Int J Pharm. 2000;199(2):167-77.

Kang BK, Lee JS, Chon SK, Jeong SY, Yuk SH, Khang G, et al. Development of self-microemulsifying drug delivery systems (SMEDDS) for oral bioavailability enhancement of simvastatin in beagle dogs. Int J Pharm. 2004;274(1):65-73.

Kipp J. The role of solid nanoparticle technology in the parenteral delivery of poorly water-soluble drugs. Int J Pharm. 2004;284(1):109-22.

Kogan A, Kesselman E, Danino D, Aserin A, Garti N. Viability and permeability across Caco-2 cells of CBZ solubilized in fully dilutable microemulsions. Colloids Surf B. 2008;66(1):1-12.

Lasa-Saracíbar B, Guada M, Sebastián V, J Blanco-Prieto M. *In vitro* intestinal co-culture cell model to evaluate intestinal absorption of edelfosine lipid nanoparticles. Curr Top Med Chem. 2014;14(9):1124-32.

Likhitwitayawuid K, Sritularak B, Benchanak K, Lipipun V, Mathew J, Schinazi, R.F. Phenolics with antiviral activity from *Millettia erythrocalyx* and *Artocarpus lakoocha*. Nat. Prod. Res. 2005; 19: 177-182.

Lin Y, Shen Q, Katsumi H, Okada N, Fujita T, Jiang X, et al. Effects of Labrasol and other pharmaceutical excipients on the intestinal transport and absorption of rhodamine123, a p-glycoprotein substrate, in rats. Biol Pharm Bull. 2007;30(7):1301-7.

Lind ML, Jacobsen J, Holm R, Müllertz A. Intestinal lymphatic transport of halofantrine in rats assessed using a chylomicron flow blocking approach: the influence of polysorbate 60 and 80. Eur J Pharm Sci. 2008;35(3):211-8.

Lipipun V, Sasivimolphan P, Yoshida Y, Daikoku T, Sritularak B, Ritthidej G, Likhitwitayawuid K, Pramyothin P, Hattori M, Shiraki K. Topical cream-based oxyresveratrol in the treatment of cutaneous HSV-1 infection in mice. Antiviral Res. 2011: 91: 154-160.

Lo Y-l. Relationships between the hydrophilic–lipophilic balance values of pharmaceutical excipients and their multidrug resistance modulating effect in Caco-2 cells and rat intestines. J Control Release. 2003;90(1):37-48.

Lundin PDP, Bojrup M, Ljusberg-Wahren H, Weström BR, Lundin S. Enhancing effects of monohexanoin and two other medium-chain glyceride vehicles on intestinal absorption of desmopressin (dDAVP). J Pharmacol Exp Ther. 1997;282(2):585-90.

Luo Y, Chen D, Ren L, Zhao X, Qin J. Solid lipid nanoparticles for enhancing vinpocetine's oral bioavailability. J Control Release. 2006;114(1):53-9.

Mei M, Ruan J-Q, Wu W-J, Zhou R-N, Lei JP-C, Zhao H-Y, et al. *In vitro* pharmacokinetic characterization of mulberroside A, the main polyhydroxylated stilbene in mulberry (*Morus alba* L.), and its bacterial metabolite oxyresveratrol in traditional oral use. J Agric Food Chem. 2012;60(9):2299-308.

Mekjaruskul C, Yang Y-T, Leed MGD, Sadgrove MP, Jay M, Sripanidkulchai B. Novel formulation strategies for enhancing oral delivery of methoxyflavones in Kaempferia parviflora by SMEDDS or complexation with 2-hydroxypropyl-β-cyclodextrin. Int J Pharm. 2013;445(1–2):1-11.

Porter CJ, Pouton CW, Cuine JF, Charman WN. Enhancing intestinal drug solubilisation using lipid-based delivery systems. Adv Drug Deliv Rev. 2008;60(6):673-91.

Pouton CW, Porter CJ. Formulation of lipid-based delivery systems for oral administration: materials, methods and strategies. Adv Drug Deliv Rev. 2008;60(6):625-37.

Rege BD, Kao JPY, Polli JE. Effects of nonionic surfactants on membrane transporters in Caco-2 cell monolayers. Eur J Pharm Sci. 2002;16:237-46.

Ritger PL, Peppas NA. A simple equation for description of solute release II. Fickian and anomalous release from swellable devices. J Control Release. 1987;5(1):37-42.

Sangsen Y, Wiwattanawongsa K, Likhitwitayawuid K, Sritularak B, Wiwattanapatapee R. Modification of oral absorption of oxyresveratrol using lipid based nanoparticles. Colloids Surf B. 2015;131:182-90.

Sangsen Y, Wiwattanawongsa K, Likhitwitayawuid K, Sritularak B, Graidist P, Wiwattanapatapee R. Influence of surfactants in self-microemulsifying formulations on enhancing oral bioavailability of oxyresveratrol: studies in Caco-2 cells and *in vivo*. Int J Pharm. 2016;498(1-2):294-303.

Sasivimolphan P, Lipipun V, Likhitwitayawuid K, Takemoto M, Pramyothin P, Hattori M., Shiraki K. Inhibitory activity of oxyresveratrol on wild-type and drug-resistantvaricella-zoster virus replication in vitro. Antiviral Res. 2009; 84: 95–97.

Seeballuck F, Lawless E, Ashford MB, O'Driscoll CM. Stimulation of triglyceride-rich lipoprotein secretion by polysorbate 80: *in vitro* and *in vivo* correlation using Caco-2 cells and a cannulated rat intestinal lymphatic model. Pharm Res. 2004;21(12):2320-6.

Sermkaew N, Ketjinda W, Boonme P, Phadoongsombut N, Wiwattanapatapee R. Liquid and solid self-microemulsifying drug delivery systems for improving the oral bioavailability of andrographolide from a crude extract of *Andrographis paniculata*. Eur J Pharm Sci. 2013;50(3):459-66.

Sha X, Yan G, Wu Y, Li J, Fang X. Effect of self-microemulsifying drug delivery systems containing Labrasol on tight junctions in Caco-2 cells. Eur J Pharm Sci. 2005;24(5):477-86.

Shono Y, Nishihara H, Matsuda Y, Furukawa S, Okada N, Fujita T, et al. Modulation of intestinal p-glycoprotein function by cremophor EL and other surfactants by an *in vitro* diffusion chamber method using the isolated rat intestinal membranes. J Pharm Sci. 2004;93(4):877-85.

Singh AK, Chaurasiya A, Awasthi A, Mishra G, Asati D, Khar RK, et al. Oral bioavailability enhancement of exemestane from self-microemulsifying drug delivery system (SMEDDS). AAPS PharmSciTech. 2009;10(3):906-16.

Souto E, Mehnert W, Müller R. Polymorphic behaviour of Compritol® 888 ATO as bulk lipid and as SLN and NLC. J Microencapsul. 2006;23(4):417-33.

Souto EB, Müller RH. Lipid nanoparticles: effect on bioavailability and pharmacokinetic changes. In: Schäfer-Korting M, editor. Drug delivery, Handbook of experimental pharmacology. Heidelberg: Springer; 2010. p. 115-41.

Tanunkat A, Absorption, metabolism and excretion of 2,3′,4,5′-tetrahydroxystilbene in volunteers after oral administration of purified extract of Paug-Haad, Mahidol University, Salaya, NakhonPathom, Thailand, 1990.

Thakkar HP, Desai JL. Influence of excipients on drug absorption via modulation of intestinal transporters activity. Asian J Pharmacol.2015;9(2):69-82.

Tiwari R, Pathak K. Nanostructured lipid carrier versus solid lipid nanoparticles of simvastatin: comparative analysis of characteristics, pharmacokinetics and tissue uptake. Int J Pharm. 2011;415(1):232-43.

Ujhelyi Z, Fenyvesi F, Váradi J, Fehér P, Kiss T, Veszelka S, et al. Evaluation of cytotoxicity of surfactants used in self-micro emulsifying drug delivery systems and their effects on paracellular transport in Caco-2 cell monolayer. Eur J Pharm Sci. 2012;47(3):564-73.

Üner M. Preparation, characterization and physico-chemical properties of solid lipid nanoparticles (SLN) and nanostructured lipid carriers (NLC): their benefits as colloidal drug carrier systems. Pharmazie. 2006;61(5):375-86.

Wu G, Lee KYC. Effects of poloxamer 188 on phospholipid monolayer morphology: an atomic force microscopy study. Langmuir. 2009;25(4):2133-9.

Yee S. *In vitro* permeability across Caco-2 cells (colonic) can predict *in vivo* (small intestinal) absorption in man-fact or myth. Pharm Res. 1997;14(6):763-6.

Zhang H, Yao M, Morrison RA, Chong S. Commonly used surfactant, Tween 80, improves absorption of p-glycoprotein substrate, digoxin, in rats. Arch Pharm Res. 2003;26(9):768-72.

Zhuang C-Y, Li N, Wang M, Zhang X-N, Pan W-S, Peng J-J, et al. Preparation and characterization of vinpocetine loaded nanostructured lipid carriers (NLC) for improved oral bioavailability. Int J Pharm. 2010;394(1):179-85.

CHAPTER II

Project 2

Structural modification of oxyresveratrol

Principle Investigator: Professor Dr. Kittisak Likhitwitayawuid
Chulalongkorn University

Background

Oxyresveratrol (2,4,3′,5′-tetrahydroxystilbene**, 1**) is present in large amounts in the heartwood of *Artocarpus lakoocha* Roxb.), and thus offers opportunities for chemical and biological studies. Our previous *in vitro* and *in vivo* experiments have shown that **1** is a potent tyrosinase inhibitor, and subsequent studies in human volunteers have confirmed it as an effective skin-whitening agent (Likhitwitayawuid et al., 2006a; Tengamnuay et al., 2006). Despite its moderate *in vitro* inhibitory activity against herpes simplex virus type I (HSV-1) (Likhitwitayawuid et al., 2005a; 2005b), compound **1**, in the form of topical cream, exhibited high therapeutic efficacy in mice cutaneously infected with HSV-1, with a magnitude comparable to that of the antiviral drug acyclovir (Lipipun et al., 2011). Currently, mounting evidence has indicated HSV-1 infection in the brain as one of the key causative factors in the pathogenesis of Alzheimer's disease (AD) (Hill et al., 2009), and this has suggested another medicinal importance for oxyresveratrol. Moreover, **1** was recently reported to exhibit inhibitory potential against H5N1 neuraminidase, an enzyme required for avian influenza virus (AIV) replication (Kongkamnerd, 2010).

It has been well documented that several other stilbenoids, including resveratrol, a stilbene with structure closely-related to **1**, possess inhibitory activity against various classes of virus (Li et al., 2006; Beyoda et al., 2006; Cardin et al., 1991). Some stilbenoids have been reported to exhibit inhibitory activity against several types of influenza virus (Liu et al., 2010; Nguyen et al., 2010). These biological data suggested stilbenes as potentially useful antiviral agents.

In our previous work, we successfully prepared, from **1**, an analog with enhanced tyrosinase inhibitory activity, as well as some derivatives with cytotoxicity against cancer cells (Likhitwitayawuid et al., 2006a). In the present investigation, we were interested in modifying the structure of **1** to improve the inhibitory activity effects against Herpes simplex virus and the AIV H5N1 neuraminidase enzyme.

Since **1** has been demonstrated to prevent DNA damage through its antioxidant property (Chatsumpun et al., 2011) and exhibited strong inhibition against α-glucosidase, an enzyme responsible for the breaking down of starch and polysaccharides into glucose in the intestine (He

et al., 2013), compound **1** and the derivatives synthesized in this study would also be subjected to assays for antioxidant and DNA protective properties, inhibitory activity against the enzyme α-glucosidase, as well as cytotoxicity against cancer cells.

1. Objectives

1. To prepare polyoxygenated stilbenes by chemically modifying the structure of oxyresveratrol using various types of chemical reactions.
2. To evaluate oxyresveratrol and the obtained derivatives for inhibitory activity against Herpes simplex virus and H5N1 neuraminidase.
3. To evaluate oxyresveratrol and derivatives for antioxidant and DNA protective properties, inhibitory activity against the enzymes α-glucosidase, and cytotoxicity against cancer cells

2. Experimental

2.1. Chemistry

2.1.1. General Information

All chemical reagents were purchased from commercial suppliers. Melting points (uncorrected) were determined on a Fisher-Johns, hot stage melting point apparatus. IR spectra were performed using UATR (Universal Attenuated Total Reflectance) on a Perkin Elmer system 2000 FT-IR and Jasco A-30 Spectrophotometer. High resolution mass spectra were taken on a MicroTOF instrument using atmospheric pressure chemical ionization (APCI) or electrospray ionization (ESI) in positive or negative mode. ^{1}H and ^{13}C- NMR were recorded on a Bruker Avance III 300 MHz spectrometer or Bruker 400 spectrometer. All chemical shift values were reported as δ (ppm) and coupling constant values *J* were measured in Hz.

2.1.2. Source of oxyresveratrol

Oxyresveratrol (**1**) was isolated and purified from the heartwood of *Artocarpus lacucha* Buch.-Ham. (*A. lakoocha* Roxb.) as previously described (Likhitwitayawuid et al., 2005a; Sritularak et al., 1988; Chuanasa et al., 2008).

2.1.3. Synthesis

2.1.3.1. 3′,5′-Dihydroxy-2,4-dimethoxystilbene (**2**), 5′-Hydroxy-2,3′,4-trimethoxystilbene (**3**), 2,3′,4,5′-Tetramethoxystilbene (**4**)

K_2CO_3 (680 mg, 4.92 mmol) and MeI (0.11 mL, 1.8 mmol) were added to the solution of **1** (200 mg, 0.82 mmol) in acetone (4 mL) at room temperature. The reaction mixture was stirred overnight. Then, the reaction mixture was diluted with water (5 mL) and extracted with EtOAc (3x5 mL). The EtOAc layer was washed with brine, dried over anhydrous Na_2SO_4, filtered and

concentrated under reduced pressure to give a crude product which, after purification by preparative TLC (50% EtOAc/hexanes), furnished **2** (19 mg, 9%), **3** (60 mg, 25%) and **4** (112 mg, 45%).

Compound **2**: viscous brown oil; IR (UATR, cm^{-1}): 3374, 2931, 1601; ^{1}H NMR (300 MHz, $CDCl_3$), δ (ppm): 7.43 (d, *J* = 8.4 Hz, 1H), 7.30 (d, *J* = 16.5 Hz, 1H), 6.82 (d, *J* = 16.2 Hz, 1H), 6.55 (d, *J* = 2.1 Hz, 2H), 6.48 (dd, *J* = 8.7, 2.1 Hz, 1H), 6.44 (d, *J* = 2.1 Hz, 1H), 6.24 (t, *J* = 2.1 Hz, 1H), 3.82 (s, 3H), 3.80 (s, 3H); ^{13}C NMR (75 MHz, $CDCl_3$), δ (ppm): 160.6, 158.1, 156.9, 141.0, 127.3, 126.2, 124.1, 119.2, 105.9, 105.1, 101.7, 98.5, 55.5, 55.4; TOF-HRMS *m/z* $[M+H]^+$, calcd for $C_{16}H_{17}O_4$: 273.1121; found: 273.1118.

Compound **3**: viscous brown oil; IR (UATR, cm^{-1}): 3408, 2938, 1590; ^{1}H NMR (300 MHz, $CDCl_3$), δ (ppm): 7.46 (d, *J* = 8.4 Hz, 1H), 7.33 (d, *J* = 16.5 Hz, 1H), 6.88 (d, *J* = 16.5 Hz, 1H), 6.62 (d, *J* = 1.8 Hz, 1H), 6.60 (d, *J* = 1.8 Hz, 1H), 6.49 (dd, *J* = 8.4, 2.4 Hz, 1H), 6.45 (d, *J* = 2.4 Hz, 1H), 6.30 (t, *J* = 2.1 Hz, 1H), 3.83 (s, 3H), 3.81 (s, 3H), 3.78 (s, 3H); ^{13}C NMR (75 MHz, $CDCl_3$), δ (ppm): 160.9, 160.5, 158.0, 156.9, 140.6, 127.3, 126.6, 123.9, 119.3, 105.8, 105.0, 104.6, 100.4, 98.5, 55.5, 55.4, 55.3; TOF-HRMS *m/z* $[M+H]^+$, calcd for $C_{17}H_{19}O_4$: 287.1278; found: 287.1285.

Compound **4**: white solid, mp 65-68 °C; ^{1}H NMR (300 MHz, $CDCl_3$), δ (ppm): 7.46 (d, *J* = 8.4 Hz, 1H), 7.36 (d, *J* = 16.2 Hz, 1H), 6.92 (d, *J* = 16.5 Hz, 1H), 6.66 (d, *J* = 2.4 Hz, 2H), 6.47 (dd, *J* = 8.4, 2.4 Hz, 1H), 6.42 (d, *J* = 2.4 Hz, 1H), 6.34 (t, *J* = 2.1 Hz, 1H), 3.81 (s, 3H), 3.79 (s, 6H), 3.77 (s, 3H); ^{13}C NMR (75 MHz, $CDCl_3$), δ (ppm): 160.8, 160.5, 158.0, 140.3, 127.2, 126.8, 123.7, 119.1, 104.9, 104.2, 99.2, 98.3, 55.3, 55.2, 55.1; TOF-HRMS *m/z* $[M+H]^+$, calcd for $C_{18}H_{21}O_4$: 301.1434; found: 301.1440. The spectroscopic data were in agreement with previously reported values (Likhitwitayawuid et al., 2006a).

2.1.3.2. 3′,5′-Dihydroxy-2,4-diisopropoxystilbene (**5**), 5′-Hydroxy-2,3′,4,-triisopropoxy-stilbene (**6**), 2,3′,4,5′-Tetraisopropoxystilbene (**7**).

To a solution of **1** (100 mg, 0.41 mmol) in DMF (2 mL), K_2CO_3 (283 mg, 2.05 mmol) and 2-bromopropane (2.30 mL, 24.6 mmol) were added. Then 2-bromopropane (1.15 mL, 12.3 mmol) was added every 24 h. The reaction mixture was stirred at 55 °C for 3 days and monitored by TLC. After completion, water (5 mL) was added, and the reaction was extracted with EtOAc (3x5 mL). The organic phase was washed with water (7x5 mL) and brine, dried over Na_2SO_4, filtered and concentrated. Column chromatographic purification with gradient EtOAc/hexanes (10% EtOAc/hexanes → 80% EtOAc/hexanes) gave **5** (32 mg, 24%), **6** (46 mg, 30%) and **7** (47 mg, 28%).

Compound **5**: brown oil; IR (UATR, cm^{-1}): 3379, 2976, 1598; ^{1}H NMR (400 MHz, $CDCl_3$), δ (ppm): 7.43 (d, *J* = 8.4 Hz, 1H), 7.31 (d, *J* = 16.4 Hz, 1H), 6.84 (d, *J* = 16.4 Hz, 1H), 6.56 (d, *J* = 2.1 Hz, 2H), 6.48 (dd, *J* = 8.5, 2.3 Hz, 1H), 6.45 (d, *J* = 2.2 Hz, 1H), 6.25 (br s, 1H), 4.52 (m, 2H), 1.35 (d, *J* = 6 Hz, 6H), 1.33 (d, *J* = 6 Hz, 6H); ^{13}C NMR (100 MHz, $CDCl_3$), δ (ppm): 158.6, 157.0,

156.5, 141.0, 127.4, 126.1, 124.3, 120.3, 107.5, 105.8, 103.2, 101.7, 71.2, 70.1, 22.1, 22.0; TOF-HRMS *m/z* $[M-H]^-$, calcd for $C_{20}H_{23}O_4$: 327.1602; found: 327.1594.

Compound **6**: brown oil; IR (UATR, cm^{-1}): 3393, 2976, 1588; ^1H NMR (400 MHz, $CDCl_3$), δ (ppm): 7.45 (d, *J* = 8.5 Hz, 1H), 7.32 (d, *J* = 16.4 Hz, 1H), 6.88 (d, *J* = 16.4 Hz, 1H), 6.61 (t, *J* = 1.5 Hz, 1H), 6.56 (t, *J* = 1.6 Hz, 1H), 6.49 (dd, *J* = 8.5, 2.3 Hz, 1H), 6.46 (d, *J* = 2.3 Hz, 1H), 6.28 (t, *J* = 2.1 Hz, 1H), 4.534 (m, 2H), 4.527 (m, 1H), 1.37 (d, *J* = 6 Hz, 6H), 1.343 (d, *J* = 6 Hz, 6H), 1.336 (d, *J* = 6 Hz, 6H); ^{13}C NMR (100 MHz, $CDCl_3$), δ (ppm): 159.2, 158.6, 156.7, 156.5, 140.8, 127.4, 126.2, 124.4, 120.2, 107.4, 107.0, 105.4, 103.0, 101.8, 71.0, 70.0, 69.9, 22.2, 22.0; TOF-HRMS *m/z* $[M-H]^-$, calcd for $C_{23}H_{29}O_4$: 369.2071; found: 369.2066.

Compound **7**: white solid, mp 58-60 °C; IR (UATR, cm^{-1}): 2976, 1585; ^1H NMR (300 MHz, $CDCl_3$), δ (ppm): 7.46 (d, *J* = 8.4 Hz, 1H), 7.33 (d, *J* = 16.4 Hz, 1H), 6.91 (d, *J* = 16.4 Hz, 1H), 6.62 (d, *J* = 2.2 Hz, 2H), 6.49 (dd, *J* = 8.5, 2.3 Hz, 1H), 6.45 (d, *J* = 3.9 Hz, 1H), 6.34 (t, *J* = 2.1 Hz, 1H), 4.55 (m, 4H), 1.37 (d, *J* = 6 Hz, 6H), 1.35 (d, *J* = 6 Hz, 12H), 1.34 (d, *J* = 6 Hz, 6H); ^{13}C NMR (75 MHz, $CDCl_3$), δ (ppm): 159.1, 158.6, 156.6, 140.5, 127.4, 126.7, 124.2, 120.4, 107.3, 106.4, 103.0, 102.5, 71.0, 69.9, 69.8, 22.2, 22.1; TOF-HRMS *m/z* $[M+H]^+$, calcd for $C_{26}H_{37}O_4$: 413.2686; found: 413.2679.

2.1.3.3. 2,3′,4,5′-Tetraacetoxystilbene (**8**)

To a well-stirred solution of **1** (50 mg, 0.21 mmol) in CH_2Cl_2 (2 mL), Et_3N (0.17 mL, 1.23 mmol), DMAP (63 mg, 0.51 mmol) and acetyl chloride (0.04 mL, 0.61 mmol) were added at room temperature, and the reaction mixture was stirred for 3 h. After completion of the reaction, it was extracted with EtOAc (3x5 mL). The EtOAc layer was washed with brine, dried over Na_2SO_4, filtered and concentrated under reduced pressure to give a crude product. Purification with column chromatography eluting with 40% EtOAc/hexanes gave **8** (60 mg, 70%).

Compound **8**: white solid, mp 129-131 °C; IR (UATR, cm^{-1}): 1762, 1605; ^1H NMR (300 MHz, $CDCl_3$), δ (ppm): 7.61 (d, *J* = 8.7 Hz, 1H), 7.08 (d, *J* = 2.1 Hz, 2H), 7.05 (d, *J* = 15.9 Hz, 1H), 7.03 (dd, *J* = 8.4, 2.4 Hz, 1H), 6.97 (d, *J* = 15.9 Hz, 1H), 6.95 (d, *J* = 2.1 Hz, 1H), 6.85 (t, *J* = 2.1 Hz, 1H), 2.36 (s, 3H), 2.31 (s, 6H), 2.29 (s, 3H); ^{13}C NMR (75 MHz, $CDCl_3$), δ (ppm): 168.93, 168.89, 168.8, 151.3, 150.5, 148.5, 139.4, 129.5, 127.2, 127.1, 123.5, 119.5, 117.0, 116.4, 114.8, 21.10, 21.09, 20.99; TOF-HRMS *m/z* $[M+Na]^+$, calcd for $C_{22}H_{20}NaO_8$: 435.1056; found: 435.1050. The spectroscopic data were in agreement with earlier reported values (Park et al., 2014).

2.1.3.4. 3′-*O*-Carbethoxymethyl-2,4,5′-triisopropoxystilbene (**9**)

To a solution of **6** (100 mg, 0.27 mmol) in DMF (4 mL), K_2CO_3 (56 mg, 0.40 mmol) and ethyl bromoacetate (0.04 mL, 0.4 mmol) were added at room temperature, and the reaction mixture was stirred overnight. After completion of the reaction, water (5 mL) was added and the mixture was extracted with EtOAc (3x5 mL). The organic layer was washed with water (7x5 mL) and brine, dried over Na_2SO_4, filtered and concentrated under reduced pressure to give a crude product, which

was purified by column chromatography on silica (15% EtOAc/hexanes) to furnish **9** (103 mg, 84%).

Compound **9**: light brown oil; IR (UATR, cm^{-1}): 2977, 1760, 1588; ^{1}H NMR (300 MHz, $CDCl_3$), δ (ppm): 7.45 (d, *J* = 8.4 Hz, 1H), 7.33 (d, *J* = 16.5 Hz, 1H), 6.90 (d, *J* = 16.5 Hz, 1H), 6.68 (d, *J* = 1.5 Hz, 1H), 6.62 (d, *J* = 1.8 Hz, 1H), 6.48 (dd, *J* = 8.7, 2.4 Hz, 1H), 6.45 (d, *J* = 2.1 Hz, 1H), 6.36 (t, *J* = 2.2 Hz, 1H), 4.62 (s, 2H), 4.54 (m, 3H), 4.26 (q, *J* = 7.1 Hz, 2H), 1.38 (d, *J* = 6 Hz, 6H), 1.344 (d, *J* = 6 Hz, 6H), 1.339 (d, *J* = 6 Hz, 6H), 1.30 (t, *J* = 6.8 Hz, 3H); ^{13}C NMR (75 MHz, $CDCl_3$), δ (ppm): 168.9, 159.0, 158.7, 156.6, 140.7, 127.4, 126.3, 124.6, 120.1, 107.6, 107.3, 104.7, 102.9, 101.4, 70.9, 69.9, 65.5, 61.8, 61.3, 22.1, 22.0, 14.1; TOF-HRMS *m/z* $[M+Na]^+$, calcd for $C_{27}H_{36}NaO_6$: 479.2404; found: 479.2388.

2.1.3.5. 3′-*O*-Carbethoxymethyl-2,4,5′-trihydroxystilbene (**10**)

A solution of BCl_3 (3.07 mL, 3. 07 mmol) was added to a solution of **9** (233 mg, 0.51 mmol) in CH_2Cl_2 (8 mL) at −78 °C under argon. Then it was allowed to warm to room temperature and stirred overnight. The reaction mixture was quenched with water (10 mL) and then extracted with EtOAc (3x10 mL). The organic phase was washed with brine, dried over Na_2SO_4, filtered and concentrated under reduced pressure to give a crude product which was purified by preparative TLC (50% EtOAc/hexanes) to give **10** (102 mg, 61%).

Compound **10**: pale yellow solid, mp 198-200 °C; IR (UATR, cm^{-1}): 3369, 1731, 1591; ^{1}H NMR (300 MHz, acetone-d_6), δ (ppm): 7.43 (d, *J* = 8.4 Hz, 1H), 7.36 (d, *J* = 16.5 Hz, 1H), 6.97 (d, *J* = 16.5 Hz, 1H), 6.70 (br s,1H), 6.63 (br s,1H), 6.49 (d, *J* = 2.1 Hz, 1H), 6.49 (br s, 1H), 6.43 (dd, *J* = 8.4, 2.1 Hz, 1H), 6.34 (t, *J* = 2.1 Hz, 1H), 4.70 (s, 2H), 4.21 (q, *J* = 6.9 Hz, 2H), 1.25 (t, *J* = 6.9 Hz, 3H); ^{13}C NMR (75 MHz, acetone-d_6), δ (ppm): 169.4, 160.4, 159.4, 159.1, 156.9, 141.7, 128.4, 126.0, 124.9, 117.1, 108.4, 107.1, 104.4, 103.5, 101.6, 65.8, 61.3, 14.4; TOF-HRMS *m/z* $[M+Na]^+$, calcd for $C_{18}H_{18}NaO_6$: 353.0996; found: 353.0989.

2.1.3.6. 3′-*O*-Carboxymethyl-2,4,5′-trihydroxystilbene (**11**)

To **10** (13 mg, 0.03 mmol), KOH (5% in EtOH, 1 mL) was added at room temperature, and the reaction mixture was stirred for 10 min. The reaction was acidified with 2 N HCl to pH 5. The material was extracted with EtOAc (3x5 mL), and the combined organic layers were dried over Na_2SO_4, filtered, and concentrated under reduced pressure to provide **11** (3 mg, 40%).

Compound **11**: brown solid; IR (UATR, cm^{-1}): 3322, 2921, 2851, 1713; ^{1}H NMR (300 MHz, methanol-d_4), δ (ppm): 7.33 (d, *J* = 8.9 Hz, 1H), 7.30 (d, *J* = 16.4 Hz, 1H), 6.86 (d, *J* = 16.4 Hz, 1H), 6.58 (d, *J* = 1.6 Hz, 1H), 6.56 (d, *J* = 1.8 Hz, 1H), 6.31 (dd, *J* = 5.9, 2.3 Hz, 1H), 6.30 (s, 1H), 6.25 (t, *J* = 2.1 Hz, 1H), 4.63(s, 2H); ^{13}C NMR (75 MHz, methanol-d_4), δ (ppm):172.9, 160.8, 159.7, 159.4, 157.4, 142.4, 128.5, 126.2, 125.4, 117.7, 108.4, 107.3, 104.8, 103.6, 101.7, 65.9; TOF-HRMS *m/z* $[M-H]^-$, calcd for $C_{16}H_{13}O_6$: 301.0718; found: 301.0708.

2.1.3.7. 2′-Chloro-2,3′,4,5′-tetrahydroxystilbene (**12**)

A mixture of **1** (100 mg, 0.41 mmol) and *N*-chlorosuccinimide (54.8 mg, 0.41 mmol) in glacial acetic acid (4 mL) was stirred at room temperature under argon for 3 h. After completion, solvent was removed under reduced pressure. Purification by column chromatography (10% MeOH/CH_2Cl_2) gave of **12** (42 mg, 36% yield).

Compound **12**: light brown solid, mp 185-187 °C; IR (UATR, cm^{-1}): 3196, 1599; ^{1}H NMR (300 MHz, acetone-d_6), δ (ppm): 7.44 (d, *J* = 8.4 Hz, 1H), 7.38 (d, *J* = 16.4 Hz, 1H), 7.32 (d, *J* = 16.4 Hz, 1H), 6.78 (d, *J* = 2.7 Hz, 1H), 6.45 (d, *J* = 2.4 Hz, 1H), 6.43 (d, *J* = 2.7 Hz, 1H), 6.41 (dd, *J* = 8.4, 2.4 Hz, 1H); ^{13}C NMR (75 MHz, acetone-d_6), δ (ppm): 158.6, 156.5, 156.3, 153.9, 137.9, 127.9, 126.3, 121.3, 116.2, 110.4, 107.6, 103.8, 102.7, 102.3; TOF-HRMS *m/z* $[M+H]^+$, calcd for $C_{14}H_{12}ClO_4$: 279.0419; found: 279.0408.

2.1.3.8. 2′-Chloro-2,3′,4,5′-tetramethoxystilbene (**13**)

To a well-stirred solution of **12** (88 mg, 0.3 mmol) in acetone (15 mL), K_2CO_3 (265 mg, 1.92 mmol) and MeI (0.11 mL, 1.8 mmol) were added. The reaction mixture was stirred at 55 °C overnight and monitored by TLC. After completion of the reaction, the mixture was diluted with water (10 mL), and extracted with EtOAc (3x10 mL). The organic phase was washed with brine. The organic extract was dried over Na_2SO_4, filtered and evaporated in vacuo. The residue obtained was purified over silica gel using 20% EtOAc/hexanes to furnish **13** (40 mg, 36%).

Compound **13**: white solid; ^{1}H NMR (300 MHz, $CDCl_3$), δ (ppm): 7.56 (d, *J* = 8.4 Hz, 1H), 7.44 (d, *J* = 16.5 Hz, 1H), 7.33 (d, *J* = 16.5 Hz, 1H), 6.83 (d, *J* = 2.7 Hz, 1H), 6.52 (dd, *J* = 8.7, 2.1 Hz, 1H), 6.46 (d, *J* = 2.1 Hz, 1H), 6.42 (t, *J* = 2.7 Hz, 1H), 3.87 (s, 3H), 3.86 (s, 3H), 3.85 (s, 3H), 3.83 (s, 3H); ^{13}C NMR (75 MHz, $CDCl_3$), δ (ppm): 160.9, 158.6, 158.2, 155.9, 137.7, 127.7, 126.0, 123.2, 119.2, 113.8, 105.0, 101.9, 98.6, 98.4, 56.2, 55.6, 55.5, 55.4; TOF-HRMS *m/z* $[M]^+$, calcd for $C_{18}H_{20}ClO_4$: 335.1045; found: 335.1035.

2.1.3.9. 2′-Formyl-2,3′,4,5′-tetraisopropoxystilbene (**14**)

$POCl_3$ (0.16 mL, 1.69 mmol) was stirred with dry DMF (4 mL) at room temperature for 2 h under argon. A solution of **7** (200 mg, 0.48 mmol) in dry DMF (4 mL) was added at 0 °C and the reaction mixture was further stirred overnight. After completion of the reaction, cool water (10 mL) was added, and the mixture was extracted with EtOAc (3x10 mL). The organic layer was washed with water (7x10 mL) and brine, dried over Na_2SO_4, filtered and concentrated under reduced pressure to give a crude product, which was purified by column chromatography on silica (15% EtOAc/hexanes) to furnish **14** (171 mg, 80%).

Compound **14**: viscous yellow oil; IR (UATR, cm^{-1}): 2976, 1671, 1586; ^{1}H NMR (300 MHz, $CDCl_3$), δ (ppm): 10.53 (s, 1H), 8.08 (d, *J* = 16.4 Hz, 1H), 7.60 (d, *J* = 8.6 Hz, 1H), 7.30 (d, *J* = 16.4 Hz, 1H), 6.75 (d, *J* = 2.1 Hz, 1H), 6.50 (dd, *J* = 8.6, 2.3 Hz, 1H), 6.44 (d, *J* = 2.4 Hz, 1H), 6.35 (d, *J* = 2.1 Hz, 1H), 4.69 (sept, *J* = 6 Hz, 1H), 4.48-4.63 (m, 3H), 1.33-1.41 (m, 24H); ^{13}C NMR

(75 MHz, $CDCl_3$), δ (ppm): 191.1, 163.6, 162.7, 158.9, 156.7, 143.9, 128.1, 127.3, 125.4, 120.4, 116.8, 107.4, 105.0, 102.9, 100.1, 71.4, 70.9, 70.1, 69.9, 22.2, 22.04, 21.98; TOF-HRMS *m/z* $[M+H]^+$, calcd for $C_{27}H_{37}O_5$: 441.2635; found: 441.2639.

2.1.3.10. 2′-Carboxy-2,3′,4,5′-tetraisopropoxystilbene (**15**)

A solution of $NaClO_2$ (260 mg, 2.88 mmol) and $NaH_2PO_4 \cdot 2H_2O$ (447 mg, 2.86 mmol) in water (1.5 mL) was added to the solution of **14** (157 mg, 0.36 mmol) and 2-methyl-2-butene (0.13 mL, 1.5 mmol) in acetone (1.5 mL) at room temperature. The reaction mixture was stirred for 1 h. After completion, water (5 mL) was added, and the reaction mixture was extracted with EtOAc (3x5 mL). The EtOAc phase was washed with brine, dried over Na_2SO_4, filtered and concentrated under reduced pressure to give crude product, which was purified by column chromatography on silica (40% EtOAc/hexanes) to furnish **15** (129 mg, 79%).

Compound **15**: pale yellow solid, mp 154-156 °C; IR (UATR, cm^{-1}): 2976, 1730, 1697, 1592; ^1H NMR (300 MHz, $CDCl_3$), δ (ppm): 7.85 (d, *J* = 16.2 Hz, 1H), 7.56 (d, *J* = 8.4 Hz, 1H), 7.19 (d, *J* = 16.2 Hz, 1H), 6.85 (d, *J* = 2.1 Hz, 1H), 6.49 (dd, *J* = 8.4, 2.1 Hz, 1H), 6.44 (d, *J* = 2.1 Hz, 1H), 6.42 (d, *J* = 2.1 Hz, 1H), 4.68 (m, 2H), 4.54 (m, 2H), 1.44 (d, *J* = 6.3 Hz, 6H), 1.40 (d, *J* = 6.3 Hz, 6H), 1.37 (d, *J* = 6.3 Hz, 6H), 1.34 (d, *J* = 6 Hz, 6H); ^{13}C NMR (75 MHz, $CDCl_3$), δ (ppm): 166.0, 160.9, 158.8, 158.0, 156.6, 145.6, 128.1, 126.6, 126.5, 120.4, 107.4, 103.0, 101.5, 74.1, 71.0, 70.2, 70.0, 22.2, 22.1, 22.0, 21.9; TOF-HRMS *m/z* $[M+H]^+$, calcd for $C_{27}H_{37}O_6$: 457.2585; found: 457.2587.

2.1.3.11. 2′-Formyl-2,3′,4,5′-tetrahydroxystilbene (**16**)

A solution of BCl_3 (2.17 mL, 2.17 mmol) was added to a solution of **14** (119 mg, 0.27 mmol) in CH_2Cl_2 (4 mL) at −78 °C under argon. The reaction was allowed to warm up to room temperature and stirred overnight. Then, water (5 mL) was added, and the reaction was extracted with EtOAc (3x5 mL). The EtOAc layer was washed with brine, dried over Na_2SO_4, filtered and concentrated under reduced pressure to give a crude product which was purified by using preparative TLC (40% EtOAc/hexanes) to give **16** (35 mg, 48%).

Compound **16**: yellow solid, decomposed > 218 °C; IR (UATR, cm^{-1}): 3337, 1602; ^1H NMR (300 MHz, methanol-d_4), δ (ppm): 10.17 (s, 1H), 7.55 (d, *J* = 15.9 Hz, 1H), 7.38 (d, *J* = 9 Hz, 1H), 7.23 (d, *J* = 15.9 Hz, 1H), 6.56 (d, *J* = 2 Hz, 1H), 6.33 (dd, *J* = 8.6, 2.3 Hz, 1H), 6.32 (br s, 1H), 6.14 (d, *J* = 2 Hz, 1H); ^{13}C NMR (75 MHz, methanol-d_4), δ (ppm): 194.3, 167.3, 167.2, 160.1, 158.0, 148.0, 131.8, 129.6, 120.4, 117.2, 112.8, 108.5, 107.4, 103.6, 102.0; TOF-HRMS *m/z* $[M-H]^-$, calcd for $C_{15}H_{11}O_5$: 271.0612; found: 271.0607.

2.1.3.12. 2′-Hydroxy-2,3′,4,5′-tetraisopropoxystilbene (**17**)

Compound **14** (121 mg, 0.27 mmol) and *p*-$TsOH \cdot H_2O$ (15 mg, 0.09 mmol) were dissolved in methanol (1 mL). Then 30% hydrogen peroxide (0.07 mL, 0.54 mmol) was added at 0 °C, and the reaction was then warmed to room temperature and stirred for 1 h. Half-saturated sodium sulfite

solution (1 mL) was added, and the mixture was extracted with CH_2Cl_2 (3x5 mL). The organic phase was washed with brine, dried over Na_2SO_4, filtered and concentrated under reduced pressure to give a crude product. Purification with preparative TLC (10% EtOAc/hexanes) gave **17** (78 mg, 66%).

Compound **17**: pale yellow solid; IR (UATR, cm^{-1}): 3536, 2975, 1600; ^1H NMR (300 MHz, CDCl3), δ (ppm): 7.53 (d, *J* = 8.4 Hz, 1H), 7.38 (d, *J* = 16.8 Hz, 1H), 7.32 (d, *J* = 16.5 Hz, 1H), 6.74 (d, *J* = 2.7 Hz, 1H), 6.48 (dd, *J* = 10.8, 2.4 Hz, 1H), 6.46 (br s, 1H), 6.40 (d, *J* = 2.4 Hz, 1H), 4.49 (m, 4H), 1.31-1.40 (m, 24H); ^{13}C NMR (75 MHz, $CDCl_3$), δ (ppm): 158.4, 156.5, 150.7, 145.0, 138.8, 127.4, 124.6, 124.1, 121.1, 120.8, 107.5, 104.9, 103.3, 102.6, 71.8, 71.1, 71.0, 69.9, 22.2, 22.14, 22.13, 22.10; TOF-HRMS *m/z* $[M+H]^+$, calcd for $C_{26}H_{37}O_5$: 429.2635; found: 429.2643.

2.1.3.13. 3-(2,4-Dihydroxyphenyl)-6,8-dihydroxyisochroman-1-one (**18**)

To a solution of **15** (104 mg, 0.23 mmol) in dry CH_2Cl_2 (2 mL), a solution of BBr_3 (0.96 mL, 0.96 mmol) in CH_2Cl_2 was added under argon at −78 °C, and the mixture was stirred for 20 min. After completion of the reaction, water (5 mL) was added, and the mixture was extracted with EtOAc (3x5 mL). The organic phase was washed with brine, dried over Na_2SO_4, filtered and concentrated under reduced pressure to give a crude product. Purification with column chromatography eluting with 5% MeOH/CH_2Cl_2 gave **18** (13 mg, 20%).

Compound **18**: light brown solid, mp 210-212 °C; IR (UATR, cm^{-1}): 3340, 3190, 1611; ^1H NMR (300 MHz, acetone-d_6), δ (ppm): 7.28 (d, *J* = 8.4 Hz, 1H), 6.48 (d, *J* = 2.1 Hz, 1H), 6.43 (dd, *J* = 8.4, 2.4 Hz, 1H), 6.35 (br s, 1H), 6.30 (d, *J* = 2.1 Hz, 1H), 5.83 (dd, *J* = 12, 3 Hz, 1H), 3.29 (dd, *J* = 16.5, 12.3 Hz, 1H), 3.04 (dd, *J* = 16.5, 3.3 Hz, 1H); ^{13}C NMR (75 MHz, acetone-d_6), δ (ppm): 171.1, 165.13, 165.07, 159.5, 156.3, 143.8, 128.9, 117.2, 107.9, 107.3, 103.4, 101.95, 101.88, 76.5, 34.4; TOF-HRMS *m/z* $[M+Na]^+$, calcd for $C_{15}H_{12}NaO_6$: 311.0526; found: 311.0529.

2.1.3.14. 2′-(*E*)-Carbethoxyethenyl-2,3′,4,5′-tetraisopropoxystilbene (**19**)

A solution of **14** in dry CH_2Cl_2 (4 mL) was added to $EtO_2CCH{=}PPh_3$ (176 mg, 0.51mmol) at 0 °C under argon. Then the reaction mixture was allowed to warm to room temperature and stirred overnight. After completion of the reaction, water (5 mL) was added, and the mixture was extracted with EtOAc (3x5 mL). The organic layer was washed with brine, dried over Na_2SO_4, filtered and concentrated under reduced pressure to give a crude product. Purification with column chromatography eluting with 50% CH_2Cl_2/hexanes gave **19** (134 mg, 68%).

Compound **19**: pale yellow oil; IR (UATR, cm^{-1}): 2977, 2932, 1706, 1589; ^1H NMR (300 MHz, $CDCl_3$), δ (ppm): 8.03 (d, *J* = 16.2 Hz, 1H), 7.45 (d, *J* = 8.4 Hz, 1H), 7.37 (d, *J* = 16.2 Hz, 1H), 7.15 (d, *J* = 16.2 Hz, 1H), 6.70 (d, *J* = 2.1 Hz, 1H), 6.50 (d, *J* = 16.2 Hz, 1H), 6.49 (dd, *J* = 8.4, 2.4 Hz, 1H), 6.48 (br s, 1H), 6.39 (d, *J* = 2.1 Hz, 1H), 4.58 (m, 4H), 4.24 (q, *J* = 7.1 Hz, 2H), 1.28-1.40 (m, 27H); ^{13}C NMR (75 MHz, $CDCl_3$), δ (ppm): 168.2, 159.4, 158.7, 156.7, 142.3, 139.0, 128.4, 127.4, 125.6, 120.3, 120.1, 115.8, 107.2, 105.6, 102.8, 100.8, 71.0, 70.7, 69.9, 69.8, 59.9,

22.09, 22.04, 22.00, 14.3; TOF-HRMS *m/z* $[M+H]^+$, calcd for $C_{31}H_{43}O_6$: 511.3054; found: 511.3077.

2.1.3.15. 3′,5′-Diacetoxy-2,4-diisopropoxystilbene (**20**)

Et_3N (0.05 mL, 0.33 mmol) and acetic anhydride (0.03 mL, 0.33 mmol) were added to a solution of **5** (50 mg, 0.15 mmol) in CH_2Cl_2 (2 mL) at room temperature. The reaction mixture was stirred for 2 h. Water (5 mL) was added, and the reaction mixture was extracted with EtOAc (3x5 mL). The organic phase was washed with brine, dried over Na_2SO_4, filtered and concentrated under reduced pressure to give a crude product. Purification with column chromatography eluting with 20% EtOAc/hexanes gave **20** (46 mg, 74%).

Compound **20**: white solid, mp 65-67 °C; IR (UATR, cm^{-1}): 2978, 1768, 1599; ^1H NMR (300 MHz, $CDCl_3$), δ (ppm): 7.41 (d, *J* = 8.4 Hz, 1H), 7.34 (d, *J* = 16.5 Hz, 1H), 7.08 (d, *J* = 2.1 Hz, 2H), 6.94 (d, *J* = 16.2 Hz, 1H), 6.78 (t, *J* = 2.1 Hz, 1H), 6.46 (dd, *J* = 8.1, 2.4 Hz, 1H), 6.45 (br s, 1H), 4.51 (m, 2H), 2.25 (s, 6H), 1.36 (d, *J* = 6 Hz, 6H), 1.31 (d, *J* = 6 Hz, 6H); ^{13}C NMR (75 MHz, $CDCl_3$), δ (ppm): 168.7, 158.8, 156.6, 151.0, 140.7, 127.6, 125.8, 124.6, 119.4, 116.3, 113.3, 106.9, 102.5, 70.6, 69.7, 21.9, 21.8, 20.8; TOF-HRMS *m/z* $[M+Na]^+$, calcd for $C_{24}H_{28}NaO_6$: 435.1778; found: 435.1796.

2.1.3.16. 3′,5′-Diacetoxy-5-formyl-2,4-diisopropoxystilbene (**21**)

$POCl_3$ (0.16 mL, 1.77 mmol) was stirred with dry DMF (1 mL) at room temperature for 2 h under argon. The solution of **20** (73 mg, 0.18 mmol) in dry DMF (1 mL) was added at 0 °C. Then the reaction mixture was allowed to warm to room temperature and stirred overnight. After completion of the reaction, cool water (5 mL) was added, and the reaction mixture was extracted with EtOAc (3x5 mL). The organic layer was washed with water (7x5 mL) and brine, dried over Na_2SO_4, filtered and concentrated under reduced pressure to give a crude product, which was purified by preparative TLC (20% EtOAc/hexanes) to furnish **21** (46 mg, 60%).

Compound **21**: viscous yellow oil; IR (UATR, cm^{-1}): 2979, 1768, 1671, 1593; ^1H NMR (300 MHz, $CDCl_3$), δ (ppm): 10.32 (s, 1H), 8.03 (s, 1H), 7.27 (d, *J* = 16.5 Hz, 1H), 7.08 (d, *J* = 1.8 Hz, 2H), 7.03 (d, *J* = 16.5 Hz, 1H), 6.81 (t, *J* = 2.1 Hz, 1H), 6.44 (s, 1H), 4.66 (m, 2H), 2.29 (s, 6H), 1.43 (d, *J* = 6 Hz, 6H), 1.40 (d, *J* = 6 Hz, 6H); ^{13}C NMR (75 MHz, $CDCl_3$), δ (ppm): 188.1, 168.7, 161.8, 161.4, 151.0, 140.1, 126.6, 126.3, 124.2, 119.6, 118.8, 116.4, 113.8, 98.1, 71.2, 70.9, 21.67, 21.66, 20.8; TOF-HRMS *m/z* $[M+Na]^+$, calcd for $C_{25}H_{28}NaO_7$: 463.1727; found: 463.1743.

2.1.3.17. 3′,5′-Diacetoxy-5-carboxy-2,4-diisopropoxystilbene (**22**)

A solution of $NaClO_2$ (85 mg, 0.93 mmol) and $NaH_2PO_4 \cdot 2H_2O$ (145 mg, 0.93 mmol) in water (0.5 mL) was added to a solution of **21** (51 mg, 0.12 mmol) and 2-methyl-2-butene (0.04 mL, 0.49 mmol) in acetone (0.5 mL) at room temperature. The reaction mixture was stirred for 1 h. After completion, water (5 mL) was added, and the reaction mixture was extracted with EtOAc (3x5 mL). The organic layer was washed with brine, dried over Na_2SO_4, filtered and concentrated under

reduced pressure to give a crude product, which was purified by column chromatography on silica (40% EtOAc/hexanes) to furnish **22** (39 mg, 73%).

Compound **22**: white solid, mp 106-108 °C; IR (UATR, cm^{-1}): 3267, 2980, 1769, 1732, 1601; ^{1}H NMR (300 MHz, $CDCl_3$), δ (ppm): 8.35 (s, 1H), 7.26 (d, *J* = 16.5 Hz, 1H), 7.09 (d, *J* = 2.1 Hz, 2H), 7.08 (d, *J* = 16.5 Hz, 1H), 6.82 (t, *J* = 2.1 Hz, 1H), 6.50 (s, 1H), 4.83 (sept, *J* = 6 Hz, 1H), 4.65 (sept, *J* = 6 Hz, 1H), 2.31 (s, 6H), 1.51 (d, *J* = 6 Hz, 6H), 1.45 (d, *J* = 6 Hz, 6H); ^{13}C NMR (75 MHz, $CDCl_3$), δ (ppm): 168.9, 165.3, 160.2, 157.2, 151.2, 140.1, 132.1, 127.5, 123.9, 121.4, 116.8, 114.2, 110.9, 99.0, 74.2, 71.4, 21.92, 21.88, 21.0; TOF-HRMS *m/z* $[M+Na]^+$, calcd for $C_{25}H_{28}NaO_8$: 479.1676; found: 479.1695.

2.1.3.18. 5-Formyl-2,3′,4,5′-tetrahydroxystilbene (**23**)

A solution of BCl_3 (0.42 mL, 0.42 mmol) was added to a solution of **21** (30 mg, 0.07 mmol) in CH_2Cl_2 (2 mL) at −78 °C under argon. Then it was allowed to warm to room temperature and stirred overnight. Water (5 mL) was then added, and the reaction mixture was extracted with EtOAc (3x5 mL). The EtOAc was washed with brine, dried over Na_2SO_4, filtered and concentrated under reduced pressure to give a crude product which was purified by preparative TLC (40% EtOAc/hexanes) to give **23** (15 mg, 78%).

Compound **23**: yellow solid, decomposed > 205 °C; IR (UATR, cm^{-1}): 3208, 1626; ^{1}H NMR (300 MHz, methanol-d_4), δ (ppm): 9.69 (s, 1H), 7.76 (s, 1H), 7.27 (d, *J* = 16.5 Hz, 1H), 6.95 (d, *J* = 16.5 Hz, 1H), 6.47 (d, *J* = 2.4 Hz, 2H), 6.25 (s, 1H), 6.16 (t, *J* = 2.1 Hz, 1H); ^{13}C NMR (75 MHz, methanol-d_4), δ (ppm): 194.9, 167.8, 164.8, 159.6, 141.6, 133.2, 128.4, 123.8, 121.0, 115.5, 105.9, 103.7, 102.7; TOF-HRMS *m/z* $[M-H]^-$, calcd for $C_{15}H_{11}O_5$: 271.0612; found: 271.0603.

2.1.3.19. 5-Carboxy-2,3′,4,5′-tetrahydroxystilbene (**24**)

A solution of BCl_3 (0.88 mL, 0.88 mmol) was added to a solution of **22** (68 mg, 0.15 mmol) in CH_2Cl_2 (2 mL) at −78 °C under argon. Then the reaction was allowed to warm to room temperature and stirred overnight. Water (5 mL) was added, and the mixture was extracted with EtOAc (3x5 mL). The organic layer was washed with brine, dried over Na_2SO_4, filtered and concentrated under reduced pressure to give a crude product which was purified by Sephadex LH20 (methanol) to give **24** (27 mg, 63%).

Compound **24**: yellow solid, decomposed > 230 °C; IR (UATR, cm^{-1}): 3337, 1616; ^{1}H NMR (300 MHz, methanol-d_4), δ (ppm): 8.01 (s, 1H), 7.24 (d, *J* = 16.5 Hz, 1H), 6.92 (d, *J* = 16.5 Hz, 1H), 6.49 (d, *J* = 2.1 Hz, 2H), 6.36 (s, 1H), 6.19 (t, *J* = 2.1 Hz, 1H); ^{13}C NMR (75 MHz, methanol-d_4), δ (ppm): 173.5, 164.2, 162.8, 159.6, 141.6, 130.0, 128.5, 123.8, 118.9, 106.3, 105.8, 103.3, 102.7; TOF-HRMS *m/z* $[M-H]^-$, calcd for $C_{15}H_{11}O_6$: 287.0561; found: 287.0549.

2.1.3.20. 5-Formyl-3′,5′-dihydroxy-2,4-diisopropoxystilbene (**25**)

To **21** (59 mg, 0.12 mmol), KOH (5% in EtOH, 1 mL) was added at room temperature, and the reaction mixture was stirred for 10 min. After completion of the reaction, the reaction was

extracted with EtOAc (3x5 mL). The EtOAc phase was washed with brine, dried over Na_2SO_4, filtered and concentrated under reduced pressure to give a crude product. Purification with column chromatography eluting with 50% EtOAc in hexanes gave **25** (41 mg, 93%).

Compound **25**: yellow solid, mp 186-188 °C; IR (UATR, cm^{-1}): 3355, 2979, 1588; ^1H NMR (300 MHz, acetone-d_6), δ (ppm): 10.32 (s, 1H), 7.99 (s, 1H), 7.30 (d, *J* = 16.5 Hz, 1H), 7.05 (d, *J* = 16.5 Hz, 1H), 6.80 (s, 1H), 6.59 (d, *J* = 2 Hz, 2H), 6.29 (t, *J* = 2 Hz, 1H), 4.91 (m, 2H), 1.43 (d, *J* = 6.3 Hz, 6H), 1.41 (d, *J* = 6.4 Hz, 6H); ^{13}C NMR (75 MHz, acetone-d_6), δ (ppm): 188.0, 162.7, 162.3, 159.6, 140.9, 129.2, 126.6, 122.9, 121.1, 120.1, 105.8, 102.9, 100.0, 72.1, 71.8, 22.2, 22.1; TOF-HRMS *m/z* $[M+H]^+$, calcd for $C_{21}H_{25}O_5$: 357.1696; found: 357.1712.

2.1.3.21. 5-Carboxy-3′,5′-dihydroxy-2,4-diisopropoxystilbene (**26**)

To **22** (30 mg, 0.07 mmol), KOH (5% in EtOH, 1 mL) was added at room temperature, and the reaction mixture was stirred for 10 min. The reaction was acidified with 2 N HCl to pH 5. The material was extracted with EtOAc (3x5 mL), and the combined organic layers were dried over Na_2SO_4, filtered, and concentrated under reduced pressure to provide **26** (10 mg, 40%).

Compound **26**: light brown solid, mp 112-114 °C; ^1H NMR (300 MHz, acetone-d_6), δ (ppm): 8.23 (s, 1H), 7.31 (d, *J* = 16 Hz, 1H), 7.07 (d, *J* = 16 Hz, 1H), 6.88 (s, 1H), 6.59 (d, *J* = 2 Hz, 2H), 6.30 (t, *J* = 2 Hz, 1H), 5.04 (sept, *J* = 6 Hz, 1H), 4.89 (sept, *J* = 6 Hz, 1H), 1.46 (d, *J* = 6.3 Hz, 6H), 1.43 (d, *J* = 6 Hz, 6H); ^{13}C NMR (75 MHz, acetone-d_6), δ (ppm): 165.7, 160.8, 159.6, 158.5, 140.8, 131.5, 129.6, 122.9, 122.0, 112.7, 108.0, 103.0, 101.1, 74.4, 71.9, 22.2, 22.1; TOF-HRMS *m/z* $[M-H]^-$, calcd for $C_{21}H_{23}O_6$: 357.1500; found: 371.1502.

2.1.3.22. 3′,5′-Diacetoxy-5-hydroxy-2,4-diisopropoxystilbene (**27**)

A solution of 30% hydrogen peroxide (0.03 mL, 0.192 mmol) was added to a methanolic mixture of **21** (44 mg, 0.10 mmol) and *p*-TsOH·H_2O (5 mg, 0.03 mmol) at 0 °C. The reaction mixture was allowed to warm to room temperature and stirred for 1 h. Half-saturated sodium sulfite solution (1 mL) was added, and the mixture was extracted with CH_2Cl_2 (3x5 mL). The CH_2Cl_2 layer was washed with brine, dried over Na_2SO_4, filtered and concentrated under reduced pressure to give a crude product. Purification with preparative TLC (30% EtOAc/hexanes) gave **27** (19 mg, 47%).

Compound **27**: pale yellow solid, mp 138-140 °C; IR (UATR, cm^{-1}): 3525, 2977, 1767; ^1H NMR (300 MHz, $CDCl_3$), δ (ppm): 7.34 (d, *J* = 16.2 Hz, 1H), 7.13 (s, 1H), 7.07 (d, *J* = 2.1 Hz, 2H), 6.87 (d, *J* = 16.2 Hz, 1H), 6.79 (t, *J* = 1.8 Hz, 1H), 6.50 (s, 1H), 4.54 (sept, *J* = 6 Hz, 1H), 4.33 (sept, *J* = 6 Hz, 1H), 2.30 (s, 6H), 1.36 (d, *J* = 6.3 Hz, 6H), 1.34 (d, *J* = 6.3 Hz, 6H); ^{13}C NMR (75 MHz, $CDCl_3$), δ (ppm): 169.0, 151.1, 149.4, 145.0, 141.4, 140.6, 125.3, 125.2, 120.9, 116.5, 113.7, 111.3, 103.7, 73.3, 71.8, 22.2, 22.0, 21.0; TOF-HRMS *m/z* $[M+Na]^+$, calcd for $C_{24}H_{28}NaO_7$: 451.1727; found: 451.1723.

2.2. Biological activities

In this study, statistical analysis of the biological data was performed using the Student's *t*-test. All results were expressed as arithmetic mean ± standard deviation (SD).

2.2.1. DPPH radical assay

The experiment was performed according to an established method (Likhitwitayawuid et al., 2006b). The experiment was performed in a 96-well plate. The reduction of the DPPH was measured by reading the absorbance at 510 nm with a Perkin Elmer Victor^3 multilabel counter. Oxyresveratrol and Trolox were used as positive controls.

2.2.2. Superoxide radical assay

The assay was based on the capacity of the sample to inhibit the reduction of nitroblue tetrazolium (NBT) in the riboflavin-light-NBT system (Chatsumpun et al. 2011; Dasgupta et al., 2004). Oxyresveratrol and Trolox were used as positive controls.

2.2.3. Inhibitory effect on supercoiled DNA breakage

The assay was performed as previously described (Chatsumpun et al. 2011). This assay measured the ability of the test sample to protect DNA against damage induced by the photochemical reaction of riboflavin, with oxyresveratrol and Trolox used as positive controls.

2.2.4. Determination of anti-herpes simplex virus activity

Anti-HSV activities of the compounds were determined using a modified plaque reduction assay, with acyclovir as a positive control (Lipipun et al., 2003).

2.2.5 Neuraminidase (NA) inhibition assay

All of the samples were evaluated for NA inhibition by the Bioassay Services of The National Center for Genetic Engineering and Biotechnology (BIOTEC). This assay was performed using the method previously described by Potier and co-workers (Poiter et al., 1979). The fluorescence was measured using SpectraMax M5 multi-detection microplate reader (Molecular Devices, USA) with excitation and emission wave lengths of 365 and 450 nm, respectively. Oseltamivir was used as a positive control.

2.2.6. Determination of α-glucosidase inhibitory activity

The assay was performed in a 96-well plate and based on the capacity of the sample to inhibit the hydrolysis of *p*-nitrophenyl-α-D-glucoside (PNPG) by α-glucosidase to release *p*-nitrophenol (PNP), a yellow color agent that can be monitored at 405 nm (He et al., 2013). Acarbose was used as a positive control.

2.2.7. Determination of cytotoxic activity

The assays for cytotoxicity were carried out according to a previous report (Tangdenpaisal et al., 2015). Cell viability was determined using MTT assay. Doxorubicin was used as the positive control.

3. Results and Discussion

3.1. Chemistry

3.1.1. *O*-Alkylation/*O*-Acylation

When **1** was allowed to react with MeI in acetone at room temperature, di-, tri- and tetra-*O*-methylated products (**2**, **3** and **4**) were obtained in 9%, 25%, and 45% yields, respectively (Scheme 1).

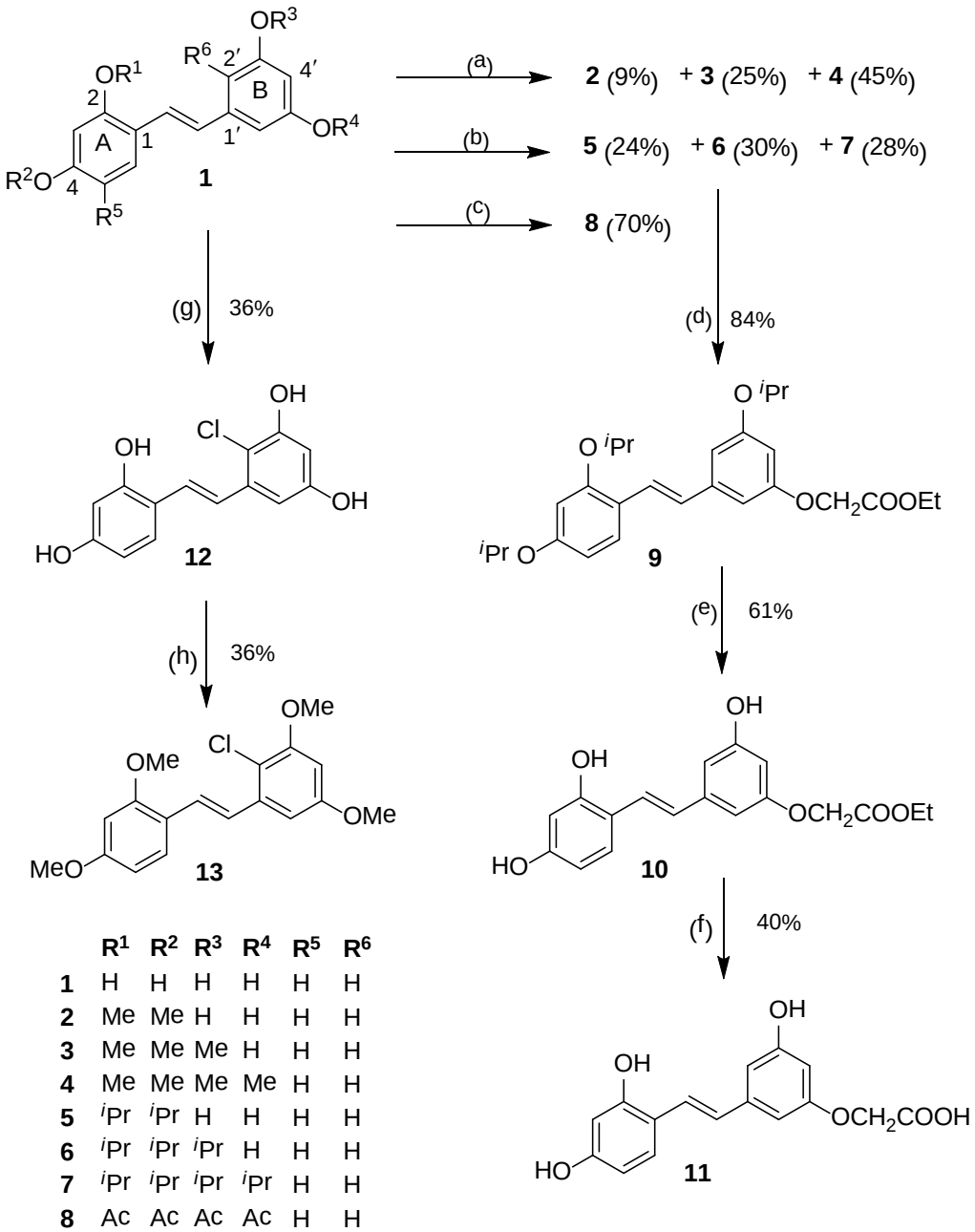

	R1	R2	R3	R4	R5	R6
1	H	H	H	H	H	H
2	Me	Me	H	H	H	H
3	Me	Me	Me	H	H	H
4	Me	Me	Me	Me	H	H
5	*i*Pr	*i*Pr	H	H	H	H
6	*i*Pr	*i*Pr	*i*Pr	H	H	H
7	*i*Pr	*i*Pr	*i*Pr	*i*Pr	H	H
8	Ac	Ac	Ac	Ac	H	H

Scheme 1. Reagent and condition: (a) MeI, K_2CO_3, acetone, rt; (b) 2-bromopropane, K_2CO_3, DMF, 55 °C; (c) AcCl, Et_3N, DMAP, CH_2Cl_2, rt; (d) ethyl bromoacetate, K_2CO_3, DMF, rt; (e) BCl_3, CH_2Cl_2, −78 °C → rt, Ar; (f) 5% KOH, EtOH, rt; (g) NCS, AcOH (glacial), rt; (h) MeI, K_2CO_3, acetone, 55 °C.

The alkylation of **1** with 2-bromopropane/K_2CO_3 in DMF gave the corresponding di-, tri- and tetra-*O*-isopropyl compounds (**5, 6** and **7**) in 24%, 30%, and 28% yields, respectively (Scheme 1). It should be noted that it was difficult to avoid the formation of **7**, perhaps due to the greater solubility of the more alkylated ethers in DMF under the reaction conditions. In both *O*-alkylation reactions, the di-*O*-alkylation occurred on the two hydroxy groups of ring A, and tri-*O*-alkylation occupied both hydroxy groups of ring A and a hydroxy group of ring B. These results suggested that the phenolic groups on ring A were more reactive than their counterparts on ring B, most likely due to the conjugation of the hydroxy groups of ring A with the olefinic bond, which is not possible for those on ring B. This difference in the reactivity of the hydroxy groups was exploited in the subsequent studies on the aromatic electrophilic substitution reactions, in which the isopropyl group was found to be a better *O*-protecting group than the methyl after some experimentation (see below). Acetylation of **1** with AcCl gave **8** in 70% yield.

O-Alkylation of the tri-*O*-isopropyl compound **6** with ethyl bromoacetate under basic conditions went smoothly, in 84% yield, to furnish the ethyl ester **9**, which then underwent BCl_3-mediated deprotection of the isopropyl groups to give the tri- hydroxyl compound **10** in 61% yield. Subsequent saponification of the ethyl ester using 5% KOH in ethanol provided the corresponding acid **11** in moderate 40% yield (Scheme 1).

3.1.2. Halogenation

It was expected that aromatic halogenation on **1** would be facile due to the high electron density contributed by the hydroxy groups. Due to the conjugation between the hydroxy groups on ring A and the olefin, the aromatic B ring should be more nucleophilic, particularly at the position 2′/6′, and this difference should give rise to regioselective electrophilic aromatic halogenation under appropriate and mild conditions. Using *N*-chlorosuccinimide (NCS) and glacial acetic acid, the corresponding 2′-mono-chlorinated product **12** was obtained from **1** in 36% yield (Scheme 1). Chlorination on **7** and **20** (prepared from **5**, Scheme 3) did not give the desired chlorinated product. Compound **12** smoothly underwent full methylation to give the tetramethylether **13** in 36% yield. Several attempts to carry out aromatic bromination on **1** or **4** with *N*-bromosuccinimide under various conditions were made, but failed to give the brominated product. Iodination of **1** with *N*-iodosuccinimide was not also successful.

3.1.3. Aromatic electrophilic substitution

When the tetra-*O*-isopropyl compound (**7**) reacted under the Vilsmeier-Haack formylation condition, the corresponding ring B-formylated product **14** was obtained in good yield (80%) (Scheme 2).

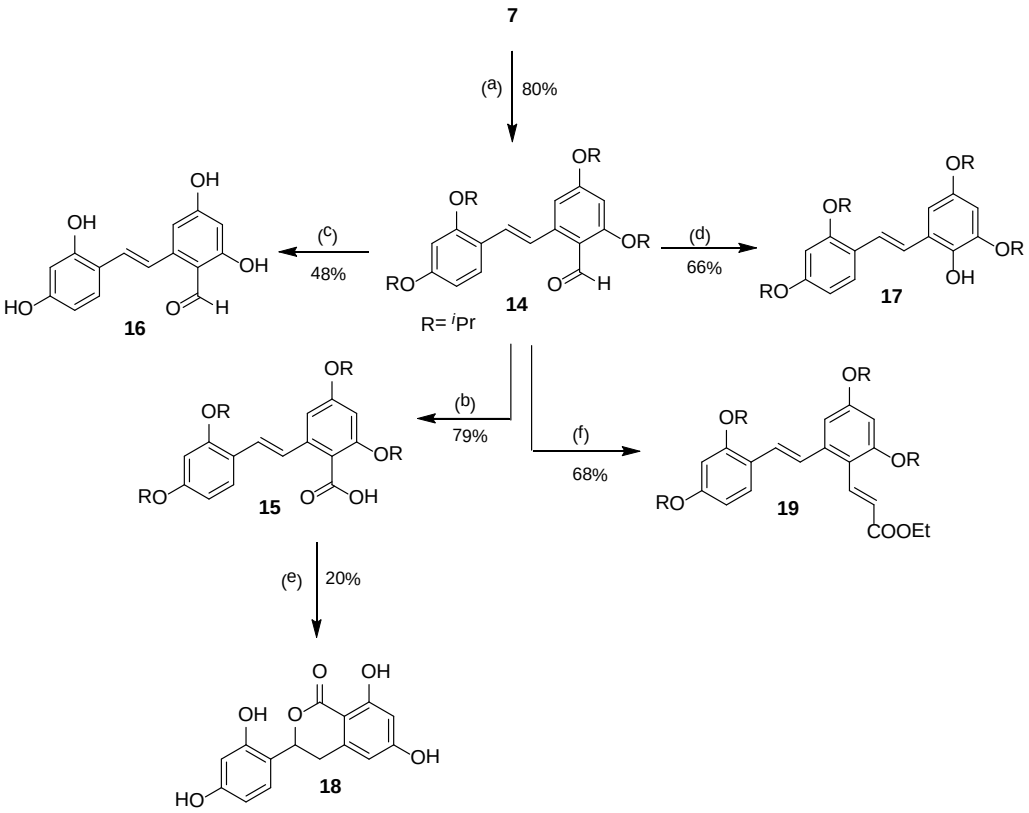

Scheme 2. Reagent and condition: (a) $POCl_3$, DMF, 0 °C, Ar; (b) $NaClO_2$, $NaH_2PO_4{\cdot}2H_2O$, 2-methyl-2-butene, acetone, rt; (c) BCl_3, CH_2Cl_2, −78 °C → rt, Ar; (d) *p*-TsOH·H_2O, H_2O_2, 0 °C, Ar; (e) BBr_3, CH_2Cl_2, −78 °C → rt, Ar; (f) EtOOCCH=PPh_3, CH_2Cl_2, 0 °C.

The aldehyde functional group could be further oxidized to the corresponding carboxylic acid **15** in 79% yield using sodium chlorite. The aldehyde **14** smoothly underwent BCl_3-mediated deprotection of the isopropyl groups to provide the 2′-formyloxyresveratrol **16** in moderate 48% yield. In addition, the aldehyde **14** could also undergo the acid-mediated Baeyer-Villiger-type, the Dakin reaction, which converted the aldehyde to the corresponding formate. Subsequent *in situ* cleavage of the formate under the reaction condition furnished 2′-hydroxy-tetra-*O*-isopropyl oxyresveratrol **17** in good yield of 66%. Unfortunately, any attempt to deprotect the isopropyl groups of **17** failed; only a mixture of decomposed products was obtained. The deisopropylation of **15** with BBr_3 under similar conditions gave the unexpected isochromanone **18** in 20% yield, a result of the Lewis acid-mediated removal of the *O*-isopropyl groups followed by C-O bond formation on the olefinic carbon of the stilbene system. In addition, the aldehyde **14** could undergo a smooth Wittig olefination to furnish the stilbenyl cinnamate **19** in 68% yield.

In order to affect the reactions on ring A of oxyresveratrol, the di-*O*-isopropyl compound **5** was acetylated under standard condition to provide ring A-di-*O*-isopropyl ring B-di-*O*-acetyl compound **20** in 74% yield (Scheme 3).

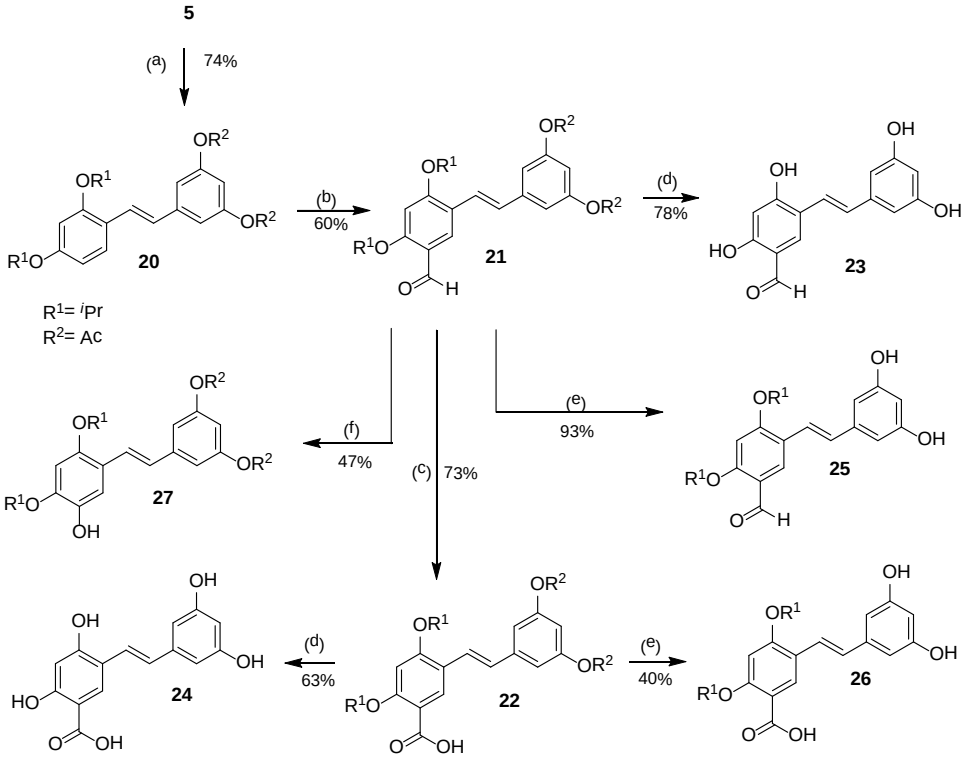

Scheme 3. Reagent and condition: (a) Ac_2O, Et_3N, CH_2Cl_2, rt; (b) $POCl_3$, DMF, 0 °C, Ar; (c) $NaClO_2$, $NaH_2PO_4{\cdot}2H_2O$, 2-methyl-2-butene, acetone, rt; (d) BCl_3, CH_2Cl_2, −78 °C → rt, Ar; (e) 5% KOH, EtOH, rt; (f) *p*-$TsOH{\cdot}H_2O$, H_2O_2, 0 °C.

After some experimentation, ring A was formylated on the 5-position to give **21** exclusively, in 60% yield under the best Vilsmeier-Haack condition (10 eq of $POCl_3$ at 0 °C → rt overnight under argon). Subsequent oxidation of the aldehyde **21** to the corresponding acid **22**, using sodium chlorite, gave the acid in 73% yield. BCl_3-mediated cleavage of all the *O*-isopropyl groups as well as the *O*-acetyl groups of **21** and **22** finally gave the desired 5-formyl- and 5-carboxy-oxyresveratrol **23** and **24** in 78% and 63% yields, respectively. Saponification of **21** and **22** using 5% KOH in ethanol to cleave the acetate groups gave 5-formyl- and 5-carboxy-di-*O*-isopropyl oxyresveratrol **25** and **26** in 93% and 40% yields, respectively. The aldehyde **21** was subjected to the Dakin reaction to give 5-hydroxy-di-*O*-acetyl-di-*O*-isopropyl oxyresveratrol **27** in 47% yield.

It is worth noting that the difference of the protecting groups could be used to manipulate the selectivity of the aromatic electrophilic reaction. In the Vilsmeier-Haack reaction of the tetra-*O*-isopropyl compound **7**, all the protecting groups were electron-donating groups, which effected the 2′ and 6′ position of ring B to be the most reactive position. But in the Vilsmeier-Haack reaction of the di-*O*-acetyl-di-*O*-isopropyl compound **20**, the acetyl groups were electron-withdrawing groups, and thus reduced the electron density of ring B. This was virtually equivalent to the deactivation of ring B, and therefore directed the formylation to occur on ring A. This synthetic strategy could be

a useful tool for the synthesis of other similar analogs derivable from exploiting the difference in electron density of each aromatic ring.

3.2. Biological activity

Since **1** was previously studied and reported to exhibit an array of biological activities including antioxidant activity and inhibitions against α-glucosidase, neuraminidase enzymes and HSV-1 (vide supra), all structurally modified analogs of **1** were subjected to the related assays to study the effects of such modification on each biological activity. In addition, these compounds were also evaluated for cytotoxic potential against four cancer cell lines of three different cancer types (breast, cervical and lung).

3.2.1. Antiherpetic activity

Compounds **1** – **27** were first evaluated for anti-HSV-1 activity at 100 μg/mL. Those that showed > 50 % inhibition at this concentration were further studied to determine their IC_{50} values (Table 2.1).

Table 2.1 Anti-herpetic activity of **1** and derivatives

Compounds	IC_{50} (μM)
1	147.1 ± 16.8
2	40.2 ± 6.8*
3	32.8 ± 5.9*
6	107.0 ± 9.8*
10	182.3 ± 28.9
14	130.3 ± 14.9
15	123.5 ± 19.3
18	289.3 ± 40.8*
21	188.3 ± 25.1
22	207.4 ± 16.9*
23	344.7 ± 32.5*
26	226.8 ± 35.7*
ACV	1.6 ± 0.0*

*****Significantly different from that of **1** ($p < 0.05$).

Three analogs, including compounds **2**, **3**, and **6**, showed IC_{50} values significantly lower than that of **1**. Stilbenes **2** and **3** (di- and tri -*O*-methylated products of **1**) displayed 3- to 4-fold higher antiherpetic activity than the parent compound. Recently, compelling evidence has suggested that HSV-1 infection of neuronal and glial cells plays a pivotal role in the pathogenesis of Alzheimer's disease (AD), and the use of antiviral drugs in the treatment of AD has been proposed (Civitelli et al., 2015). As mentioned earlier, **1**, despite its moderate anti-herpetic activity *in vitro*, exhibited potent activity *in vivo* in mice cutaneously infected with HSV-1 (Lipipun et al., 2011). However,

due to its poor BBB permeability (Breuer et al., 2006), oxyresveratrol (**1**) seems to have limited clinical application. In this regard, stilbenes **2** and **3**, with their higher lipophilicity, may be better candidates for further investigation on HSV infection of the CNS, as well as neurodegenerative diseases such as AD or PD.

3.2.2. Neuraminidase inhibitory activity

In this study, oxyresveratol and all of its derivatives (**2** – **27**) exhibited no activity against the enzyme neuraminidase (positive control oseltamivir, IC_{50} 0.5 nM), although **1** has been earlier described as having modest activity (Kongkamnerd, 2010). It should be mentioned that resveratrol, a closely related stilbene, and several of its synthetic and semisynthetic analogs have been recently reported to possess significant inhibitory activity against influenza neuraminidase (Li et al., 2015).

3.2.3. α-Glucosidase inhibitory activity

Almost all of the stilbenoids prepared from oxyresveratrol (**2 – 27**) exhibited reduced or lost inhibitory activity against α-glucosidase (the positive control acarbose: IC_{50} 745.9 ± 88.4 μM). The only exception was **6**, which showed activity (IC_{50} 19.6 ± 3.6 μM) comparable to that of **1** (IC_{50} 19.5 ± 1.7 μM). In a previous study, **1** has been suggested to be a promising structure for anti-diabetic drug development (He et al., 2013). However, the compound, after oral absorption, was found to undergo extensive hepatic metabolism and rapid urinary elimination, resulting in a short half-life time (~ 0.96 h) (Huang et al., 2010). Compound **6**, with three isopropoxy groups, is predicted to have much slower metabolism and may be considered as a better candidate for the preclinical and clinical studies for anti-DM drugs.

3.2.4. Free radical scavenging activity

First, examinations were conducted on the relationships between the phenolic and olefinic functionalities of the core stilbene structure and the free radical scavenging and the DNA protective activities. Then, investigations were carried out to study how the nature and position of substituents with electron-withdrawing (i.e. Cl, CHO and COOH) or electron-donating (i.e. OH) properties on the aromatic rings affected these biological activities. Compounds were first evaluated at 100 μg/mL, and those that showed >80% inhibition were further analyzed for their IC_{50} values.

Oxyresveratrol (**1**) showed weaker DPPH free radical scavenging activity than Trolox (Table 2.2). The phenolic groups were essential since the activity was reduced or lost when some or all of the phenolic groups of **1** were esterified/etherified as observed in compounds **2** – **8** and **20**. The only exception was compound **3**, the 2,4,3′-tri-*O*-methylation product of **1**, which showed higher activity against the superoxide anion radical than the parent compound. Interestingly, this compound also showed higher DNA protective property.

The olefinic bridge, which provided conjugation (and thus electron delocalization) between the two aromatic rings, was also required for DPPH radical scavenging ability, as demonstrated from the marked decrease in activity of **18**. However, when evaluated against the superoxide anion,

18 displayed higher activity than **1**. This enhanced activity was most likely due to the electron-withdrawing effect of the C=O of the dihydropyrone ring which helped to stabilize the negatively-charged stilbene radical formed from **18** after interaction with the superoxide anion.

Introducing an electron-donating group such as OH to the aromatic rings could recover the loss of DPPH scavenging activity caused by phenolic esterification/etherification. This was inferred from comparing the activity of the following pairs of structures: **7** (no activity) *vs* **17**, and **20** (no activity) *vs* **27**. However, these sets of compounds did not give similar results in the superoxide assay.

Placing an electron-withdrawing substituent, such as Cl, CHO and COOH, onto the aromatic ring of **1** yielded compounds **12**, **16**, **23** and **24** which showed weaker activity against the DPPH radical, but enhanced activity against the superoxide anion. The improved activity was likely attributable to the electron-withdrawing nature of these groups that helped to distribute the negative charge of the radicals generated from the reactions of these stilbenoids (**12**, **16**, **23** or **24**) with the superoxide anion.

3.2.5. DNA protective property

Riboflavin (RF), when exposed to light, generates several kinds of free radicals, including triplet ($^3RF^{\bullet}$), neutral oxidized ($RF(-H)^{\bullet}$) and cation ($RF^{\bullet+}$) riboflavin radical. The ($^3RF^{\bullet}$) radical then transfers energy to oxygen to form reactive oxygen species (ROS) such as singlet oxygen ($^1O_2$) and superoxide ($O_2^{\bullet-}$) radicals (Joshi, 1985; Lu et al., 1999). These free radicals, with their high energy, can each cause damage to the DNA by attacking the purine base guanine to form 8-hydroxyguanine and 2,6-diamino-4-hydroxy-5-formamidopyrimidine (Joshi, 1985; Korycka-Dahl et al., 1977; Cardoso et al., 2007; Mori et al., 1988). Any compound that can efficiently protect DNA from the damage induced by photo-sensitized riboflavin must be capable of scavenging or neutralizing these free radicals. In this study, compounds were first evaluated at 100 μg/mL, and those with >80% inhibition were further analyzed for their IC_{50} values (Table 2).

Compound **1** showed higher DNA protective activity than Trolox despite its inferior activity in the DPPH assay (Table 2.2). Total *O*-alkylation or *O*-acylation of **1** destroyed the activity, as observed in the lost or diminished activity for **4**, **7**, **8**, **9**, **14**, **15**, **17**, **19** and **20**. The lost activity of **20** could be rescued by placing an OH substituent on ring B (**27**), an outcome similar to the case of the DPPH radical. The partially *O*-alkylated products of **1,** including **3**, **10**, and **11** showed enhanced DNA protective activity, but the tri-*O*-isopropylated product **6** displayed markedly reduced activity.

Table 2.2 IC_{50} values (μM) for free radical scavenging activities and DNA protective properties of **1** and derivatives

Compound	Free radical scavenging activity		DNA protective activity
	DPPH	Superoxide	
1	11.7 ± 0.4	303.1 ± 7.9	43.3 ± 6.7
2	77.0 ± 6.4*	nd#	39.4 ± 1.2
3	nd	120.1 ± 14.9*	6.3 ± 0.8*
5	147.7± 9.8*	nd	59.1 ± 9.9
10	9.7 ± 0. 2*	154.9 ± 14.7*	19.9 ± 2.8*
11	19.4 ± 3.1*	81.9 ± 12.3*	28.6 ± 3.8*
12	14.7 ± 0.6*	98.4 ± 7.0*	32.0 ± 1.4*
16	16.5 ± 2.8*	43.4 ± 4.4*	32.2 ± 4.8
17	11.7 ± 0.3	nd	nd
18	nd	107.3 ± 8.7*	28.3 ± 4.3*
22	nd	17.7 ± 3.5*	81.4 ± 4.2*
23	nd	88.3 ± 9.7*	54.7 ± 8.3
24	48.3 ± 5.8*	38.6 ± 1.4*	79.4 ± 14.9*
25	nd	nd	111.8 ± 7.3*
26	nd	nd	104.7 ± 8.5*
27	7.0 ± 0.2*	nd	18.6 ± 3.7*
Trolox	8.7 ± 1.1*	293.5 ± 19.3	113.1 ± 4.6*

#nd = not determined due to < 80 % inhibition at 100 μg/mL.
*Significantly different from that of **1** ($p < 0.05$).

Compound **18** did not lose DNA protective activity despite the disappearance of the C=C bond. With the aid of the C=O of the dihydro-α-pyrone ring, this compound (**18**) showed even higher activity than **1**. The placement of the electron-donating group OH on ring A of **20** could recover the lost activity, giving **27** which is a better DNA protectant than **1**. The introduction of an electron-withdrawing substituent to the aromatic rings of **1** gave unclear results. Placing Cl on ring B slightly increased the activity (**12**), but introducing COOH to ring A reduced the activity (**24**).

3.2.6. Cytotoxicity against cancer cells

All compounds (**1** – **27**) were initially evaluated at 50 μg/mL, and those demonstrating > 50% inhibition were subjected to IC_{50} determination (Table 2.3).

Seventeen derivatives demonstrated higher cytotoxicity than the parent compound (**1**), which was virtually non-cytotoxic against all cancer cell lines. The partially (di- or tri-) *O*-alkylated products (**2**, **3**, **5** and **6**) showed increased cytotoxicity against all types of cancer cells. The fully *O*-methylated product (**4**) showed enhanced cytotoxicity selectively against HeLa and H69AR cells, but no activity against T47-D and A549 cells. Interestingly, the IC_{50} value of **4** against the multidrug-resistant small lung cancer cells (H69AR) was in the same range as that of doxorubicin ($p > 0.05$). The fully *O*-isopropylated products, including **7**, **9**, **17**, and **19**, did not show cytotoxicity

in the assays, probably a result of their poor aqueous solubility. With regard to the esterified analogs, the fully *O*-acetylated compound **8** showed slightly improved activity selectively against T47-D cells, but lessened activity against HeLa and A549 cells when compared with **1**. Compound **20**, a di-*O*-isopropylated-di-*O*-acetylated product of **1**, showed better cytotoxicity than **1** in all cancer cell lines, with selective potency against HeLa cells.

Table 2.3 Cytotoxicity against cancer cells of **1** and some derivatives

Compounds	IC_{50} (μM)			
	T47-D	HeLa	A549	H69AR
1	152.7 ± 4.5	126.2 ± 0.3	159.8 ± 0.0	nd#
2	114.2 ± 2.0*	28.4 ± 7.0*	117.0 ± 11.1*	180.7 ± 3.4
3	87.1 ± 9.5*	13.1 ± 2.1*	52.4 ± 0.9*	36.7 ± 3.3
4	nd	12.1 ± 1.5*	nd	26.8 ± 7.6
5	117.4 ±	11.0 ± 2.7*	55.5 ± 3.5*	39.2 ± 6.5
6	37.7 ± 12.9*	25.7 ± 2.1*	28.8 ± 5.1*	54.5 ±3.0
8	103.0 ± 4.3*	nd	nd	nd
10	88.6 ± 2.9*	100.9 ± 4.7*	137.7 ± 8.4*	nd
12	156.6 ± 6.0	33.4 ± 2.9*	120.7 ± 2.9*	111.2 ± 3.1
13	nd	18.7 ± 4.2*	nd	65.7 ± 3.2
14	nd	69.1 ± 3.3*	nd	nd
15	101.4 ± 9.1*	83.2 ± 9.1*	nd	nd
16	99.3 ± 3.1*	74.4 ± 4.8*	138.0 ± 3.1*	nd
20	81.3 ± 0.6*	5.7 ± 0.6*	51.7 ± 1.7*	38.0 ± 2.2
21	54.5 ± 2.0*	18.9 ± 0.7*	71.3 ± 3.2*	nd
23	82.9 ± 2.2*	77.9 ± 2.1*	143.2 ± 3.3*	nd
25	44.7 ± 2.6*	22.4 ± 0.4*	75.1 ± 0.7*	111.0 ± 2.3
27	83.2 ± 10.6*	79.8 ± 4.7*	104.4 ± 5.3*	nd
Doxorubicin	0.5 ± 0.00*	0.7 ± 0.2*	0.4 ± 0.1*	21.7 ± 0.9

#nd = not determined due to < 50 % inhibition at 50 μg/mL.
*****Significantly different from that of **1** ($p < 0.05$).
Cell lines: T47D= human hormone-dependent breast cancer, HeLa= human cervical adenocarcinoma, A549= human non-small-cell lung carcinoma, H69AR= human multidrug-resistant small-cell lung carcinoma

Different impacts on the cytotoxicity were observed when an electron-withdrawing substituent was attached to the aromatic rings of **1**. Chlorination of **1** at C-2′ gave **12**, a product with increased cytotoxicity against almost all cancer cell lines, except T47D cells. Similar profiles of cytotoxicity were observed for compounds **16** and **23**, the 5- and the 2′-formylated analogs, both of which displayed increased activity against T47-D, HeLa and A549, but with no activity against H69AR cells. Further structural modification of **23** by converting the CHO into a COOH group destroyed cytotoxicity in all cancer cell lines (**24**). When **7**, the fully *O*-isopropylated analog, was formylated or carboxylated at C-2′, partial restoration of cytotoxicity was observed (**14** and **15**).

For **20**, placing a CHO group at C-5 gave a product (**21**) with mixed results since the cytotoxicity against TD47-D cells was enhanced, but the activity against HeLa A549 and H69AR cells was weakened ($p < 0.05$). Transforming the CHO at this position of **21** into a COOH group abolished the activity (**22**). An electron-donating group such as hydroxy group, when added to the aromatic rings, could not induce cytotoxicity, as reflected from the non-cytotoxicity of both **7** and **17**, but instead seemed to weaken the cytotoxicity, as evident when comparing the strong activity of **20** with that of **27** which showed less cytotoxicity in HeLa and A549 cancer cells ($p< 0.05$).

4. Conclusions

A total of 26 derivatives were prepared from oxyresveratrol (**1**) through several types of reactions. Selective di-*O*-alkylation is possible because the two hydroxy groups at C-2 and C-4 of ring A of **1** are obviously more reactive than those on ring B. Electrophilic substitution on the B ring is more facile than those on the A ring. However, the relative reactivity can be reversed by manipulating the type and the number of protecting groups. Through this strategy, electrophilic substitution reactions can be selectively directed to ring A or B. This finding has provided a new and useful approach for the future chemical modification of similarly oxygenated aromatic structures.

Compound **1** and analogs (**2** - **27**) were evaluated for a number of biological activities including antiherpetic activity, inhibition against the enzymes neuraminidase and α-glucosidase, free radical scavenging activity, DNA protective property, and cytotoxicity against some cancer cell lines.

The most interesting products are the partially etherified analogs, namely 3′,5′-dihydroxy-2,4-dimethoxystilbene **(2**) and 5′-hydroxy-2,3′,4-trimethoxy-stilbene (**3**), which displayed 3- to 4-fold higher antiherpetic activity than the parent compound (**1**). Because of the ether functionalities, stilbenes **2** and **3** should have higher lipophilicity as compared with **1**, and thus greater potential as preventive agents for neurological disorders triggered by cerebral HSV infection. It is recommended that further studies of these two compounds (**2** and **3**) *in vivo* should be pursued.

Regarding the inhibitory activity against H5N1 neuraminidase, surprisingly **1** was found to be inactive against the enzyme in this study, in contrast to the earlier report (Kongkamnerd, 2010). Moreover, none of its derivatives (**2** – **27**) showed the activity.

In addition, it should be noted that 5′-hydroxy-2,3′,4,-triisopropoxystilbene (**6**), an etherified analog with retained anti-α-glucosidase activity but with a potentially slower rate of metabolism than that of **1**, should be a better lead compound for oral anti-diabetic drug development. Finally, the mixed esterified/etherified derivative 3′,5′-diacetoxy-2,4-diisopropoxy-stilbene (**20**) displayed pronounced *in vitro* cytotoxicity against HeLa cells, and warrants further investigation in animals.

Output

(13) Nutputsorn Chatsumpun, Taksina Chuanasa, Boonchoo Sritularak, Vimolmas Lipipun, Vichien Jongbunprasert, Somsak Ruchirawat, Poonsakdi Ploypradith, and Kittisak Likhitwitayawuid. Oxyresveratrol: Structural modification and evaluation of biological activities. Molecules **21**: 489; doi:10.3390/molecules21040489 (2016). (IF = 2.465)

References

Beyoda, L.M.; del Olmo, E.; Sancho, R.; Barboza, B.; Beltrán, M.; Garcia-Cadenas, A.E.; Sánchez-Palomino, S.; López-Pérez, J.L.; Muñoz, E.; Feliciano, A.S.; Alcamí, J. Anti-HIV activity of stilbene-related heterocyclic compounds. Bioorg. Med. Chem. Lett. 2006, 16, 4075-4079.

Breuer, C.; Wolf, G.; Andrabi, S.A.; Lorenz, P.; Horn, T.F. Blood-brain barrier permeability to the neuroprotectant oxyresveratrol. Neurosci. Lett. 2006, 393, 113-118.

Cardin, A.D.; Smith, P.L.; Hyde, L.; Blankenship, D.T.; Bowlin, T.L.; Schroeder, K.; Stauderman, K.A.; Taylor, D.L.; Tyms A. S. Stilbene disulfonic acids. J. Biol. Chem. 1991, 266, 13355-13363.

Cardoso, D.R.; Olsen, K.; Skibsted, L.H. Mechanism of deactivation of triplet-excited riboflavin by ascorbate, carotenoids, and tocopherols in homogeneous and heterogeneous aqueous food model systems. J. Agric. Food Chem. 2007, 55, 6285-6291.

Chatsumpun, M.; Chuanasa, T.; Sritularak, B.; Likhitwitayawuid, K. Oxyresveratrol protects against DNA damage induced by photosensitized riboflavin. Nat. Prod. Commun. 2011, 6, 41-44.

Chuanasa, T.; Phromjai, J.; Lipipun, V.; Likhitwitayawuid, K.; Suzuki, M.; Pramyothin, P.; Hattori, M.; Shiraki, K. Anti-herpes simplex virus (HSV-1) activity of oxyresveratrol derived from Thai medicinal plant: mechanism of action and therapeutic efficacy on cutaneous HSV-1 infection in mice. Antiviral Res. 2008, 80, 62-70.

Civitelli, L.; Marcocci, M.E.; Celestino, I.; Piacentini, R.; Garaci, E.; Grassi, C.; De Chiara, G.; Palamara, A.T. Herpes simplex virus type 1 infection in neurons leads to production and nuclear localization of APP intracellular domain (AICD): implications for Alzheimer's disease pathogenesis. J. Neurovirol. 2015, 21, 480-490.

Dasgupta, N.; De, B. Antioxidant activity of *Piper betle* L. leaf extract in vitro. Food Chem. 2004, 88, 219-224.

He, H.; Lu, Y.-H. Comparison of inhibitory activities and mechanisms of five mulberry plant bioactive components against α-glucosidase. J. Agric. Food Chem. 2013, 61, 8110-8119.

Hill, J.M.; Zhao, Y.; Clement, C.; Neumann, D.M.; Lukiw, W.J.; HSV-1 infection of human brain cells induces miRNA-146a and Alzheimer-type inflammatory signaling. NeuroReport. 2009, 20, 1500-1505.

Huang, H.; Chen, G.; Lu, Z.; Zhang, J.; Guo, D.A. Identification of seven metabolites of oxyresveratrol in rat urine and bile using liquid chromatography/tandem mass spectrometry. Biomed. Chromatogr. 2010, 24, 426-432.

Joshi, P.C. Comparison of the DNA-damaging property of photosensitised riboflavin via singlet oxygen ($^1O_2$) and superoxide radical (O_2^-) mechanisms. Toxicol. Lett. 1985, 26, 211-217.

Kongkamnerd, J. Development of non-cell based assays for screening of inhibitiors against avian influenza neuraminidase. Ph.D. Dissertation, Chulalongkorn University, Thailand, 2010.

Korycka-Dahl, M.; Richardson, T. Photogeneration of superoxide anion in serum of bovine milk and in model systems containing riboflavin and amino acids. J. Dairy Sci. 1977, 61, 400-407.

Li, C.; Fang, J.S.; Lian, W.W.; Pang, X.C.; Liu, A.L.; Du, G.H. In vitro antiviral effects and 3D QSAR study of resveratrol derivatives as potent inhibitors of influenza H1N1 neuraminidase. Chem. Biol. Drug. Des. 2015, 85, 427-438.

Li, Y.-Q.; Li, Z.-L.; Zhao, W.-J.; Wen, R.-X.; Meng, Q.-W.; Zeng, Y. Synthesis of stilbene derivatives with inhibition of SARS coronavirus replication. Eur. J. Med. Chem. 2006, 41, 1084-1089.

Likhitwitayawuid, K.; Sritularak, B.; Benchanak, K.; Lipipun, V.; Mathew, J.; Schinazi, R.F. Phenolics with antiviral activity from *Millettia erythrocalyx* and *Artocarpus lakoocha*. Nat. Prod. Res. 2005a, 19, 177-182.

Likhitwitayawuid, K., Supudompol, B., Sritularak, B., Lipipun, V., Rapp, K. and Schinazi, R.F. Phenolics with anti-HSV and anti-HIV activities from *Artocarpus gomezianus*, *Mallotus pallidus* and *Triphasia trifolia*. Pharm. Biol. 2005b, 43, 651-657.

Likhitwitayawuid, K.; Sornsute, A.; Sritularak, B.; Ploypradith, P. Chemical transformations of oxyresveratrol (*trans*-2,4,3′,5′-tetrahydroxystilbene) into a potent tyrosinase inhibitor and a strong cytotoxic agent. Bioorg. Med. Chem. Lett. 2006a, 16, 5650-5653.

Likhitwitayawuid, K.; Klongsiriwet, C.; Jongbunprasert, V.; Sritularak, B.; Wongseripipatana, S. Flavones with free radical scavenging activity from *Goniothalamus tenuifolius*. Arch. Pharm. Res. 2006b, 29, 199-202.

Lipipun, V.; Kurokawa, M.; Suttisri, R.; Taweechotipatr, P.; Pramyothin, P.; Hattori, M.; Shiraki, K. Efficacy of Thai medicinal plant extracts against herpes simplex virus type 1 infection in vitro and in vivo. Antiviral Res. 2003, 60, 175-180.

Lipipun, V.; Sasivimolphan, P.; Yoshida, Y.; Daikoku, T.; Sritularak, B.; Ritthidej, G.; Likhitwitayawuid, K.; Pramyothin, P.; Hattori, M.; Shiraki, K. Topical cream-based oxyresveratrol in the treatment of cutaneous HSV-1 infection in mice. Antiviral Res. 2011, 91, 154-160.

Liu, A.-L.; Yang, F.; Zhu, M.; Zhou, D.; Lin, M.; Lee, S. M-Y.; Wang, Y.-T.; Du, G.-H. In vitro anti-influenza viral activities of stilbenoids from the Lianas of *Gnetum pendulum*. Planta Med. 2010, 76, 1874–1876.

Lu, C.-Y.; Wang, W.-F.; Lin, W.-Z.; Han, Z.-H.; Yao, S.-D.; Lin, N.-Y. Generation and photosensitization properties of the oxidized radical of riboflavin: a laser flash photolysis study. J. Photochem. Photobiol. B: Biol. 1999, 52, 111-116.

Mori, T.; Tano, K.; Takimoto, K.; Utsumi, H. Formation of 8-hydroxyguanine and 2,6-diamino- 4-hydroxy-5-formamidopyrimidine in DNA by riboflavin mediated photosensitization. Biochem. Biophys. Res. Commun. 1998, 242, 98-101.

Nguyen, P.-H.; Na, M.-K.; Dao, T.-T.; Ndinteh, D. T.; Mbafor, J. T.; Park J.-Y.; Cheong, H.-S.; Oh, W.-K. New stilbenoid with inhibitory activity on viral neuraminidases from *Erythrina addisoniae*. Bioorg. Med. Chem. Lett. 2010, 20, 6430–6434.

Park, J.; Park, J.H.; Suh, H.J.; Lee, I.C.; Koh, J.; Boo, Y.C. Effects of resveratrol, oxyresveratrol, and their acetylated derivatives on cellular melanogenesis. Arch. Dermatol. Res. 2014, 306, 475-487.

Potier, M.; Mameli, L.; Bélisle, M.; Dallaire, L.; Melançon, S.B. Fluorometric assay of neuraminidase with a sodium (4-methylumbelliferyl-α-D-N-acetylneuraminate) substrate. Anal. Biochem. 1979, 94, 287-296.

Sritularak, B.; De-Eknamkul, W.; Likhitwitayawuid, K. Tyrosinase inhibitors from Artocarpus lakoocha. Thai J. Pharm. Sci. 1988, 22, 149-155.

Tangdenpaisal, K.; Worayuthakarn, R.; Karnkla, S.; Ploypradith, P.; Intachote, P.; Sengsai, S.; Saimanee, B.; Ruchirawat, S.; Chittchang, M. Designing new analogs for streamlining the structure of cytotoxic lamellarin natural products. Chem. Asian. J. 2015, 10, 925-937.

Tengamnuay, P.; Pengrungruangwong, K.; Pheansri, I.; Likhitwitayawuid, K. Artocarpus lakoocha heartwood extract as a novel cosmetic ingredient: evaluation of the in vitro anti-tyrosinase and in vivo skin whitening activities. Int. J. Cosmetic. Sci. 2006, 28, 269-276.

CHAPTER III

Project 3

Search for new antiviral agents from Thai medicinal plants

Principle Investigator: Professor Dr. Kittisak Likhitwitayawuid
Chulalongkorn University

Background

In our earlier reports (Likhitwitayawuid et al., 2005a; 2005b), we made a comment that antiviral activity, or antiherpetic potential in particular, has been frequently observed in a number of compounds with a *bis*-aryl partial structure [**a**]. These include several classes of plant secondary metabolites, for example, phloroglucinol dimers (C_6-C_1-C_6) [**b**], stilbenoids (C_6-C_2-C_6) [**c**], flavonoids (C_6-C_3-C_6) [**d**] and lignans (C_6-C_4-C_6) [**e**].

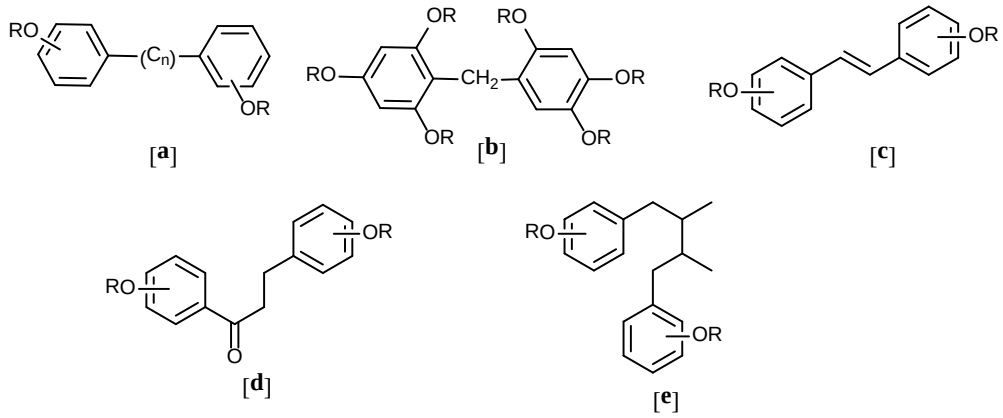

Based on our previously accumulated chemical and biological data, these naturally occurring aromatic compounds have been frequently located in some groups of plants in the Angiosperm, as illustrated in Table 3.1A.

Table 3.1A Potential sources of antiviral compounds

Class of compound	Plant genus	Family	Reference
Stilbenoids, flavonoids	*Artocarpus*	Moraceae	Likhitwitayawuid et al., 2006
	Dendrobium	Orchidaceae	Srirularak et al., 2009
Lignans, neolignans	*Miliusa*	Annonaceae	Swasdee et al., 2010
Phloroglucinols dimers	*Mallotus*	Euphorbiaceae	Supudompol et al., 2004

With the above concept in mind, we selected, from our repository, some extracts of plants/plant parts with no records of antiviral activity studies. The extracts were evaluated for inhibitory activity against Herpes simplex virus (HSV), and the enzyme H5N1 neuraminidase in some cases. Extracts with promising bioassay results were subjected to further chemical and biological investigations (see Table 3.1B).

Table 3.1B Selected plant extracts and their antiviral potential

Plant extract			**% inhibition at 100 μg/mL**		**H5N1 neuraminidase inhibitory activity**
Plant name	**Solvent**	**Plant part**	**HSV-1**	**HSV-2**	
1. *Artocarpus lakoocha*	EtOAc	root bark	80	80	NA
2. *Miliusa mollis*	MeOH	leaves	60	60	NA
3. *Miliusa fragrans*	MeOH	leaves	70	60	NA
4. *Miliusa fragrans*	MeOH	stems	80	80	NA
5. *Miliusa umpangensis*	MeOH	leaves	80	60	*NT*
6. *Mallotus plicatus*	EtOAc	stem bark	70	60	*NT*
7. *Mallotus plicatus*	MeOH	stem bark	80	80	*NT*
8. *Dendrobium venustum*	MeOH	whole plant	80	80	*NT*
9. *Dendrobium williamsonii*	MeOH	whole plant	80	80	*NT*

NA = no activity at 50 μg/mL; *NT* = not tested due to limited research funding.

From the available preliminary data (Tables 1A and 1B), we decided to carry out our chemical and biological studies on 9 plant samples, which were prepared from 7 plant species, i.e. *Artocarpus. Lakoocha* Roxb., *Miliusa fragrans* Chaowasku & Kessler, *Miliusa mollis* Pierre *Miliusa umpangensis* Chaowasku & Kessler, *Mallotus plicatus* (Müller.Arg) Airy Shaw, *Dendrobium venusum* Teijsm. & Binn. and *Dendrobium williamsonii* Day & Rchb. f.. These plants belong to 4 genera (*Artocarpus*, *Miliusa*, *Mallotus* and *Dendrobium*) distributed in 4 families (Moraceae, Annonaceae, Euphorbiaceae and Orchidaceae). It was hoped that the diverse chemical compositions of these selected plants would offer new structural scaffolds for the development of novel antiviral agents.

It should be mentioned here that due to our limited research funding, we were not able to test all of the plant extracts and isolated compounds for inhibitory activity against AIV H5N1 neuraminidase. Only compounds isolated from *Miliusa mollis* were evaluated for this activity.

1. Objectives

1. To isolate and determine the structures of the chemical constituents of the extracts obtained from: roots of *Artocarpus lakoocha*; leaves of *Miliusa mollis*; stems and leaves of *Miliusa fragrans*; leaves of *Miliusa umpangensis*; stem bark of *Mallotus plicatus,* whole plants of *Dendrobium venusum* and *D. williamsonii*
2. To evaluate the antiherpetic activity of the isolated compounds.

Notes: Only pure compounds obtained from the leaves of *Miliusa mollis* were evaluated for inhibitory effects against H5N1 neuraminidase. Other compounds were not tested, due to the expected inactivity, as well as insufficiency of research funding.

2. Experimental

2.1 Isolation

General experimental procedures

Mass spectra were recorded on a Micromass LCT mass spectrometer (ESI-MS). NMR spectra were recorded on a BrukerAvance DPX-300 FT-NMR spectrometer or a Varian Unity INOVA-500 NMR spectrometer. Microtiter plate reading was performed on a Perkin-Elmer VictorTM 1420 multilabel counter. Vaccuum-liquid chromatography (VLC) and column chromatography (CC) were performed on silica gel 60 (Merck, Kieselgel 60, 70-320 mesh) and silica gel 60 (Merck, Kieselgel 60, 230-400 mesh), respectively. Size-exclusion chromatography was conducted on Sephadex LH-20 (25-100 μm, Pharmacia Fine Chemical Co. Ltd.).

Roots of *Artocarpus lakoocha*

Roots of *Artocarpus lakoocha* were collected from the plant growing in the botanical garden of Faculty of Pharmaceutical Sciences, Chulalongkorn University. Dried powdered roots of *A. lakoocha* (2.4 kg) were extracted with ethylacetate (3 × 20 L) and methanol (3 × 20 L) to give an EtOAc extract (111 g) and a MeOH extract (369 g) after removal of the organic solvents. The EtOAc extract (at 100 μg/ml) showed 80% inhibition against HSV-1, whereas the MeOH extract showed no activity.

The EtOAc extract (111 g) was fractionated by vacuum liquid chromatography (VLC) on SiO_2 with hexane-EtOAc in a polarity gradient manner to give 13 fractions (A – M). Fraction L was further separated repeatedly by column chromatography (CC) to give compounds **I** (54 mg) and cudraflavone C (**II**, 5 mg). A portion of the MeOH extract (10 g) was passed through Diaion HP220SS (H_2O-MeOH) to give 6 fractions. The first fraction was subjected to CC (SiO2, CH_2Cl_2-MeOH) and then size exclusive chromatography (Sephadex LH20, MeOH) to give (+)-afzelechin-3-*O*-α-L-rhamnoside (**III**, 8 mg) and (+)-catechin (**IV**, 15 mg).

*5,7,2′,4′-Tetrahydroxy-3-prenyl-6-geranylflavone (**I**)*

Compound **I**: yellow powder; UV (MeOH) λ_{max} nm (log ε): 220 (3.83), 262 (3.69), 308 (3.44); IR (film) ν_{max} cm^{-1}: 3328, 2968, 2873, 1701, 1648, 1619, 1560, 1459, 1360, 1309; HR-ESIMS: *m/z* 491.2430 $[M+H]^+$ calcd for $C_{30}H_{35}O_6$ 491.2434; ^1H NMR (500 MHz, acetone-d_6): δ 1.41 (3H, s, H_3-13), 1.55 (6H, s, H_3-12, H_3-22), 1.60 (3H, s, H_3-23), 1.78 (3H, s, H_3-17), 1.95 (2H, m, H2-18), 2.04 (2H, m, H_2-19), 3.09 (2H, d, *J* = 7.0 Hz, H_2-9), 3.36 (2H, d, *J* = 7.0 Hz, H_2-14), 5.07 (1H, t, *J* = 7.0 Hz, H-20), 5.11 (1H, t, *J* = 7.0 Hz, H-10), 5.28 (1H, t, *J* = 7.0 Hz, H-15), 6.38 (1H, s, H-8), 6.48 (1H, dd, *J* = 8.5, 2.5 Hz, H-5′), 6.54 (1H, d, *J* = 2.5 Hz, H-3′), 7.16 (1H, d, *J* = 8.5 Hz, H-6′), 13.42 (1H, s, OH-5). ^{13}C NMR (125 MHz, acetone-d_6): δ 16.2 (C-17), 17.6 (C-13, C-22), 21.8 (C-14), 24.6 (C-9), 25.7 (C-12, C-23), 27.3 (C-19), 40.4 (C-18), 93.4 (C-8), 103.8 (C-3′), 104.9 (C-4a), 107.9 (C-5′), 111.7 (C-6), 113.0 (C-1′), 121.4 (C-3), 122.7 (C-10), 123.2 (C-15), 125.1 (C-20), 131.5 (C-21), 131.9 (C-11), 132.2 (C-6′), 135.1 (C-16), 157.0 (C-8a), 157.1 (C-2′), 160.0 (C-5), 161.3 (C-4′), 161.9 (C-2), 162.4 (C-7), 182.9 (C-4).

Leaves of *Miliusa mollis*

Dried and powdered leaves (198.0 g) were extracted with MeOH (3 × 3L) to give, after removal of the solvent, 36.0 g of a dried extract, which was then subjected to VLC on silica gel using solvent mixtures of increasing polarity [*n*-hexane-CH_2Cl_2 (100:0 - 0:100), CH_2Cl_2-EtOAc (100:0 - 0:100), MeOH] to give eight fractions (A-H). Fraction D (314 mg) was further fractionated by CC on silica gel with gradient elution [*n*-hexane-CH_2Cl_2 (100:0-0:100)] to give nine fractions (D1 – D9). Fraction D5 (90 mg) was separated by CC on silica gel with isocratic elution [*n*-hexane-EtOAc (98:2)] to give three fractions (E5-1 - E5-3). Fraction D5-2 (32 mg) was purified by CC on silica gel using isocratic elution [*n*-hexane-CH_2Cl_2 (4:1)] to give **VI** (10 mg). Fraction E (2.2 g) was separated by MPLC on silica gel with gradient elution [*n*-hexane-CH_2Cl_2 (100:0-0:100)] to give seven fractions (E1 - E7). Fraction E4 (790 mg) was separated on Sephadex LH-20 [CH_2Cl_2-MeOH (1:1)] to give five fractions (E4-1 to E4-5). Fraction E4-2 (84 mg) was purified by CC on silica gel with solvent mixtures of *n*-hexane-EtOAc (96:4) to give **X** (11 mg). Fraction E4-4 (531 mg) was purified by CC on silica gel (21.3 g) with isocratic elution [*n*-hexane-EtOAc (94:6)] to give **VII** (162 mg). Fraction F (5.2 g) was fractionated by VLC on silica gel with gradient elution [*n*-hexane-EtOAc (100:0 - 0:100] to give seven fractions (F1-F7). Fraction F4 (647 mg) was separated with Sephadex LH-20 [CH_2Cl_2-MeOH (1:1)] to give seven fractions (F4-1 to F4-7). Fraction F4-5 (121 mg) was purified by CC on silica gel with gradient elution [*n*-hexane-EtOAc (100:0-0:100)] to give **V** (8 mg) and **VIII** (6 mg). Fraction F5 (991 mg) was separated with Sephadex LH-20 [CH_2Cl_2-MeOH (1:1)] to give five fractions (F5-1 to F5-5). Fraction F5-4 (174 mg) was purified by CC on silica gel with gradient elution [*n*-hexane-EtOAc (100:0-0:100)] to give **IX** (27 mg) and. decurrenal **XI** (64 mg).

*4′-O-Methylmiliumollin (**V**)*

Compound **V**: colorless viscous liquid; $[\alpha]_D^{20}$ –25.00 ($CHCl_3$, *c* 0.12); CD (MeOH, *c* 0.0009): $[\theta]_{284}$ +863, $[\theta]_{238}$ −25,323; UV λ_{max} (MeOH) nm (log ε): 212 (3.95), 229 (4.09), 283 (3.63); IR ν_{max} (film): 1513, 1484, 1237 cm^{-1}; HR-ESI-TOF-MS *m/z* 281.1593 $[M+H]^+$ (calcd. for $C_{19}H_{21}O_2$, 281.1542); ^1H NMR and ^{13}C NMR ($CDCl_3$): see Tables 3.2 and 3.3.

*Miliusamollin (**VI**)*

Compound **VI**: colorless viscous liquid; $[\alpha]_D^{20}$ –55.40 ($CHCl_3$, *c* 0.20); CD (MeOH, *c* 0.0014): $[\theta]_{278}$ −2366, $[\theta]_{230}$ −13,098; UV λ_{max} (MeOH) nm(log ε): 228 (4.31), 273 (3.84); IR ν_{max} (film): 1734,
1507, 1227 cm^{-1}; HR-ESI-TOF-MS *m/z* 363.1578 $[M+Na]^+$ (calcd. for $C_{21}H_{24}O_4Na$, 363.1572); ^1H NMR and ^{13}C NMR ($CDCl_3$): see Tables 3.2 and 3.3.

*3′-Methoxymiliumollin (**VII**)*

Compound **VII**: clorless viscous liquid; $[\alpha]_D^{20}$ +8.60 ($CHCl_3$, *c* 0.18); CD (MeOH, *c* 0.0017): $[\theta]_{290}$ −2751, $[\theta]_{240}$ +4197; UV λ_{max} (MeOH) nm (log ε): 208 (4.46), 233 (4.22), 283 (3.95); IR ν_{max} (film): 3431, 1515, 1484, 1234 cm^{-1}; HR-ESI-TOF-MS *m/z* 319.1921 $[M+Na]^+$ (calcd. for $C_{19}H_{20}O_3Na$, 319.1310); ^1H NMR and ^{13}C NMR (acetone-d_6): see Tables 3.2 and 3.3.

*Miliumollin (**VIII**)*

Compound **VIII**: colorless viscous liquid; $[\alpha]_D^{20}$ +32.40 ($CHCl_3$, *c* 0.17); CD (MeOH, *c* 0.0005): $[\theta]_{290}$ −6930, $[\theta]_{236}$ +22,491; UV λ_{max} (MeOH) nm (log ε): 209 (4.30), 230 (4.31), 285 (3.82); IR ν_{max} (film): 3392, 1517, 1485, 1237 cm^{-1}; HR-ESI-TOF-MS *m/z* 265.1225 $[M-H]^-$ (calcd. for $C_{18}H_{17}O_2$, 265.1229); ^1H NMR and ^{13}C NMR ($CDCl_3$): see Tables 3.2 and 3.3.

*7-Methoxymiliumollin (**IX**)*

Compound **IX**: colorless viscous liquid; $[\alpha]_D^{20}$ +15.70 ($CHCl_3$, *c* 0.07,); CD (MeOH, *c* 0.0004): $[\theta]_{286}$ −4440, $[\theta]_{242}$ +17,023; UV λ_{max} (MeOH) nm (log ε): 211 (4.46), 228 (4.30), 280 (3.82); IR ν_{max} (film): 3408, 1516, 1494, 1205, 1138 cm^{-1}; HR-ESI-TOF-MS *m/z* 319.1304 $[M+Na]^+$ (calcd. for $C_{19}H_{20}O_3Na$, 319.1310); ^{1}HNMR and ^{13}C NMR ($CDCl_3$): see Tables 3.2 and 3.3.

*Miliumollinone (**X**)*

Compound **X**: white amorphous powder; $[\alpha]_D^{20}$ +23.00 ($CHCl_3$, *c* 0.14,); CD (MeOH, *c* 0.0004): $[\theta]_{290}$ −7913, $[\theta]_{236}$ +23,272; UV λ_{max} (MeOH) nm (log ε): 207 (4.35), 229 (4.34), 284 (3.90); IR ν_{max} (film): 3378, 1704, 1517, 1485, 1237 cm_{-1}; HR-ESI-TOF-MS *m/z* 305.1158 $[M+Na]^+$ (calcd. for $C_{18}H_{18}O_3Na$, 305.1154); ^1H NMR and ^{13}C NMR ($CDCl_3$): see Tables 3.2 and 3.3.

Leaves of *Miliusa fragrans*

Dried and powdered leaves (199.0 g) were macerated in MeOH (9 x 1L) to give an extract (40.1 g) after removal of the organic solvent. This extract was then subjected to vacuum liquid chromatography (VLC) on silica gel using solvent mixtures of increasing polarity (*n*-hexane-CH_2Cl_2 (1:0 to 0:1), CH_2Cl_2-EtOAc (1:0 to 0:1) and EtOAc-MeOH (1:0 to 0:1)) to give eight fractions (A-H).

Fraction E (8.3 g) was further fractionated by column chromatography (CC) on Sephadex LH-20 (CH_2Cl_2-MeOH 1:1) to give four fractions (E1–E4). Fraction E3 (2.8 g) was separated on a silica gel column with gradient elution of cyclohexane-EtOAc to give thirteen fractions (E3-1 to E3-13), including two pure compounds **XII** (112 mg) and **XIII** (524 mg). Fraction E3-2 (52 mg) was purified by CC on Sephadex LH-20 (CH_2Cl_2-MeOH 1:1) to give**XX** (12 mg). Fraction E3-4 (126 mg) was separated by CC on silica gel using a mixture of cyclohexane-CH_2Cl_2 (1:9) to give four fractions (E3-4-1 to E3-4-4). Fraction E3-4-3 (74 mg) was purified on Sephadex LH-20 column (CH_2Cl_2-MeOH 1:1) to give **XXIV** (17 mg). Fraction E3-5 (967 mg) was separated on silica gel column with isocratic elution of cyclohexane-CH_2Cl_2 (1:9) to give **XV** (126 mg) and **XVI** (366 mg).

Fraction F (1.8 g) was separated by CC on silica gel with gradient elution of cyclohexane-acetone to give eight fractions (F1–F8). Fraction F3 (328 mg) was separated on Sephadex LH-20 column (CH_2Cl_2-MeOH 1:1) to give three fractions (F3-1 to F3-3). Fraction F3-3 (82 mg) was purified by CC on silica gel with a mixture of CH_2Cl_2-EtOAc (95:5) to yield 28 mg of **XXIII**.

Fraction G (973 mg) was fractionated by CC on silica gel with gradient elution of CH_2Cl_2-MeOH to give seven fractions (G1–G7). Fraction G4 (190 mg) was separated on Sephadex LH-20 column (MeOH) to give **XXVIII** (140 mg).

Stems of *Miliusa fragrans*

The dried and powdered stems (1.2 kg) were extracted with MeOH (3 x 4 L), and the solution was filterd and evaporated to dryness. The residue (99.3 g) was then subjected to VLC on silica gel using solvent mixtures of increasing polarity (*n*-hexane-EtOAc (1:0 to 0:1) and EtOAc-MeOH (1:0 to 0:1)) to give seven fractions (A-G). Fraction D (6.6 g) was further fractioned by CC on silica gel with gradient elution (cyclohexane-EtOAc) to give fifteen fractions (D1–D15). Fraction D2 (72 mg) was purified on Sephadex LH-20 column (CH_2Cl_2-MeOH 1:1) to give **XXI** (38 mg). Fraction D4 (896 mg) was purified by CC on silica gel with the mixture solvent of CH_2Cl_2-EtOAc (98:2) to give **XVII** (87 mg). Fraction D5 (1.2 g) was purified by CC on silica gel with gradient elution of CH_2Cl_2-EtOAc to give **XV** (301 mg), **XVI** (32 mg), **XVIII** (58 mg) and **XXII** (46 mg). Fraction D6 (702 mg) was purified on silica gel column using CH_2Cl_2-EtOAc mixtures of increasing polarity to give **XIV** (347 mg). Fraction D8 (660 mg) was separated with Sephadex LH-20 column (CH_2Cl_2-MeOH 1:1) to give four fractions (D8-1 to D8-4). Fraction D8-2 (532 mg) was

purified on silica gel column with the mixture of cyclohexane-EtOAc (96:4) to give **XXVI** (205 mg) and **XXVII** (50 mg). Fraction D12 (454 mg) was fractionated on silica gel column using the isocratic elution of CH_2Cl_2-EtOAc (95:5) to give six fractions (D12-1 to D12-6). Fraction D-12-1, after evaporation of the solvent, gave **XIII** (118 mg). Fraction D12-5 (100 mg) was purified on silica gel column with gradient elution of CH_2Cl_2-EtOAc to give **XXV** (58 mg). Fraction E (1.9 g) was separated with Sephadex LH-20 column (MeOH) to give six fractions (E1-E6). Fraction E2 (609 mg) was purified by CC on silica gel by using gradient solvent mixtures of CH_2Cl_2-EtOAc to give **XIX** (7 mg). Fraction E6 (579 mg) was separated by CC on silica gel with gradient elution of CH_2Cl_2-MeOH to give four fractions (E6-1 to E6-4). Fraction E6-2 (80 mg) was purified on Sephadex LH-20 column (MeOH) to give **XXVIII** (47 mg).

*(+)-3-O-Demethyleusiderin C (**XII**)*

Compound **XII**: colorless viscous liquid; $[\alpha]_D^{20}$ +65.5 (*c* 0.46, $CHCl_3$); CD (*c* 0.0005, MeOH): $[\theta]_{286}$ +795, $[\theta]_{246}$ −9,662; UV (MeOH)/nm λ_{max} (log ε) 220 (4.51), 275 (3.63); IR (film) ν_{max}: 3438 (br), 2937, 2841, 1597, 1506, 1454, 1432, 1211, 1121 cm^{-1}; HRESI-TOFMS *m/z* 395.1456 $[M+Na]^+$ (calcd. for $C_{21}H_{24}O_6Na$, 395.1471); ^1H and ^{13}C NMR see Tables 3.4 and 3.5.

*(+)-4-O-Demethyleusiderin C (**XIII**)*

Compound **XIII**: colorless viscous liquid; $[\alpha]_D^{20}$ +96.9 (*c* 0.16, $CHCl_3$); CD (*c* 0.0013, MeOH): $[\theta]_{284}$ +2,403, $[\theta]_{248}$ −5,969; UV (MeOH)/nm λ_{max} (log ε) 215 (4.59), 276.0 (4.43); IR (film) ν_{max}: 3436 (br), 2937, 1598, 1506, 1455, 1213, 1117 cm^{-1}; HRESI-TOFMS *m/z* 395.1473 $[M+Na]^+$ (calcd. for $C_{21}H_{24}O_6Na$, 395.1471); ^1H and ^{13}C NMR see Tables 3.4 and 3.5.

*(−)-Miliusfragrin (**XVI**)*

Compound **XVI**: white solid; $[\alpha]_D^{20}$ −23.6 (*c* 0.33, $CHCl_3$); CD (*c* 0.0009, MeOH): $[\theta]_{288}$ −1,824, $[\theta]_{238}$ −7,940; UV (MeOH)/nm λ_{max} (log ε) 215 (4.42), 281 (3.73); IR (film) ν_{max}: 3440 (br), 2936, 1560, 1509, 1453, 1433, 1225, 1149, 1103 cm^{-1}; HRESI-TOFMS *m/z* 341.1392 $[M-H]^-$ (calcd. for $C_{20}H_{21}O_5$, 341.1389); ^1H and ^{13}C NMR see Tables 3.4 and 3.5.

*(−)-4-O-Methylmiliusfragrin o (**XVII**)*

Compound **XVII**: colorless viscous liquid; $[\alpha]_D^{20}$ −15.3 (*c* 0.28, $CHCl_3$); CD (*c* 0.0007, MeOH): $[\theta]_{284}$ −1,166, $[\theta]_{238}$ −7,707; UV (MeOH)/nm λ_{max} (log ε) 215 (4.97), 278 (4.09); IR (film) ν_{max}: 2936, 2838, 1599, 1509, 1453, 1263, 1225, 1148, 1104, 1028 cm^{-1}; HRESI-TOFMS *m/z* 379.1514 $[M+Na]^+$ (calcd. for $C_{21}H_{24}O_5Na$, 379.1521); ^1H and ^{13}C NMR see Tables 3.4 and 3.5.

*(+)-Eusiderin A (**XVIII**)*

Compound **XVIII**: white solid; $[\alpha]_D^{20}$ +13.6 (*c* 0.33, $CHCl_3$); CD (*c* 0.0008, MeOH): $[\theta]_{294}$ −1,409, $[\theta]_{238}$ +3,787; UV (MeOH)/nm λ_{max} (log ε) 215 (4.77), 273 (3.60); IR (film) ν_{max}: 2938,

2840, 1597, 1508, 1463, 1226, 1148, 1127, 1105 cm^{-1}; HRESI-TOFMS *m/z* 409.1629 $[M+Na]^+$ (calcd. for $C_{22}H_{26}O_6Na$, 409.1627); ^1H and ^{13}C NMR see Tables 3.4 and 3.5.

*(–)-Miliusfragranol A (**XIX**)*

Compound **XIX**: colorless viscous liquid; $[\alpha]_D^{20}$ −18.7 (*c* 0.17, $CHCl_3$); CD (*c* 0.0019, MeOH): $[\theta]_{284}$ −453, $[\theta]_{244}$ −1,458, $[\theta]_{228}$ −799; UV (MeOH)/nm λ_{max} (log ε) 215 (3.67), 277 (3.16); IR (film) ν_{max}: 3521 (br), 2934, 1515, 1463, 1264, 1236, 1126 cm^{-1}; HRESI-TOFMS *m/z* 411.1768 $[M+Na]^+$ (calcd. for $C_{22}H_{28}O_6Na$, 411.1784); ^1H and ^{13}C NMR see Tables 3.4 and 3.5.

*(–)-Miliusfragranol B (**XX**)*

Compound **XX**: colorless viscous liquid; $[\alpha]_D^{20}$ −20.0 (*c* 0.11, $CHCl_3$); CD (*c* 0.0019, MeOH): $[\theta]_{276}$ −1,185, $[\theta]_{240}$ −6,575; UV (MeOH)/nm λ_{max} (log ε) 210 (4.20), 229 (4.07), 281 (3.70); IR (film) ν_{max}: 3441 (br), 2967, 2936, 1514, 1464, 1268, 1232 cm^{-1}; HRESI-TOFMS *m/z* 351.1568 $[M+Na]^+$ (calcd. for $C_{20}H_{24}O_4Na$, 351.1572); ^1H and ^{13}C NMR see Tables 3.4 and 3.5.

*(+)-3-Hydroxyveraguensin (**XXV**)*

Compound **XXV**: colorless viscous liquid; $[\alpha]_D^{20}$ +37.7 (*c* 0.17, $CHCl_3$); CD (*c* 0.0017, MeOH): $[\theta]_{292}$ −1,240, $[\theta]_{276}$ +655, $[\theta]_{256}$ −100, $[\theta]_{236}$ +4,828, $[\theta]_{228}$ +9,107, $[\theta]_{218}$ +1,378; UV (MeOH)/nm λ_{max} (log ε) 216 (4.30), 233 (4.25), 279 (3.67); IR (film) ν_{max}: 3422 (br), 2958, 2933, 1593, 1513, 1463, 1258, 1234, 1136, 1102, 1028, 1005 cm^{-1}; HRESI-TOFMS *m/z* 411.1770 $[M+Na]^+$ (calcd. for $C_{22}H_{28}O_6Na$, 411.1784); ^1H and ^{13}C NMR see Tables 3.4 and 3.5.

Leaves of *Miliusa umpangensis*

The dried and powdered leaves of *M. umpangensis* (199 g) were extracted with MeOH to give 46.8 g of an extract after removal of the solvent. This MeOH extract was then fractionated by vacuum liquid chromatography on silica gel using solvent mixtures of increasing polarity (*n*-hexane-EtOAc (100:0-0:100), EtOAc-MeOH (100:0-0:100) to give seven fractions (A-G). Further chromatographic separations of these fractions yielded 10 pure compounds (**XXIX**-**XXXVIII**). They were were identified as (+)-miliusate (**XXIX**), (+)-miliusol (**XXX**), (+)-miliusane I (**XXXI**), methyl 2-(1′*β*-geranyl-5′*β*-hydroxy-2′-oxocyclohex-3′-enyl) acetate (**XXXII**), 7,3′,4′-trimethylquercetin (**XXXIII**), ayanin (**XXXIV)**, ombuin (**XXXV**), quercetin 3,7-dimethyl ether (**XXXVI**), chrysosplenol-D (**XXXVII**) and rutin (**XXXVIII**) through analysis of their spectroscopic data (^1H and ^{13}C NMR and ESI-MS), as well as their optical properties, in comparison with literature values.

Stem bark of *Mallotus plicatus*

The dried and powdered stem bark of *Mallotus plicatus* (7.5 kg) was successively extracted with EtOAc and MeOH to give an EtOAc (56 g) and a MeOH (890 g) extract after removal of the solvent. The EtOAc extract was then fractionated by VLC (silica gel, *n*-hexane–CH_2Cl_2 gradient)

to obtain 14 fractions (I–XIV). Fraction VIII (2.2 g) was further separated on a silica gel column (*n*-hexane–CH_2Cl_2 polarity gradient) to give 17 fractions. Fractions 12−17 were combined and dried, and the obtained residue was recrystallized from petroleum ether to give aleuritolic acid acetate (**XLIII**) as colorless needles (188 mg). Fraction XII (3.1 g) was subjected to CC (silica gel, CH_2Cl_2–MeOH gradient) to yield 9 subfractions. Fraction 7 from this column, after drying, was purified by recrystallization from acetone to afford daucosterol (**XLIV**) as a white powder (31 mg). Fraction 9, upon standing, gave brown crystals. The crystals were collected, dried and purified by washing with acetone to furnish colorless needles of bergenin (**XLI**) (62 mg). The mother liquor, after drying, was separated by preparative TLC (silica gel, CH_2Cl_2–acetone 4:6) to afford protocatechuic acid (**XLV**) (8 mg). The MeOH extract was partitioned between H_2O and *n*-BuOH to give an *n*-BuOH extract (38 g) and a water extract (54 g) after evaporation of the solvents. Separation of the *n*-BuOH extract by CC (silica gel, CH_2Cl_2–MeOH gradient) gave 7 fractions (A–G). Fraction B was fractionated on a silica gel column (CH_2Cl_2–acetone gradient) to provide 26 fractions (B1−B26). Fractions B6−B9 were pooled and dried, and further purified by high performance liquid chromatography (ODS, H_2O–CH_3CN 6:4) to give scopoletin (**XLVI**, 2 mg). Fraction B24, after purification by HPLC using similar stationary and mobile phases, presented blumenol A (**XLVII**) as a yellow gum (17 mg). Purification of fraction B26 by recrystallization from CH_2Cl_2 afforded 11-*O*-acetylbergenin (**XLII**) as colorless needles (28 mg). Separation of the water extract on an MCI column (H_2O-MeOH gradient) gave 5 fractions (1−5). Fraction 2 was separated on a silica gel column (EtOAc–MeOH gradient) to give 8 fractions (W1−W8). Fraction W2 was further separated by CC (CH_2Cl_2–MeOH gradient) and then by preparative TLC (silica gel, $CHCl_3$–MeOH 8:2) with double development to give compound **XXXIX** as colorless needles (42 mg). Fraction W8 was separated by prep. TLC (silica gel, *n*-BuOH–CH_3COOH–H_2O 8:1:1) and then purified by CC (silica gel, CH_2Cl_2–MeOH 1:1) to furnish compound **XL** as colorless cubic crystals (6 mg).

*Bergenin-8-O-α-L-rhamnoside (**XXXIX**)*

Colorless needles; mp 198-203 °C; $[\alpha]_D^{20}$ −62.3 (*c* = 0.001, MeOH); UV (MeOH) λ_{max} nm (log ε): 223 (4.42), 274 (3.67); IR (KBr) ν_{max}: 3400, 1722, 1612, 1510, 1460, 1374, 1337, 1093 cm^{-1}; HR-ESI-MS: $[M+Na]^+$ at *m/z* 497.1287 (calcd. for $C_{20}H_{26}O_{13}Na$, 497.1271); ^1H (300 MHz) and ^{13}C (75 MHz) NMR spectral data see Table 3.6.

*seco-Bergenin-8-O-α-L-rhamnoside (**XL**)*

Cubic crystals; mp 146-149 °C; $[\alpha]_D^{20}$ −10.4 (*c* = 0.0003, MeOH); UV (MeOH) λ_{max} nm (log ε): 219 (3.12); IR (KBr) ν_{max}: 3434, 1623, 1573, 1402, 1384, 1094 cm^{-1}; HR-ESI-MS: $[M-H]^-$ at *m/z* 491.1399 (calcd. for $C_{20}H_{27}O_{14}$, 491.1406); ^1H (300 MHz) and ^{13}C (75 MHz) NMR spectral data see Table 3.6.

Whole plant of *Dendrobium venustum*

The dried and powdered whole plant (2 kg) was macerated with MeOH (3 x 10 L) to afford a MeOH extract (164 g) after removal of the solvent. This material was subjected to vacuum-liquid chromatography (VLC) on silica gel (*n*-hexane-EtOAc gradient) to give 8 fractions (A-H). Fraction G was selected for further investigation as it showed antimalarial and antiherpetic effects. Fraction G (16.3 g) was fractionated by CC over silica gel eluting with a CH_2Cl_2-EtOAc gradient to give 10 fractions (GI-GX). Fraction GIV (1.5 g) was separated by CC (silica gel; CH_2Cl_2-EtOAc gradient) to afford 8 fractions (GIV1-GIV8). Fractions GIV3 (218 mg), GIV6 (104 mg) and GIV7 (48 mg) were further purified on Sephadex LH-20 (acetone) to give flavanthrinin (**XLVIII**) (452 mg), gigantol (**XLIX**) (25 mg) and densiflorol B (**L**) (25 mg), respectively. Fraction GV (1.0 g) was separated by CC (silica gel; CH_2Cl_2-EtOAc gradient) and then further purified on Sephadex LH-20 (acetone) to afford lusianthridin (**LI**) (618 mg). Fraction GVI (45 mg) was separated on Sephadex LH-20 (acetone) and then purified by CC (silica gel; CH_2Cl_2-EtOAc gradient) to yield batatasin III (**LII**) (19 mg). Fraction GVII (2.2 g) was separated by CC over silica gel (CH_2Cl_2-MeOH gradient) and then further purified by preparative TLC (CH_2Cl_2-MeOH 9.5:0.5) to give phoyunnanin E (**LIII**) (16 mg). Fraction GVIII (5.0 g) was separated by CC (silica gel; CH_2Cl_2-MeOH gradient) and then by preparative TLC (CH_2Cl_2-MeOH 9.5:0.5) to afford phoyunnanin C (**LIV**) (31 mg).

Whole plant of *Dendrobium williamsonii*

Dried and powdered whole plant of *D. williamsonii* (1.8 kg) was extracted with MeOH(3 × 10 L) at room temperature to give a viscous mass of dried extract (165 g) after evaporation of the solvent. This material was initially subjected to vacuum-liquid chromatography (VLC) on silica gel (*n*-hexane-EtOAc, gradient) to give 6 fractions (A-F). Fraction D (9.1 g) was further separated by column chromatography (CC) over silica gel, eluted with *n*-hexane- EtOAc (gradient) to give 10 fractions (D1-D10). Fraction D3 (650 mg) was subjected to CC (silica gel; *n*-hexane-CH_2Cl_2, gradient) to give 33 fractions. Compound **LV** (3 mg) was obtained from fraction 26 after recrystallization from *n*-hexane. Fraction 16 was purified on Sephadex LH-20 (CH_2Cl_2-MeOH, 1:1) to furnish **LVI** (38 mg). Fraction D5 (790 mg) was separated by CC (silica gel; *n*-hexane-EtOAc, gradient) and then further purified on Sephadex LH-20 (CH_2Cl_2-MeOH, 1:1) to furnish **LVII** (20 mg). Fraction D6 (1.7 g) was subjected to repeated CC (silica gel; *n*-hexane- EtOAc, gradient) to give 7 fractions (D6.1-D6.7). Fraction D6.5 (30 mg) was separated on Sephadex LH-20 (CH2Cl2-MeOH, 1:1) to yield **LVIII** (5 mg). Compound **LIX** 5 (5 mg) was obtained from fraction D6.6 after purification on Sephadex LH-20 (CH_2Cl_2-MeOH, 1:1). Fraction D-7 (863 mg) was separated by CC (silica gel; CH_2Cl_2-acetone, gradient) to give 13 fractions. Separation of fraction 3 (50 mg) was performed by CC over silica gel (CH_2Cl_2-MeOH, gradient) to give **LX** (3 mg).

2.2 Biological activity evaluation

Assay for Anti-Herpes Simplex Activity

Anti-HSV activity of the isolated compounds was determined using a modified plaque reduction method (Lipipun et al., 2003). Briefly, Vero cells in 96-well tissue culture plate were infected with 30 plaque forming units of HSV-1 (KOS) or HSV-2 (Baylor186). After 1 hr incubation at room temperature for virus adsorption, the cells were added with overlay media containing various concentrations of the test compound. The infected cultures were incubated at 37 °C for 2 days. The infected cells were fixed and stained, and then the number of plaques was counted. The 50% effective concentration (EC_{50}) was determined from the curve relating the plaque number to the concentration of the compound. Acyclovir was used as a positive control.

Assay for Neuraminidase inhibitory activity

Samples were evaluated by the Bioassay Services of The National Center for Genetic Engineering and Biotechnology (BIOTEC). This assay was performed using the method previously described by Potier and co-workers (Potier et al., 1979). The fluorescence was measured using SpectraMax M5 multi-detection microplate reader (Molecular Devices, USA) with excitation and emission wave lengths of 365 and 450 nm, respectively. Oseltamivir was used as a positive control.

3. Results and discussion

3.1 Structural characterization

Melting points (uncorrected) were determined on a Fisher-Johns hot stage melting point apparatus. Optical rotations were measured on a Perkin-Elmer 341polarimeter, and the CD spectra were recorded on a JASCO J-715 spectropolarimeter. UV spectra were obtained on a Shimadzu UV-160A UV/VIS spectrometer and IR spectra on aPerkin-Elmer FT-IR spectrum 65 spectrophotometer and Nicolet FT-IR 510 spectrophotometer. Mass spectra were recorded on Thermo Finnergan LCQ Advantage (ESI-ion trap) or a LCT Premier Waters (ESI-TOF) mass spectrometer. NMR spectra were obtained with a Bruker AC300 spectrometer (300 MHz) or a Bruker Avance 400 spectrometer (400 MHz).

Root bark of *Artocarpus lakoocha*

Compound **I** (Figure 3.1) was obtained as a new compound. The positive HR-ESI-MS exhibited the $[M+H]^+$ ion at *m/z* 491.2430 (calcd. for $C_{30}H_{35}O_6$, 491.2434), suggesting the molecular formula $C_{30}H_{34}O_6$. The IR bands at 3328 (hydroxyl), 1701 (conjugated carbonyl) and 1459-1648 (aromatic ring) cm^{-1} and the UV absorptions at 220, 262 and 308 nm, were suggestive of a flavone skeleton. Similar to cudraflavone (**IV**), compound **I** showed ^1H NMR signals for H-8 (δ 6.38 1H, s), H-3′ (δ 6.54, 1H, d, *J* = 2.5 Hz), H-5′ (δ 6.48, 1H, dd, *J* = 8.5, 2.5 Hz), H-6′ (δ 7.16, 1H, d, *J* = 8.5 Hz), and OH-5 (δ 13.42, 1H, s). The ^1H NMR spectrum of **I** also exhibited signals for a prenyl group [δ 1.41 (3H, s, H_3-13), δ 1.55 (3H, s, H_3-12), δ 3.09 (2H, d, *J* = 7.0 Hz, H_2-9) and δ 5.11 (1H,

t, *J* = 7.0 Hz, H-10)] and a geranyl group [δ 1.55 (3H, s, H_3-22), δ 1.60 (3H, s, H_3-23), 1.78 (3H, s, H_3-17), δ 1.95 (2H, m, H_2-18), δ 2.04 (2H, m, H_2-19), δ 3.36 (2H, d, *J* = 7.0 Hz, H_2-14), 5.07 (1H, t, *J* = 7.0 Hz, H-20) and δ 5.28 (1H, d, *J* = 7.0 Hz, H-15)]. Important NMR properties observed for the geranyl group were the HMBC connectivities from H-18 to C-15 (δ 123.2), C-17 (δ 16.2), C-19 (δ 27.3) and C-20 (δ 125.1). The prenyl group should be attached at C-3 (δ 121.4) of ring C, as suggested from the HMBC correlations from H_2-9 to C-2 (δ 161.9), C-4 (δ 182.9) and C-11 (δ 131.9). The HMBC correlations of H_2-14 with C-6 (δ 111.7) and C-5 (δ 160.0) placed the geranyl group at C-6 of ring A. Based on above spectral evidence, compound **I** was characterized as 5,7,2′,4′-tetrahydroxy-3-prenyl-6-geranylflavone.

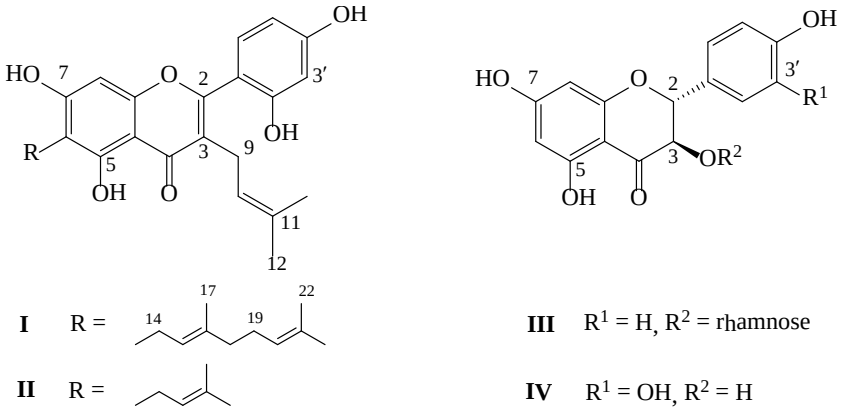

Figure 3.1 Flavonoids isolated from roots of *Artocarpus lakoocha*

Through analysis of the spectroscopic properties, known compounds were identified as (+)-afzelechin-3-*O*-α-L-rhamnopyranoside (**II**) (Drewes et al., 1992), (+)-catechin (**III**) (Davis et al., 1996) and cudaflavone C (**IV**) (Hano et al., 1990).

Leaves of *Miliusa mollis*

Six new polyphenolics were isolated, and their structures were established through NMR and MS studies. They included five new dihydrobenzofuran neolignans (**V**, **VII**-**X**) and a new 8-*O*-4′-neolignan (**VI**). In addition, decurrenal (**XI**) (Chauret et al., 1996) was also obtained (Figure 3.2).

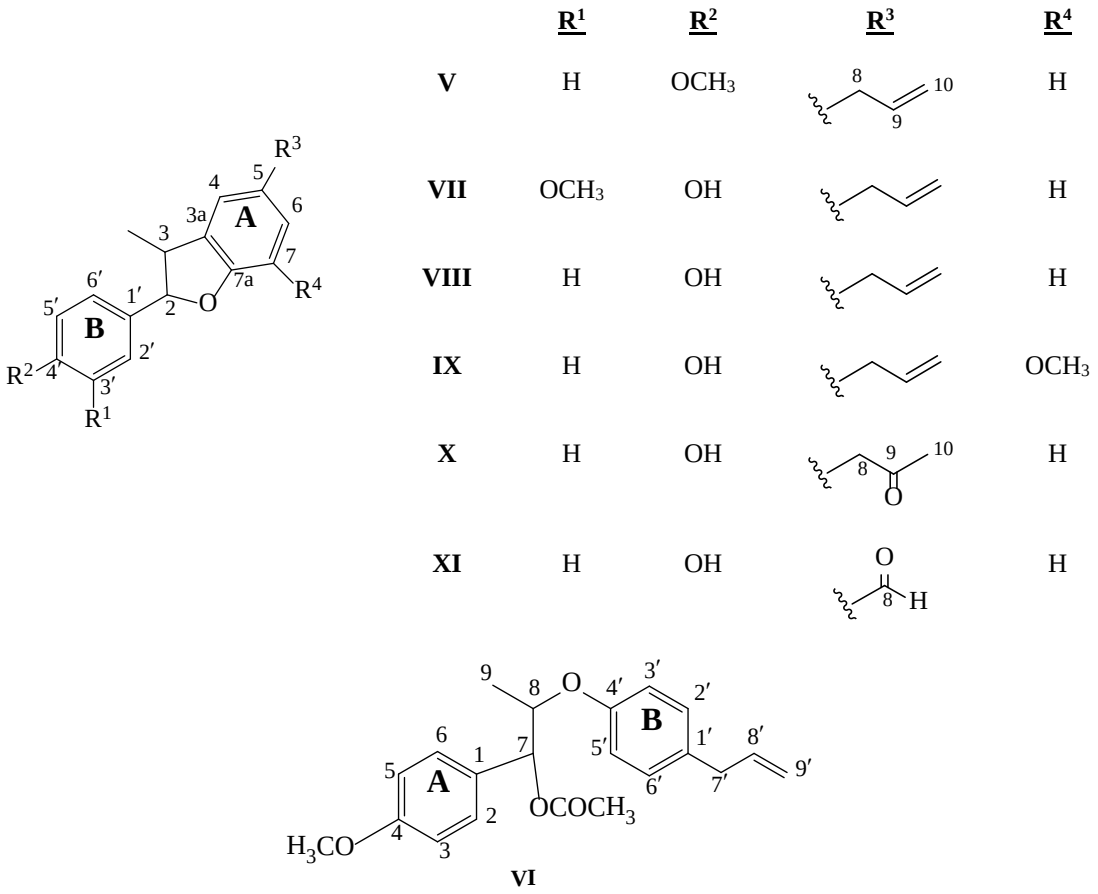

VI

Figure 3.2 Neolignans isolated from leaves of *Miliusa mollis*

Compounds **V**, **VII**-**X** could be preliminarily characterized as neolignans containing a dihydrobenzofuran structure from the three UV maxima at 207-212, 228-233 and 280-285 nm. Spectroscopic data confirming the dihydrobenzofuran nucleus in these compounds were the sets of ^{1}H NMR signals observed for the following protons: H-2 [δ 5.07 – 5.13 (1H, d, *J* = 8.8 – 9.6 Hz)]; H-3 [δ 3.40 – 3.46 (1H, apparent quintet, *J* = 7.0 – 7.9 Hz)]; and CH_3-3 [δ 1.37 – 1.41 (3H, d, *J* = 6.8 Hz)] (Table 1). These protons, as expected, showed HSQC correlations to C-2 [δ 92.5 – 93.2], C-3 [δ 45.2 – 45.8] and CH_3-3 [δ 17.0 – 17.7] (Table 3.2).

Miliumollin (**VIII**) was obtained as a colorless viscous liquid. The molecular formula was established by HR-ESI-TOF-MS as $C_{18}H_{18}O_2$, which was the same as that of conocarpan, a dihydrobenzofuran-type neolignan previously identified from *Krameria cystisoides*. Characteristic NMR signals for the dihydrofuran ring were HSQC cross-peaks for H-2/C-2 [δ_H 5.10 (1H, d, *J* = 8.8 Hz)/δ_C 92.5] and H-3/C-3 [δ_H 3.43 (1H, apparent quintet, *J* = 7.7 Hz)/δ_C 45.3] (Tables 3.2 and 3.3). The large coupling constant (*J* = 8.8 Hz) between H-2 and H-3 indicated a *trans* relative configuration, and this was confirmed by the NOESY interaction of H-2 with C<u>H</u>$_3$-3. The ^{1}H and

^{13}C NMR data for both aromatic rings of **VIII** were also similar to those of conocarpan; however differences were found in the propenyl side-chain. In **VIII**, this three-carbon unit should be an allyl moiety, as reflected by the NMR signals for vinyl protons at δ 5.04 (1H, br dd, *J* = 9.9, 1.7 Hz) and δ 5.11 (1H, br dd, *J* = 16.9, 1.7 Hz), both being correlated to the same carbon at δ 115.4 in the HSQC spectrum. This was also corroborated by the ^{13}C NMR signals for a methine and a methylene olefinic carbon at δ 138.1 and 115.4, respectively. The above spectroscopic evidence suggested that **VIII** should be 5-allyl-2,3-dihydro-2-(4-hydroxyphenyl)-3-methylbenzofuran. Key HMBC correlations observed from H-8 to C-4 and C-6, and from H-2 to C-2′ and C-6′ confirmed the proposed structure. To determine the absolute configuration at C-2 and C-3, the optical rotation and circular dichroism properties of **VIII** were studied. It is known that a *trans*-2-aryl-3-methyl-2,3-dihydrobenzofuran structure with 2*R*,3*R* configuration shows a negative Cotton effect at about 281 nm and a positive Cotton effect at about 233 nm, whereas the reverse is true for the 2*S*,3*S*-isomer. Compound **VIII** was found to be dextrorotatory ($[\alpha]_D^{20}$ +32.40), and its CD spectrum showed a negative and a positive Cotton effect at 290 nm and 236 nm, respectively. Therefore, it was concluded that miliumollin (**VIII**) possessed 2*R*,3*R* configuration, and its structure was established as (*2R,3R*)-5-allyl-2,3-dihydro-2-(4-hydroxyphenyl)-3-methylbenzofuran.

The molecular formula of 4′-*O*-methylmiliumollin (**V**) was defined as $C_{19}H_{20}O_2$ by HR-ESI-TOF-MS. The ^{1}H-NMR and ^{13}C-NMR spectral properties of **V** (Tables 3.2 and 3.3) were very close to those of **VIII**, except that **V** possessed NMR signals for a methoxy group [δ_H 3.84 (3H, s); δ_C 55.3]. This methoxy group should be placed at C-4′, as indicated by the NOESY interaction of the C$\underline{H}_3$O protons with H-3′/H-5′ (δ 6.94, 2H, d, *J* = 8.7 Hz), and the HMBC correlations from the C$\underline{H}_3$O and H-2′/H-6′ protons to C-4′. In the dihydrofuran ring, the large vicinal coupling constant (*J* = 9.1 Hz) between H-2 and H-3, together with the NOESY interaction of H-2 with the C$\underline{H}_3$-3 protons, indicated *trans*-relative configuration for these methine protons. Compound **V** was levorotatory ($[\alpha]_D^{20}$ −25.00), and the absolute configuration was determined to be 2*S*,3*S* from the positive and negative Cotton effect at 284 and 238 nm, respectively in the CD spectrum. Thus, **V** was characterized as (2*S*,3*S*)-5-allyl-2,3-dihydro-2-(4-methoxyphenyl)-3-methylbenzofuran.

3′-Methoxymiliumollin (**VII**) had a molecular formula of $C_{19}H_{20}O_3$ as determined by HR-ESI-TOF-MS. This compound (**VII**), similar to **VIII,** showed ^{1}H-NMR and ^{13}C-NMR signals for the dihydrobenzofuran system, but on ring B of **VII**, one of the aromatic protons was replaced by a methoxy group [δ_H 3.84 (3H, s); δ_C 55.4] (Tables 3.2 and 3.3). This CH_3O group should be located on C-3′, as supported by the NOESY interaction between these C$\underline{H}_3$O protons and H-2′ [δ 7.10, (1H, d, *J* = 1.7 Hz)], and the HMBC connectivity from H-2 to C-2′ and C-6′. The absolute configuration of **VII** was determined to be 2*R*,3*R* based on the negative and positive Cotton effect

at 290 nm and 240 nm in the CD spectrum, respectively. Thus, the structure of **VII** was elucidated as (*2R,3R*)-5-allyl-2,3-dihydro-2-(4-hydroxy-3-methoxyphenyl)-3-methylbenzofuran.

The molecular formula of 7-methoxymiliumollin (**IX**) was deduced to be $C_{19}H_{20}O_3$ by HR-ESI-TOF-MS, which was the same as that of **VII**. However, this neolignan (**IX**) had the methoxy group located on ring A at C-7. This was indicated from the NOESY cross-peak between the C$\underline{H}_3$O protons and H-6 (δ 6.64, 1H, br s), and the HMBC correlation from H-6 to C-8 (δ 40.2) (Figure 2). A positive optical rotation ($[\alpha]_D^{20}$ +15.70) was observed for (**IX**), and its CD curve demonstrated a negative and a positive Cotton effect at 286 and 242 nm, respectively, indicating *2R,3R* configuration. Thus, the structure of (**IX**) was established as (2*R*,3*R*)-5-allyl-2,3-dihydro-2-(4-hydroxyphenyl)-7-methoxy-3-methylbenzofuran.

Miliumollinone (**X**) possessed ^{1}H and ^{13}C NMR properties similar to those of **VIII**, but with a different three-carbon substituent at C-5 (Tables 3.2 and 3.3). This was evident from three ^{13}C NMR signals representing keto (δ 208.4, C-9), methylene (δ 50.5, C-8) and methyl (δ 29.3, C-10) carbons. These two aliphatic carbons showed HSQC coupling with the protons at δ 3.69 (2H, s, C$\underline{H}_2$-8) and 2.22 (3H, s, C$\underline{H}_3$-10), respectively. The HMBC connectivity from C$\underline{H}_2$-8 to C-4 (δ 124.6), C-6 (δ 129.3) and C-9 (δ 208.4) showed that the substituent at C-5 was a 2-oxopropyl group (Figure 2). Compound **X** was optically active ($[\alpha]_D^{20}$ +23.00), and the negative and positive Cotton effect at 290 and 236 nm in the CD spectrum justified *2R,3R* configuration. Hence, **X** was characterized as (*2R,3R*)-2,3-dihydro-2-(4-hydroxyphenyl)-3-methyl-5-(2-oxopropyl)-benzofuran.

Miliusamollin (**VI**) exhibited UV maxima at 228 and 273 nm, suggesting a 8-*O*-4′-neolignan structure. Its molecular formula $C_{21}H_{24}O_4$ was established by HR-ESI-TOF-MS. The ^{1}H and ^{13}C NMR spectra of (**VI**) (Tables 3.2 and 3.3) were generally similar to those of (7*S*,8*S*)-*threo*-$\Delta^{8'}$-4-methoxyneolignan, an 8-*O*-4′-neolignan earlier identified from the twigs of this plant]. However, in **VI**, additional NMR signals for an acetoxy group [δ_H 2.02 (3H, s); δ_C 21.2 (q) and 170.2 (s)] were observed. This acetoxy moiety should be located at C-7, as evidenced by the upfield shift of C-8 in **VI** due to the γ-steric effect caused by the carbonyl carbon, as compared with its counterpart in (7*S*,8*S*)-*threo*-$\Delta^{8'}$-4-methoxyneolignan. This was confirmed by the HMBC correlation from H-7 (δ 5.89, 1H, d, J = 7.2 Hz) to the carbonyl carbon (δ 170.2). The large vicinal coupling constant (J = 7.2 Hz) between H-7 and H-8 indicated a *threo* relative configuration. In support of this, NOESY interactions were observed between H-7 and CH_3-9 protons. The absolute configuration of **VI** was then determined by comparison of its optical properties with those of ligraminol C. Compound **VI** was levorotatory ($[\alpha]_D^{20}$ −55.40), and had 7*R*,8*R* absolute configuration, as indicated by the negative Cotton effects at 278 and 230 nm in the CD spectrum. Based on the above spectroscopic evidence, miliusamollin (**VI**) was characterized as (7*R*,8*R*)-*threo*-$\Delta^{8'}$-7-acetoxy-4-methoxy-8-*O*-4′-neolignan.

Table 3.2 ^{1}H NMR spectroscopic data of compounds **V - X** (300 MHz, δ ppm, *J* in Hz).

Position	**V**[a]	**VI**[a]	**VII**[b]	**VIII**[a]	**IX**[a]	**X**[a]
2	5.11 (*d*, 9.1)	7.33 (*d*, 8.7)	5.07 (*d*, 9.1)	5.10 (*d*, 8.8)	5.13 (*d*, 9.6)	5.09 (*d*, 9.2)
3	3.43 (*apparent quint*, 7.9)	6.91 (*d*, 8.7)	3.41 (*apparent quint*, 7.9)	3.43 (*apparent quint*, 7.7)	3.46 (*apparent quint*, 7.5)	3.40 (*apparent quint*, 7.0)
3a	-	-	-	-	-	-
4	6.98 (*br s*)	-	7.03 (*br s*)	6.99 (*br s*)	6.62 (*br s*)	6.98 (*br s*)
5	-	6.91 (*d*, 8.7)	-	-	-	-
6	7.00 (*br d*, 9.3)	7.33 (*d*, 8.7)	6.99 (*br d*, 8.1)	7.00 (*br d*, 9.2)	6.64 (*br s*)	7.01 (*d*, 7.9)
7	6.80 (*d*, 9.3)	5.89 (*d*, 7.2)	6.73 (*d*, 8.1)	6.79 (*d*, 9.2)	-	6.81 (*d*, 7.9)
7a	-	-	-	-	-	-
8	3.38 (*br d*, 6.7)	4.61 (*apparent quint*, 6.5)	3.35 (*br d*, 6.8)	3.38 (*br d*, 6.8)	3.38 (*br d*, 6.8)	3.69 (*s*)
9	6.00 (*ddt*, 16.9, 9.3, 6.7)	1.15 (*d*, 6.5)	5.98 (*ddt*, 17.8, 11.6, 6.8)	6.00 (*ddt*, 16.9, 9.9, 6.8)	6.00 (*ddt*, 16.7, 11.4, 6.8)	-
10	5.08 (*br dd*, 9.3, 1.7)	-	5.03 (*br dd*, 11.6, 1.8)	5.04 (*br dd*, 9.9, 1.7)	5.08 (*br dd*, 11.4, 1.7)	2.22 (*s*)
	5.11 (*br dd*, 16.9, 1.7)	-	5.09 (*br dd*, 17.8, 1.8)	5.11 (*br dd*, 16.9, 1.7)	5.13 (*br dd*, 16.7, 1.7)	-
1′	-	-	-	-	-	-
2′	7.38 (*d*, 8.7)	7.12 (*d*, 8.7)	7.10 (*d*, 1.7)	7.32 (*d*, 8.7)	7.32 (*d*, 8.6)	7.29 (*d*, 8.5)
3′	6.94 (*d*, 8.7)	6.91 (*d*, 8.7)	-	6.85 (*d*, 8.7)	6.83 (*d*, 8.6)	6.84 (*d*, 8.5)
4′	-	-	-	-	-	-
5′	6.94 (*d*, 8.7)	6.91 (*d*, 8.7)	6.87 (*d*, 8.1)	6.85 (*d*, 8.7)	6.83 (*d*, 8.6)	6.84 (*d*, 8.5)
6′	7.38 (*d*, 8.7)	7.12 (*d*, 8.7)	6.92 (*dd*, 8.1, 1.7)	7.32 (*d*, 8.7)	7.32 (*d*, 8.6)	7.29 (*d*, 8.5)
7′	-	3.35 (*br d*, 6.7)	-	-	-	-
8′	-	5.97 (*ddt*, 17.0, 10.1, 6.7)	-	-	-	-
9′	-	5.07 (*br dd*, 10.1, 1.7)	-	-	-	-
	-	5.09 (*br dd*, 17.0, 1.7)	-	-	-	-
CH_3-3	1.41 (*d*, 6.8)	-	1.37 (*d*, 6.8)	1.41 (*d*, 6.8)	1.39 (*d*, 6.8)	1.37 (*d*, 6.8)
CH_3O	3.84 (*s*)	3.83 (*s*)	3.84 (*s*)	-	3.89 (*s*)	-
$OOCCH_3$	-	2.02 (*s*)	-	-	-	-

[a]Measured in $CDCl_3$
[b]Measured in acetone-d_6

Table 3.3 ^{13}C NMR spectroscopic data of compounds **V - X** (75 MHz, δ in ppm).

Position	**V**[a]	**VI**[a]	**VII**[b]	**VIII**[a]	**IX**[a]	**X**[a]
1	-	129.3	-	-	-	-
2	92.6	128.9	92.8	92.5	93.2	92.8
3	45.4	113.9	45.3	45.3	45.8	45.2
3a	132.7	-	132.5	132.7	133.1	132.8
4	123.7	159.6	123.8	123.7	115.7	124.6
5	132.2	113.9	132.2	132.2	133.5	126.3
6	128.3	128.9	128.1	128.2	111.8	129.3
7	109.2	77.7	108.8	109.1	144.0	109.6
7a	157.6	-	157.8	157.5	145.7	158.3
8	39.8	76.2	39.5	39.8	40.2	50.5
9	138.1	16.4	138.5	138.1	137.9	208.4
10	115.4	-	114.6	115.4	115.6	29.3
1′	132.4	132.7	132.2	132.4	132.6	132.2
2′	127.7	129.6	109.7	127.9	128.2	127.9
3′	114.0	116.2	147.6	115.4	115.3	115.5
4′	159.6	156.7	146.7	155.7	155.6	156.1
5′	114.0	116.2	114.8	115.4	115.3	115.5
6′	127.7	129.6	119.4	127.9	128.2	127.9
7′	-	39.4	-	-	-	-
8′	-	137.8	-	-	-	-
9′	-	115.5	-	-	-	-
CH_3-3	17.7	-	17.0	17.7	17.7	17.6
CH_3O	55.3	55.3	55.4	-	56.0	-
$OOC\underline{CH_3}$	-	21.2	-	-	-	-
$\underline{COO}$	-	170.2	-	-	-	-

[a]Measured in $CDCl_3$
[b]Measured in acetone-d_6

Leaves and stems of *Miliusa fragrans*

Chemical investigations of the leaves and stems of *Miliusa fragrans* resulted in the isolation of thirteen neolignans (**XII** – **XXIV**), three lignans (**XXV** –**XXVII**), and a flavonoid (**17 XXVIII**). They were characterized as seven new neolignans **(XII, XIII, XVI-XX**) and a new lignan (**XXV**). Furthermore, nine known polyphenolic compounds were identified, including eusiderins C and D (**XIV** and **XV**) (Fernandes, et al., 1980), 2-(4-allyl-2,6-dimethoxyphenoxy)-1-(3,4-dimethoxyphenyl)propane (**XXI**) (Yang et al., 2008), virolongin B (**XXII**)(Bárbosa-Filho et al., 1989), (7*S*,8*R*)-7-hydroxy-3,4,3′-trimethoxy-$\Delta^{1,3,5,1',3',5',8'}$-8.O.4′-neolignan (**XXIII**) (Morais et al., 2009), licarin A (**XXIV**) (Achenbach et al, 1987), veraguensin (**XXVI**) (Fonseca et al, 1979), (7*S*,8*S*,7′*R*,8′*S*)-3,4,5,3′,4′-pentamethoxy-7,7′-epoxylignan (**XXVII**) (Lopes et al., 1996) and (–)-epicatechin (**XXVIII**) (Sun et al., 2006) (Figure 3.3).

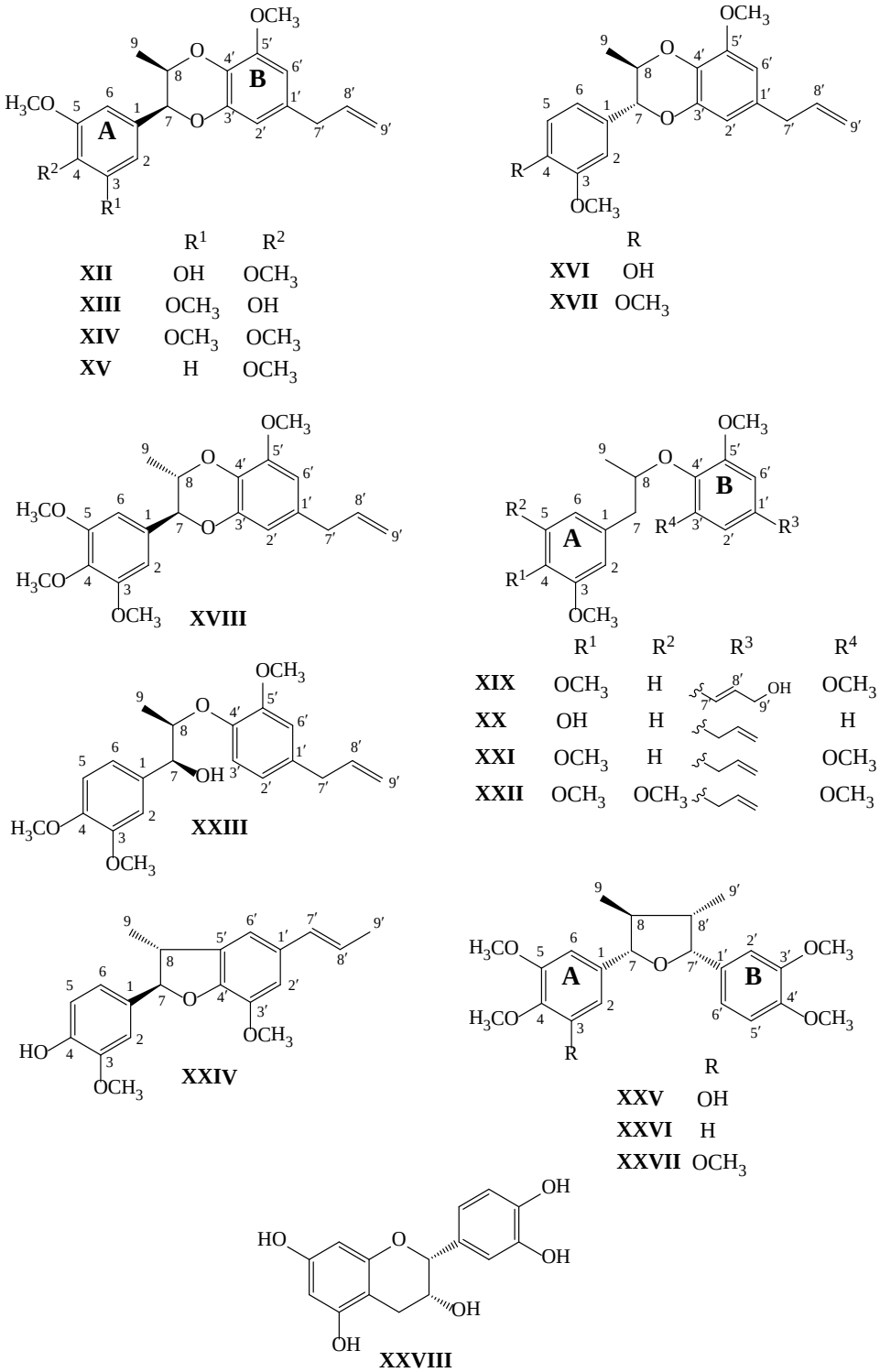

Figure 3.3 Neolignans, lignans and a flavonoid isolated from stems and leaves of *Miliusa fragrans*

The 7.*O*.3′,8.*O*.4′-neolignans (**XII** – **XVIII**) showed UV absorptions at about 220 and 275 nm. These compounds had a dioxane ring formed as a bridge linking the two phenylpropanoid units, as was evident from the HMBC 3-bond connectivities from the oxybenzylic methine protons (H-7 and H-8) to the aromatic carbons (i.e. C-2 and C-6 of ring A, and C-3′ and C-4′ of ring B)

(Tables 3.4 and 3.5). In addition, the ^{1}H and ^{13}C NMR spectroscopic data of these compounds revealed that their B rings shared the same substitution pattern, having an allyl and a methoxy group located at C-1′ and C-5′, respectively. The structural differences were: (1) the number and the positions of the oxygen functionalities on ring A (OH and/or OMe); (2) the spatial orientation of the A ring and the methyl group on the benzodioxane structure.

Compound **XII** had a molecular formula of $C_{21}H_{24}O_6$ as determined by HRESI-TOFMS. The molecular mass, together with the COSY and HSQC correlations, suggested that the oxygenation pattern of ring A of **XII** was similar to that of eusiderin C (**XIV**), but one of the methoxy groups was replaced with a hydroxy. The lack of symmetry in ring A of **XII**, as reflected by the different chemical shifts of H-2 [δ 6.65 (1H, d, *J* = 1.8 Hz)] and H-6 [δ 6.56 (1H, d, *J* = 1.8 Hz)] (Table 3.4), required that the hydroxy group be placed at C-3. This was confirmed by the downfield shift of C-2 and the upfield shift of C-3 in the ^{13}C NMR spectrum of **XII** in comparison with their counterparts in **XIV** (Table 3.5). The *cis*-arrangement of the *sec*-methyl and the aryl on the benzodioxane ring of **XII** was verified by analysis of the chemical shift of the methyl protons (δ 1.15) and the coupling constant (*J* = 2.3 Hz) between H-7 and H-8, and this was ascertained by the NOESY interaction between H-7 and H-8. The absolute stereochemistry was then determined by measurement of the circular dichroism (CD) spectrum. It has been well established for 7.*O*.3′,8.*O*.4′-neolignans that a *cis*-benzodioxane derivative with 7*S*,8*R* configuration shows a negative Cotton effect at *ca* 246 nm, whereas the (7*R*,8*S*) antipodal isomer shows a positive effect at this position. For the *trans*-series, an analogue with 7*R*,8*R* configuration exhibits a negative Cotton effect at about 242 nm and the reverse is true for an isomer with 7*S*,8*S* configuration (da Silva et al., 1989). Since **XII** showed a negative Cotton effect at 246 nm, it should have the absolute configuration 7*S*,8*R*. Based on the above data, isolate **XII** was characterized as (7*S*,8*R*)-$\Delta^{8'}$-3-hydroxy-4,5,5′-trimethoxy-7.*O*.3′,8.*O*.4′-neolignan, and named (+)-3-*O*-demethyleusiderin C.

Neolignan **XIII** was a structural isomer of **XII**, as was evident from its molecular formula ($C_{21}H_{24}O_6$) as determined by HRESI-TOFMS. Similar to **XII**, compound **XIII** had H-7 and H-8 placed in a *cis*-relationship, as suggested from their vicinal coupling (*J* = 2.4 Hz) (Table 3.4) and NOESY interaction. The negative Cotton effect at 248 nm in the CD spectrum indicated the 7*S*,8*R* absolute configuration for **XIII**. Thus, the structure of **XIII** was established as (7*S*,8*R*)-$\Delta^{8'}$-4-hydroxy-3,5,5′-trimethoxy-7.*O*.3′,8.*O*.4′-neolignan, and the trivial name (+)-4-*O*-demethyl-eusiderin C was thus given.

For (−)-miliusfragrin (**XVI**), the ^{1}H and ^{13}C NMR spectral signals for ring B were similar to those of **XII** and **XIII** (Tables 3.4 and 3.5). However, the A ring of **XVI** was dioxygenated at positions 3 and 4, as suggested from the ^{13}C NMR spectral signals at δ 146.9 (C-3) and 146.2 (C-4), and the ^{1}H NMR coupling system at δ 6.88 (1H, br s, H-2), δ 6.89 (1H, br d, *J* = 8.6 Hz, H-6) and δ 6.96 (1H, d, *J* = 8.6 Hz, H-5) (Tables 2 and 3). The molecular formula $C_{20}H_{22}O_5$, together

with the HSQC cross peak at δ_H (3.81, 3H, s)/δ_C (56.1, q), necessitated the presence of methoxy and hydroxy groups on ring A. The methoxy group, due to the NOESY correlation with H-2, should be placed at C-3. Protons H-7 and H-8 had a *trans*-relative relationship, as was evident from their *J* values (7.9 Hz) and the NOESY correlation from H-7 to CH_3-9. Based on the negative CD Cotton effect at 238 nm, **XVI** was assigned the absolute configuration 7*R*,8*R*. Thus, the structure of **5** was elucidated as (7*R*,8*R*)-$\Delta^{8'}$-4-hydroxy-3,5′-dimethoxy-7.*O*.3′,8.*O*.4′-neolignan.

(−)-4-*O*-Methylmiliusfragrin (**XVII**) possessed NMR features similar to those of **XVI**, except for the presence of an additional HSQC correlation peak at δ_H 3.92 (3H, s)/δ_C 56.0. Compound **XVII** had a molecular mass ($C_{21}H_{24}O_5$) 14 amu higher than **XVI**, implying that **XVII** was a 4-*O*-methyl derivative of **XVI**. The ^{1}H and ^{13}C NMR spectroscopic data relevant to the 1,4-dioxane ring of **XVII** (Tables 3.4 and 3.5)**,** as well as the NOESY correlation between H-7 and CH_3-9, resembled those of **XVI**, suggesting the same *trans* H-7/H-8 relative configuration. The 7*R*,8*R* absolute stereochemistry was assigned to **XVII**, due to the negative peak at 238 nm in the CD curve. On the basis of these spectroscopic data, the structure of **XVII** was concluded to be (7*R*,8*R*)-$\Delta^{8'}$-3,4,5′-trimethoxy-7.*O*.3′,8.*O*.4′-neolignan.

Compound **XVIII** exhibited ^{1}H and ^{13}C NMR spectral and MS properties (Tables 3.4 and 3.5) which were superimposable with those reported for (−)-eusiderin A, a (7*R*,8*R*)-benzodioxane-type neolignan isolated earlier from *Virola pavonis* and *Licaria chrysophylla* (Fernandes et al., 1980; da Silva etal., 1989). However, **7 XVIII** showed a positive CD Cotton effect at *ca* 238 nm, in contrast with (−)-eusiderin A, which exhibited a negative sign at this position.[21] Thus, **XVIII** was characterized as (+)-eusiderin A, the (7*S*,8*S*)-antipodal isomer of (−)-eusiderin A, which was unknown prior to this study.

Regarding the 8.*O*.4′-neolignans **XIX -XXII**, nearly all of them, except for **XX**, possessed a symmetric B ring, with two methoxy groups at C-3′ and C-5′, and an allyl or a propenyl moiety at C-1′.

For (−)-miliusfragranol A (**XIX**), the HRESI-TOFMS established a molecular formula of $C_{22}H_{28}O_6$, indicating an additional oxygen atom with respect to *erythro*-2-(4-allyl-2,6-dimethoxyphenoxy)-1-(3,4-dimethoxyphenyl)propane, a neolignan also found in this plant, and earlier isolated from the seeds of *Myristica fragrans*. However, **XIX** should have a hydroxypropenyl group at C-1′. This was confirmed by the HMBC 3-bond connectivities from H-7′ to C-2′, C-6′ and C-9′. Further examination of the COSY, HSQC and HMBC data led us to establish the structure of **XIX** as $\Delta^{7'}$-9′-hydroxy-3,4,3′,5′-tetramethoxy-8.*O*.4′-neolignan.

(−)-Miliusfragranol B (**XX**) was also an 8.*O*.4′-neolignan, but with only one methoxy group on the B ring. This was apparent from the appearance of H-2′ (δ 6.70, 1H, dd, *J* = 8.1 and 1.7 Hz), H-3′ (δ 6.80, 1H, br d, *J* = 8.1 Hz) and H-6′ (δ 6.73, 1H, br s), which showed HSQC correlations

to C-2′ (δ 120.5), C -3′ (δ 116.1) and C-6′ (112.6), respectively (Tables 3.4 and 3.5). The ^{1}H NMR data for the A ring of **XX** were similar to those of 2-(4-allyl-2,6-dimethoxyphenoxy)-1-(4-hydroxy-3-methoxyphenyl)propane, a neolignan earlier found in *Myristica fragrans*, suggesting that **XX** had methoxy and hydroxy groups at C-3 and C-4, respectively. This was confirmed by the ^{3}J coupling between H-6 and C-4 observed in the HMBC spectrum. On the basis of these data, the structure of **XX** was elucidated as $\Delta^{8'}$-4-hydroxy-3,5′-dimethoxy-8.*O*.4′-neolignan. It should be noted that this structure has been described as 2-methoxy-4-{2-[2-methoxy-4-(2-propen-1-yl)phenoxy]-propyl}phenol on the Scifinder® data base, but so far neither its source nor its physicochemical properties have been provided.

It is important to mention that the neolignans **XIX** – **XXII** were found to show the same sign of specific rotations and closely similar CD properties, suggesting that they should share the same absolute stereochemistry. Unfortunately, no CD data of 8.*O*.4′-neolignans with established absolute configurations are available, so the absolute configurations of this group of 8.*O*.4′-neolignans still await further investigation.

Compound **XXIII**, an 8.*O*.4′neolignan with oxygenation at position 7, was earlier isolated from *Virola pavonis*, and initially proposed to have the relative 7*S**,8*R***erythro*-configuration. In this study, negative CD cotton effects at 240 and 276 nm[24] were observed, confirming the absolute configuration of **XXIII** to be 7*S*,8*R*.

Compounds **XXV -XXVII** were tetrahydrofuran lignans. The new compound **XXV** had a molecular formula of $C_{22}H_{28}O_6$, as established by HRESI-TOFMS. Similar to **XXVI** and **XXVII**, lignan **XXV** had a tetrahydrofuran ring with the relative stereochemistry *trans* (H-7/H-8), *trans* (H-8/H-8′), *cis* (H-8′/H-7′), as suggested from the ^{1}H NMR spectral signals for the following pairs of protons: H-7 (δ 4.38, 1H, d, J = 9.2 Hz) / H-7′ (δ 5.14, 1H, d, J = 8.6 Hz); H_3-9 (δ 1.10, 3H, d, J = 6.5 Hz) / H_3-9′ (δ 0.67, 3H, d, J = 7.0 Hz) (Table 3.4). The large coupling constants of the oxybenzylic protons were attributed to the dihedral angles of about 150° and 0° between H-7 and H-8, and between H-7′ and H-8′, respectively. This relative configuration of the tetrahydrofuran ring was confirmed by the NOESY interactions between H-7 and H_3-9 and between H-7′ and H-8′. Further examination of the ^{1}H and ^{13}C NMR data revealed that the B rings in **XXV** –**XXVII** were similarly substituted. However, ring A of **XXV** was unsymmetrically trioxygenated with one hydroxy and two methoxy substituents, as suggested from the three carbon resonances at δ 152.3 (C-3), 134.9 (C-4) and 149.2 (C-5) (Table 3.5), and the proton signals for H-2 (δ 6.67, 1H, d, J = 1.8 Hz) and H-6 (δ 6.78, 1H, d, J = 1.8 Hz). The two methoxys [δ_H 3.89 (3H, s) / δ_C 55.9 and δ_H 3.91 (3H, s) / δ_C 61.0] should be situated adjacently at C-4 and C-5, leaving the hydroxy group to be placed at C-3. This was corroborated by the NOESY correlation from H-6 to O$C\underline{H}_3$-5 (δ 3.89). Finally, the proposed structure of **XXV** was confirmed from the HMBC spectrum, which showed

^{3}J-correlations from C-7 to H-2, H-6 and H-7′, and from C-7′ to H-2′ and H-6′. Compound **XXV** was dextrorotatory optically and possessed a CD spectrum closely comparable to those of **XXVI** and **XXVII**, and therefore its absolute stereochemistry was established as 7*S*,8*S*,7′*R*,8′*S*. Since **XXV** can be considered as a hydroxylated derivative of **XXVI**, it was given the trivial name (+)-3-hydroxyveraguensin

.**Leaves of *Miliusa umpangensis***

The isolates (Figure 3.4), through analysis of their spectroscopic data (^{1}H and ^{13}C NMR and ESI-MS), as well as their optical properties, were identified as (+)-miliusate (**XXIX**), (+)-miliusol (**XXX**), (+)-miliusane I (**XXXI**) (Zhang et al., 2006), methyl 2-(1′*β*-geranyl-5′*β*-hydroxy-2′-oxocyclohex-3′-enyl) acetate (**XXXII**) (Mbah et al., 2004), 7,3′,4′-trimethylquercetin (**XXXIII**) (Chen et al., 2009), ayanin (**XXXIV)** (Wang et al., 1989; Matsuda et al., 2002), ombuin (**XXXV**(Huong et al., 2004), quercetin 3,7-dimethyl ether (**XXXVI**) (Guerrero et al., 2002), chrysosplenol-D (**XXXVII**) (Ling et al., 2010) and rutin (**XXXVIII**) (Slimestad et al., 2008), in comparison with literature values

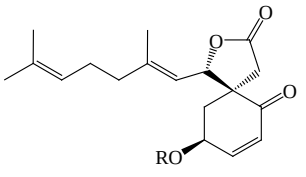

XXIX R = Ac
XXX R = H

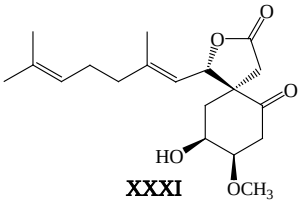

XXXI

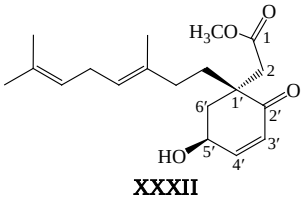

XXXII

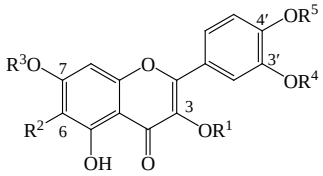

	R^1	R^2	R^3	R^4	R^5
XXXIII	H	H	CH_3	CH_3	CH_3
XXXIV	CH_3	H	CH_3	H	CH_3
XXXV	H	H	CH_3	H	CH_3
XXXVI	CH_3	H	CH_3	H	H
XXXVII	CH_3	OCH_3	CH_3	H	H
XXXVIII	rutinose	H	H	H	H

Figure 3.4 Compounds isolated from the leaves of *Miliusa umpangensis*

Table 3.4 ^{1}H NMR (300 MHz, $CDCl_3$) spectral data for compounds **XII**, **XIII**, **XVI**, **XVII**, **XVIII**, **XX** and **XXV**

Position	**XII**	**XIII**	**XVI**	**XVII**	**XVIII**	**XX**	**XXV**
1	–	–	–	–	–	–	–
2	6.65 (d, 1.8)	6.60 (br s)	6.88 (br s)	6.88 (d, 1.7)	6.79 (d, 2.0)	6.83 (d, 1.9)	6.67 (d, 1.8)
3	–	–	–	–	–	–	–
4	–	–	–	–	–	–	–
5	–	–	6.96 (d, 8.6)	6.93 (d, 7.3)	6.80 (d, 8.1)	6.85 (d, 8.2)	–
6	6.56 (d, 1.8)	6.60 (br s)	6.89 (br d, 8.6)	6.95 (dd, 7.3, 1.7)	6.77 (br d, 8.1)	6.75 (dd, 8.2, 1.9)	6.78 (d, 1.8)
7	5.10 (d, 2.3)	5.08 (d, 2.4)	4.59 (d, 7.9)	4.61 (d, 7.9)	2.76 (dd, 13.5, 8.2) 3.14 (dd, 13.5, 5.0)	2.77 (dd, 13.7, 6.7) 3.11 (dd, 13.7, 6.0)	4.38 (d, 9.2)
8	4.62 (dq, 2.3, 6.6)	4.56 (dq, 2.4, 6.6)	4.12 (dq, 7.9, 6.4)	4.13 (dq, 6.4, 7.9)	4.40 (m)	4.46 (m)	1.80 (m)
9	1.15 (d, 6.6)	1.11 (d, 6.6)	1.25 (d, 6.4)	1.26 (d, 6.4)	1.23 (d, 6.2)	1.32 (d, 6.1)	1.10 (d, 6.5)
1′	–	–	–	–	–	–	–
2′	6.53 (d, 1.9)	6.50 (d, 1.9)	6.58 (d, 1.7)	6.50 (d, 1.7)	6.63 (br s)	6.70 (dd, 8.1, 1.7)	6.90 (d, 1.7)
3′	–	–	–	–	–	6.80 (br d, 8.1)	–
4′	–	–	–	–	–	–	–
5′	–	–	–	–	–	–	6.86 (d, 7.9)
6′	6.40 (d, 1.9)	6.37 (d, 1.9)	6.40 (d, 1.7)	6.39 (d, 1.7)	6.63 (br s)	6.73 (br s)	6.89 (dd, 7.9, 1.7)
7′	3.33 (br d, 6.8)	3.29 (br d, 6.8)	3.31 (br d, 6.8)	3.31 (br d, 6.8)	6.57 (d, 15.9)	3.35 (br d, 6.7)	5.14 (d, 8.6)
8′	5.98 (ddt, 16.1, 10.2, 6.8)	5.94 (ddt, 17.0, 10.0, 6.8)	5.97 (ddt, 16.7, 9.0, 6.8)	5.97 (ddt, 16.7, 9.9, 6.8)	6.31 (dt, 15.9, 5.8)	5.98 (ddt, 17.1, 10.0, 6.7)	2.25 (m)
9′	5.10 (br dd, 10.2, 1.6)	5.10 (br dd, 10.0, 1.9)	5.08 (br dd, 9.5, 1.6)	5.08 (br dd, 9.9, 1.6)	4.35 (d, 4.7)	5.08 (br dd, 10.0, 1.6)	0.67 (d, 7.0)
	5.13 (br dd, 16.1, 1.6)	5.12 (br dd, 17.0, 1.9)	5.12 (br dd, 16.7, 1.6)	5.11 (br dd, 16.7, 1.6)	–	5.10 (br dd, 17.1, 1.6)	–
OCH_3-3	–	3.88(s)	3.81 (s)	3.92 (s)	3.87 (s)	3.88 (s)	–
OCH_3-4	3.87 (s)	–	–	3.92 (s)	3.87 (s)	–	3.91 (s)
OCH_3-5	3.86 (s)	3.88(s)	–	–	–	–	3.89 (s)
OCH_3-3′	–	–	–	–	3.84 (s)	–	3.90 (s)
OCH_3-4′	–	–	–	–	–	–	3.90 (s)
OCH_3-5′	3.86 (s)	3.87(s)	3.88 (s)	3.91 (s)	3.84 (s)	3.85 (s)	–

Table 3.5 ^{13}C NMR (75 MHz, $CDCl_3$) spectral data for compounds **XII**, **XIII**, **XVI**, **XVII**, **XVIII**, **XX** and **XXV**

Position	XII	XIII	XVI	XVII	XVIII	XX	XXV
1	133.0	128.0	128.9	129.5	131.6	130.5	137.2
2	105.9	102.8	109.6	110.0	112.8	112.2	102.7
3	149.3	147.1	146.9	149.5	148.6	146.2	152.3
4	135.1	134.4	146.2	149.3	147.3	144.0	134.9
5	152.5	147.1	114.5	111.1	110.9	114.0	149.2
6	101.9	102.8	121.0	120.3	121.4	122.1	105.9
7	76.8	77.0	80.9	80.8	42.8	42.4	87.3
8	73.1	73.4	74.2	74.2	80.2	76.9	47.9
9	12.6	12.5	17.3	17.3	19.6	19.5	15.2
1′	132.2	132.2	132.4	132.4	132.1	133.3	133.7
2′	109.7	109.7	109.6	109.6	103.6	120.5	110.3
3′	143.3	143.4	144.5	144.4	153.8	116.1	148.5
4′	129.5	129.5	131.3	131.3	135.9	145.6	148.0
5′	149.2	149.2	148.6	148.5	153.8	150.4	110.6
6′	104.9	104.9	104.5	104.5	103.6	112.6	119.2
7′	40.1	40.1	40.0	40.1	131.2	39.9	83.2
8′	137.4	137.4	137.4	137.4	127.8	137.2	46.0
9′	115.9	115.9	115.8	115.9	63.7	116.0	15.0
OCH_3-3	–	56.4	56.1	56.0	55.8	55.9	–
OCH_3-4	61.0	–	–	56.0	55.9	–	61.0
OCH_3-5	56.1	56.4	–	–	–	–	55.9
OCH_3-3′	–	–	–	–	56.0	–	55.8
OCH_3-4′	–	–	–	–	–	–	55.8
OCH_3-5′	56.0	56.1	56.0	56.1	56.0	55.8	_

Stembark of *Mallotus plicatus*

Two new structures (**XXXIX** and **XL**) were isolated and structurally determined, along with seven known compounds including bergenin (**XLI**) (Wang et al., 2005), 11-*O*-acetylbergenin (**XLII**) (Wang et al., 2008), aleuritolic acid acetate (**XLIII**) (Chaudhuri et al., 1995), daucosterol (**XLIV**) (Paulo et al., 2000), protocatechuic acid (**XLV**) (Keawsa-ard, et al., 2012), scopoletin (**XLVI**) (Vasconcelos et al., 1998) and blumenol A(**XLVII**) (Liu et al., 1999).

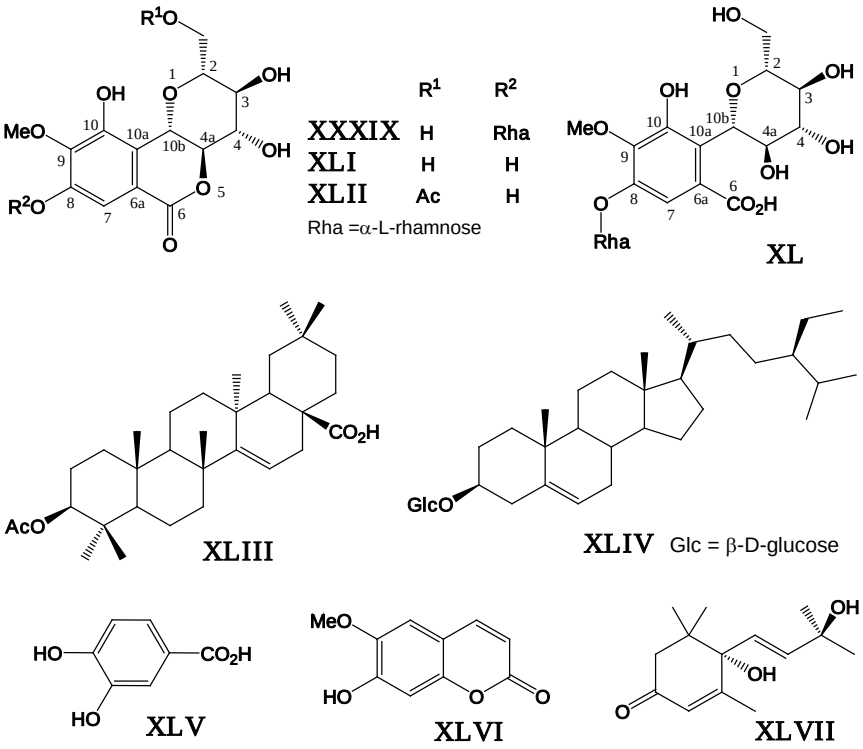

Figure 3.5 Compounds isolated from the leaves of *Mallotus plicatus*

Compound **XXXIX** was obtained as colorless needles. The HR-ESI mass spectrum of **XXXIX** showed $[M+Na]^+$ at *m/z* 497.1287 (calcd. for $C_{20}H_{26}O_{13}Na$ 497.1271), suggesting the molecular formula $C_{20}H_{26}O_{13}$. The UV maximal absorptions at 223 and 274 nm and the IR bands at 1721 (lactone) and 3000-3200 (aromatic ring) cm^{-1} of **XXXIX** were similar to those of bergenin (**XLI**), a gallic acid *C*-glucoside. In the ^1H NMR spectrum (Table 3.6), **XXXIX** exhibited characteristic proton resonances for the bergenin skeleton at δ 4.07 (1H, t, *J* = 10.1 Hz, H-4a) and δ 5.04 (1H, d, *J* = 10.1 Hz, H-10b). This was further supported by correlation peaks for these two protons at δ 79.7 (C-4a) and δ 72.1 (C-10b) in the HSQC spectrum. Further comparison of the ^1H and ^{13}C NMR data, and the molecular formula of **XXXIX** with those of **XLI** suggested that **XXXIX** should be a derivative of **XLI** with an additional sugar moiety with the composition $C_6H_{11}O_4$. This second sugar unit was suggested to be rhamnose by six HSQC correlation peaks that represented one acetal methine [C-1′, δ_H 5.33 (1H, br s)/δ_C 99.7], four oxymethines [C-2′, δ_H 3.87 (1H, m)/δ_C 70.2; C-3′, δ_H 3.64 1(1H, m)/δ_C 70.5; C-4′, δ_H 3.30 (1H, t, d, *J* = 9.2 Hz)/δ_C 71.7; C-5′, δ_H 3.53 (1H, m)/δ_C 70.1] and one methyl carbon [C-6′, δ_H 1.11 (3H, d, *J* = 6.0 Hz)/δ_C 18.0].

A NOESY experiment was then performed to locate the point of attachment of this rhamnose unit to the aglycone structure. In the NOESY spectrum, a correlation peak was observed between H-7 (δ 7.24, s) and H-1′ (δ 5.33, br s), indicating that the rhamnose should be attached to C-8 of bergenin through an ether [(C-1′)-*O*-(C-8)] linkage. In addition, in the rhamnopyranose moiety H-1′ displayed a NOESY cross peak with H-2′, in agreement with their di-equatorial relation.

The presence of the ether bridge that connected the two structural parts was further corroborated by the 3-bond HMBC connectivity from H-1′ to C-8, which was already assigned through its a 2-bond coupling with H-7. Finally, to confirm the proposed structure, **XXXIX** was subjected to acid hydrolysis with 2N HCl under reflux. The reaction was completed after 3 h, and the products were identified by TLC to be bergenin (**XLI**) and L-rhamnose. It should be noted here that under this reaction condition, the structure of the alycone bergenin was still intact, meaning that both the *C/C*-glycosidic bond and the lactone functionality were resistant to acid hydrolysis. Thus, based on the above-discussed spectroscopic data and chemical evidence, together with the known fact that natural rhamnose occurs in L-form, **XXXIX** was concluded to be bergenin-8-*O*-α-L-rhamnoside.

Compound **XL** was isolated as colorless cubic crystals. The ^{1}H and ^{13}C NMR spectra obtained for **XL** (Table 3.6) showed strong resemblance to those obtained for **XXXIX**. However, substantial differences were observed for the ^{13}C NMR resonances of the three carbons that were supposed to be part of the lactone ring, i.e. C-4a, C-6 and C-6a (Table 3.6). In **XL**, C-4a was moved to a more upfield position, showing at δ 74.3, whereas C-6 and C-6a were downfield shifted, resonating at δ 176.1 and 137.3, respectively. It could be inferred from the downfield shift of C-6 that in **XL**, the lactone functionality was missing, and in its place, an open carboxyl group and a free hydroxyl appeared. This was also reflected by the higher resonance frequency of C-10b of **XL** (δ 80.1) as compared with that of **XXXIX** (δ 72.1), which was due to the dissapearance of γ-steric interaction with C-6. The fact that the molecular mass of **XL**, which was deduced from the $[M-H]^-$ at *m/z* 491.1399 (calcd. for $C_{20}H_{27}O_{14}$ 491.1406) in the HR-ESIMS, was 18 amu higher than that of **XXXIX** further supported this argument. A NOESY correlation peak observed between H-7 and H-1′ indicated that **XL** had the deoxyhexosyl moiety attached to C-8 of the alycone through an ether bridge, which was similar to that of **XXXIX**. In support of this, a three-bond coupling was observed between H-1′ and C-8 in the HMBC spectrum. Upon complete acid hydrolysis, compound **XL** gave bergenin (**XLI**) and L-rhamnose. It is important to note that the final aglycone product was bergenin (**XLI**), not *seco*-bergenin. This means that during the reaction, the initial product *seco*-bergenin underwent cyclization rapidly and spontaneously to produce **XLI**. At present, there are no reports on the isolation of *seco*-bergenin from natural sources. Hence, **XL** was characterized as a new naturally occurring compound, and named *seco*-bergenin-8-*O*-α-L-rhamnoside.

Table 3.6 ^{1}H and ^{13}NMR data of compounds XXIX and XL

Position	**XXXIX** (DMSO-d_6)		**XL** (methanol-d_4)	
	δ_H	δ_C	δ_H	δ_C
2	3.59 (m)	81.9 d	3.40 (m)	82.8 d
3	3.21 (t, 9.0)	70.7 d	3.50 (t, 9.6)	80.7 d
4	3.67 (m)	73.7 d	3.43 (t, 9.6)	73.9 d
4a	4.07 (t, 10.1)	79.7 d	3.69 (m)	74.3 d
6	–	163.3 s	–	176.1 s
6a	–	119.2 s	–	137.3 s
7	7.24 (s)	110.0 d	7.02 (s)	109.3 d
8	–	149.8 s	–	150.4 s
9	–	142.8 s	–	140.2 s
10	–	148.3 s	–	150.4 s
10a	–	118.3 s	–	117.8 s
10b	5.04 (d, 10.1)	72.1 d	5.14 (d, 9.9)	80.1 d
11	3.44 (m), 3.85 (m)	61.2 t	3.83 (2H, m)	62.1 t
MeO	3.83 (3H, s)	60.4 q	3.83 (3H, s)	61.4 q
1′	5.33 (br s)	99.7 d	5.48 (br s)	100.5 d
2′	3.87 (m)	70.2 d	4.06 (dd, 3.3, 1.7)	72.2 d
3′	3.64 (m)	70.5 d	3.9 (dd, 9.6, 3.3)	72.4 d
4′	3.30 (t, 9.2)	71.7 d	3.54 (m)	71.1 d
5′	3.53 (m)	70.1 d	3.71 (m)	71.0 d
6′	1.11 (d, 6.0)	18.0 q	1.23 (d, 6.2)	18.1 q

(δ in ppm and J in Hz).

Whole plant of *Dendrobium venustum*

Seven isolated compounds were identified as flavanthrinin (**XLVIII**) (Zhang et al., 2008), gigantol (**XLIX**) (Chen et al., 2008), densiflorol B (**L**) (Fan et al., 2001), lusianthridin (**LI**) (Guo et al., 2007), batatasin III (**LII**) (Sachdev et al., 1986), phoyunnanin E (**LIII**) (Guo et al., 2006) and phoyunnanin C (**LIV**) (Guo et al., 2007).

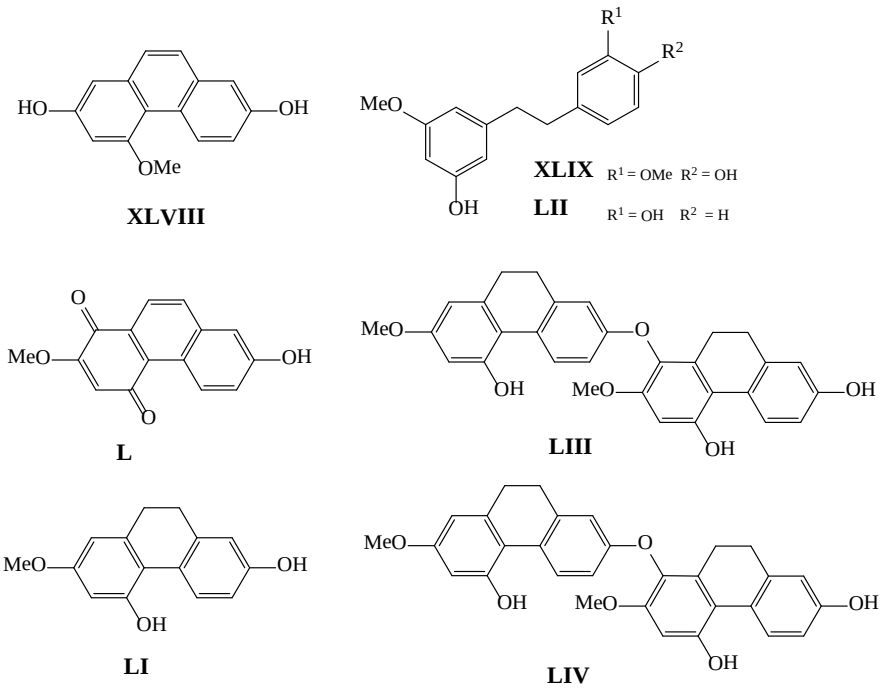

Figure 3.6 Compounds isolated from *Dendrobium venustum*

Whole plant of *Dendrobium williamsonii*

The isolates were determined through analysis of their spectroscopic data in comparison with reported values as tetratriacontanyl-*trans*-*p*-coumarate (**LV**) (Mahmood et al., 2003), *trans*-docosanoylferulate (**LVI**) (Ulubelen et al., 1994), 3,3′-dihydroxy-4, 5-dimethoxybibenzyl (**LVII**) (Arriaga-Giner et al., 1993), moscatilin (**LVIII**) (Majumder et al., 1987), apigenin (**LIX**) (Han et al., 2007) and vanillic acid (**LX**) (Sakushima et al., 1995).

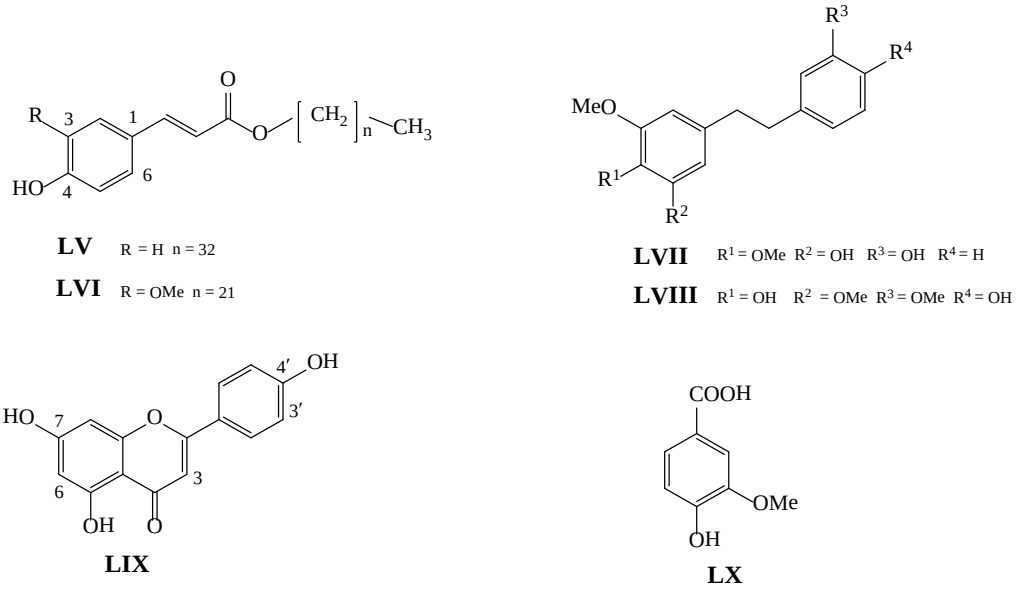

Figure 3.7 Compounds isolated from *Dendrobium williamsonii*

3.2 Biological activity

Aniherpetic activity

Evaluation of the anti-HSV activity of the isolated compounds was performed by the plaque reduction assay (inactivation). Due to limited amounts of the isolates, only some of them were subjected to the bioassay, and the results are shown in Table 3.7.

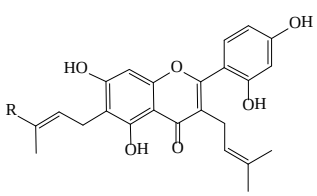

I R = $CH_2CH_2CH=C(CH_3)_2$

II R = H

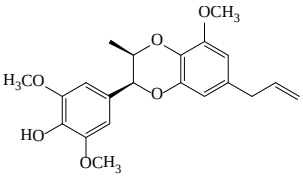

XIII

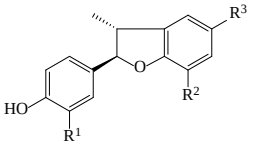

X $R^1 = R^2 = H$; $R^3 = CH_2(CO)CH_3$

XXIV $R^1 = R^2 = OCH_3$; $R^3 = CH=CHCH_3$

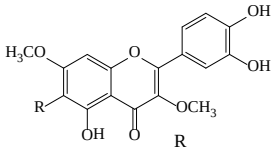

XXXVI H
XXXVII OCH_3

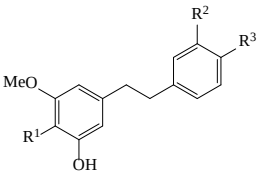

XLIX $R^1 = H$ $R^2 = OMe$ $R^3 = OH$
LII $R^1 = H$ $R^2 = OH$ $R^3 = H$
LVII $R^1 = OMe$ $R^2 = OH$ $R^3 = H$

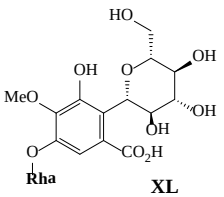

Rha **XL**

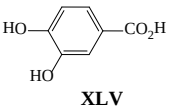

XLV

Among the compounds evaluated in this study, 5,7,2′,4′-tetrahydroxy-3-prenyl-6-geranylflavone (**I**) was the strongest, with IC_{50} values of 25.5 and 25.5 μM against HSV-1 and HSV-2, respectively. The C_{10}-isoprenyl unit at C-6 seemed to play an important role since the activity was weakened in **2**, in which this position was replaced with a C_5-isoprenyl unit. However, the antiherpetic activity of **1** was considered moderate when compared with that of the antiviral drug acyclovir (IC_{50} 1.08 and 2.18 μM, respectively).

Some of the *bis*-aryl structures, such as the flavonoids: cudraflavone C (**II**), quercetin 3,7-dimethyl ether (**XXXVI**) and chrysosplenol-D (**XXXVII**); the neolignans: miliumollinone (**X**), (+)-4-*O*-demethyleusiderin C (**XIII**) and licarin A (**XXIV**); the dihydrostilbenoids (bibenzyls): gigantol (**XLIX**), batatasin III (**LII**) and 3,3′-dihydroxy-4, 5-dimethoxybibenzyl (**LVII**), displayed marginal antiherpetic activity, whereas the others were devoid of activity at the concentration of 100 μg/ml. Very weak activity against HSV-1 was also observed for some simple benzoic acid derivatives, such as *seco*-bergenin-8-*O*-α-L-rhamnoside (**XL**) and protocatechuic acid (**XLV**).

Table 3.7 Antiherpetic activity of compounds isolated from *Artocarpus lakoocha*, *Miliusa mollis*, *Miliusa fragrans*, *Miliusa umpangensis*, *Mallotus plicatus*, *Dendrobium venustum* and *Dendroium williamsonii*

Compound	IC_{50} (μM)	
	HSV-1	HSV-2
I	25.5	25.5
II	237.0	237.0
III	NA	NA
IV	NA	NA
V	*NT*	*NT*
VI	*NT*	*NT*
VII	NA	NA
VIII	NA	NA
IX	*NT*	*NT*
X	155.3	222.0
XI	NA	NA
XII	NA	NA
XIII	62.5	87.5
XIV	NA	NA
XV	NA	NA
XVI	NA	NA
XVII	NA	NA
XVIII	NA	NA
XIX	*NT*	*NT*
XX	*NT*	*NT*
XXI	NA	NA
XXII	NA	NA
XXIII	NA	NA
XXIV	66.7	87.5
XXV	NA	NA
XXVI	NA	NA
XXVII	NA	NA
XXVIII	NA	NA
XXIX	NA	NA
XXX	NA	NA
acyclovir	1.08	2.18

Compound	IC_{50} (μM)	
	HSV-1	HSV-2
XXXI	NA	NA
XXXII	NA	NA
XXXIII	NA	NA
XXXIV	NA	NA
XXXV	NA	NA
XXXVI	94.7	189.5
XXXVII	86.8	86.7
XXXVIII	NA	NA
XXXIX	NA	NA
XL	193.1	NA
XLI	NA	NA
XLII	NA	NA
XLIII	NA	NA
XLIV	NA	NA
XLV	616.8	NA
XLVI	NA	NA
XLVII	NA	NA
XLVIII	NA	NA
XLIX	304.1	319.3
L	NA	NA
LI	NA	NA
LII	341.5	384.2
LIII	NA	NA
LIV	NA	NA
LV	NA	NA
LVI	NA	NA
LVII	304.1	334.5
LVIII	NA	NA
LIX	NA	NA
LX	NA	NA

*NA =No activity at 100 μg/ml; *NT* = not tested due to insufficient amounts.

Inhibition of neuraminidase

Due to limited research funding, only some compounds (**V** - **X**), which were isolated from the leaves of *Miliusa mollis*, were evaluated for this activity at 50 μg/ml, but none of them showed observable activity.

4. Conclusion

Sixty secondary plant metabolites were isolated and structurally characterized from seven plants which belong to 4 plant families, including *Artocarpus lakoocha* (Moraceae), *Miliusa mollis, M. fragrans, M. umpangensis* (Annonaceae), *Mallotus plicatus* (Euphorbiacea), *Dendrobium venustum* and *Dendroium williamsonii* (Orchidaceae). Sixteen of theses isolates have been determined as new compounds by spectroscopic analysis, consisting of a prenylated flavonoid, a lignan, twelve neolignans, and two glycosidic gallic acid derivatives.

Antiherpetic activity was observed in 10 compounds, including 4 flavonoids, 3 neolignans and 3 dihydrostilbenes (bibenzyls). All are polyphenolic compounds containing a *bis*-aryl structure. These findings are in line with our earlier proposed hypothesis. Among the active isolates, 5,7,2′,4′-tetrahydroxy-3-prenyl-6-geranylflavone was the most potent, but its activity was considered moderate, as compared with acyclovir.

Regarding the neuraminidase inhibitory activity, only some of the isolates were subjected to the assay, owing to limited financial resources. None of them showed recognizable activity.

The chemical and biological data obtained in this study have produced scientific knowledge useful for future research on the chemistry and bioactivity of Thai medicinal plants.

Outputs

(1) Boonchoo Sritularak, Kullasap Tantrakarnsakul, Vimolmas Lipipun and Kittisak Likhitwitayawuid. Flavonoids with anti-HSV activity from the root bark of *Artocarpus lakoocha*. Natural Product Communications **8**: 1079-80 (2013). (Impact Factor =0.884)

(2) Kanokporn Sawasdee, Tanawat Chaowasku, Vimolmas Lipipun, Thi-Hanh Dufat, Sylvie Michel and Kittisak Likhitwitayawuid. Neolignans from leaves of *Miliusa mollis*. Fitoterapia **85**: 49–56 (2013). (IF = 2.408)

(3) Kanokporn Sawasdee, Tanawat Chaowasku, Vimolmas Lipipun, Thi-Hanh Dufat, Sylvie Michel and Kittisak Likhitwitayawuid. New neolignans and a lignan from *Miliusa fragrans*, and their anti-herpetic and cytotoxic activities. Tetrahedron Letters **54**: 4259–4263 (2013). (IF = 2.347)

(4) Kanokporn Sawasdee, Tanawat Chaowasku, Vimolmas Lipipun, Thi-Hanh Dufat, Sylvie Michel, Vichien Jongbunprasert and Kittisak Likhitwitayawuid. Geranylated homogentisic acid derivatives and flavonols from *Miliusa umpangensis*. Biochemical Systematics and Ecology **54**: 179–181 (2014). (IF = 0.988)

(5) Kongsin Luangruangrong, Boonchoo Sritularak, Vimolmas Lipipun and Kittisak Likhitwitayawuid. New gallic acid glycosides from *Mallotus plicatus*. Heterocycles **89**: 1237–1244 (2014). (IF = 1.107)

(6) Prapapun Sukphan, Boonchoo Sritularak, Wanwimon Mekboonsonglarp, Vimolmas Lipipun and Kittisak Likhitwitayawuid. Chemical constituents of *Dendrobium venustum* and their antimalarial and anti-herpetic properties. Natural Product Communications 9: 825-827 (2014). (IF = 0.884)

(7) Pathrapa Rungwichaniwat, Boonchoo Sritularak and Kittisak Likhitwitayawuid. Chemical Constituents of *Dendrobium williamsonii*. Pharmacognosy Journal **6**: 36-41 (2014).

References

Achenbach H, Grob J, Dominguez XA., Cano G, Star JV, Brussolo LDC, Munõz G, Salgado F, López, L. Phytochemistry. 1987, 26, 1159–1166.

Arriaga-Giner FJ, Wollenweber E, Dörr M. Bibenzyls from crowberry leaves. Phytochemistry. 1993, 33, 725–726.

Bárbosa-Filho JM, da Silva, MS, Yoshida, M, Gottlieb OR. Neolignans from *Licaria aurea* Phytochemistry. 1989, 28, 2209–2211.

Chaudhuri SK, Fullas F, Brown DM, Wani MC, Wall ME, Cai L, Mar W, Lee SK, Luo Y, Zaw K, Fong HHS, Pezzuto JM, Kinghorn AD. Isolation and structural elucidation of pentacyclic triterpenoids from *Maprounea Africana*. J. Nat. Prod. 1995, 58, 1–9.

Chauret DC, Bernard CB, Arnason JT, Durst T, Krishnamurty HG,Sanchez-Vindas P, et al. Insecticidal neolignans from *Piper decurrens*. J. Nat. Prod. 1996, 59, 152–5.

Chen Y, Xu J, Yu H, Qing C, Zhang Y, Wang L, Liu Y, Wang J. Cytotoxic phenolics from *Bulbophyllum odoratissimum*. Food Chem. 2008, 107, 169–173.

Chen B-N, Yang G-E, Li J-K, Du H-J, Li Q-S, Zhang Z-M Cytotoxic constituents from *Viscum coloratum* Chem. Nat. Comp. 2009, 45, 547–549.

Davis AL, Cai Y, Davies AP, Lewis JR. ^{1}H and ^{13}C NMR assignments of some green tea polyphenols. Magn. Reson. Chem. 1996, 34, 887–890.

da Silva MS, Barbosa-Filho JM, Yoshida M, Gottlieb OR. Benzodioxane and β-aryloxy-arylpropane type neolignans from *Licaria chrysophylla*. Phytochemistry 1989, 28, 3477–3482.

Drewes SE, Taylor CW, Cunningham AB. (+)-Afzelechin 3-rhamnoside from *Cassipourea gerrardii*. Phytochemistry. 1992, 31, 1073–1075.

Fan C, Wang W, Wang Y, Qin G, Zhao W. Chemical constituents from *Dendrobium densiflorum*. Phytochemistry. 2001, 57, 1255–1258.

Fernandes JB, Ribeiro MN, Gottlieb OR, Gottlieb HE. Eusiderins and 1,3-diarylpropanes from *Virola* species. Phytochemistry. 1980, 19, 1523–1525.

Fonseca SF, Barata LES, Rúveda EA, Baker PM. ^{13}C nuclear magnetic resonance spectral and conformational analysis of naturally occurring tetrahydrofuran lignans. Can. J. Chem. 1979, 57, 441–444.

Guerrero MF, Puebla P, Carrón R, Martín ML, San Román L. Quercetin 3,7-dimethyl ether : a vasorelaxant flavonoid isolated from *Croton schiedeanus* Schlecht J. Pharm. Pharmacol. 2002, 54, 1373–1378.

Guo XY, Wang J, Wang NL, Kitanaka S, Liu HW, Yao XS. New stilbenoids from *Pholidota yunnanensis* and their inhibitory effects on nitric oxide production. Chem. Pharm. Bull. 2006, 54, 21–25.

Guo XY, Wang J, Wang NL, Kitanaka S, Yao XS. 9,10-Dihydrophenanthrene derivatives from *Pholidota yunnanensis* and scavenging activity on DPPH free radical. J. Asian Nat. Prod. Res. 2007, 9, 165–174.

Han XH, Hong SS, Hwang JS, Lee MK, Hwang BY, Ro JS, Monoamine oxidase inhibitory components from *Cayratia japonica*. Arch. Pharm. Res. 2007, 30, 13–17.

Hano Y, Matsumoto Y, Shinohara K, Sun JY, Nomura T. Cudraflavones C and D, two new prenylflavones from the root bark of *Cudrania tricuspidata* (Carr.) Bur. Heterocycles. 1990, 31, 1339-1344.

Huong DT, Kamperdick C, Sung TV. Homogentisic acid derivatives from *Miliusa balansae*. J. Nat. Prod. 2004, 67, 445–447.

Keawsa-ard S, Natakankitkul S, Liawruangrath S, Teerawutgulrag A, Trisuwan K, Charoenying P, Pyne SG, Liawruangrath B. Anticancer and antibacterial activities of the isolated compounds from *Solanum spirale* Roxb. Leaves. Chiang Mai J. Sci. 2012, 39, 445–454.

Likhitwitayawuid K, Sritularak B, Benchanak K, Lipipun V, Mathew J, Schinazi RF. Phenolics with antiviral activity from *Millettia erythrocalyx* and *Artocarpus lakoocha*. Nat. Prod. Res. 2005a, 19, 177–182.

Likhitwitayawuid K, Supudompol B, Sritularak B, Lipipun V, Rapp K, Schinazi RF. Phenolics with anti-HSV and anti-HIV activities from *Artocarpus gomezianus*, *Mallotus pallidus* and *Triphasia trifolia*. Pharm. Biol. 2005b, 43, 651–657.

Likhitwitayawuid K, Chaiwiriya S, Sritularak B, Lipipun, V. Anti-HSV Flavones from the heartwood of *Artocarpus gomezianus* Chem. Biod. 2006, 3, 1138–1143.

Ling T-J, Ling W-W, Chen Y-J, Wan X-C, Xia T, Du X-F, Zhang Z-Z. Antiseptic activity and phenolic constituents of the aerial parts of *Vitex negundo* var. *cannabifolia* Molecules. 2010, 15, 8469–8477.

Lipipun V, Kurokawa M, Suttisri R, Taweechotipatr P, Pramyothin P, Hattori M, et al. Efficacy of Thai medicinal plant extracts against herpes simplex virus type 1 infection in vitro and in vivo. Antiviral Res. 2003, 60,175–80.

Liu X, Tian F, Zhang HB, Pilarinou E, Mclaughlin JL. Biologically active blumenol A from the leaves of *Annona Glabra*. Nat. Prod. Lett. 1999, 14, 77–81.

Lopes NM, de Almeida Blumenthal EE, Cavalheiro, AJ, Kato MJ, Yoshida M. Lignans, γ-lactones and propiophenones of *Virola surinamensis*. Phytochemistry. 1996, 43, 1089–1092.

Mahmood U, Kaul VK, Acharya R, Jirovetz L. *p*-Coumaric acid esters from *Tanacetum longifolium*. Phytochemistry. 2003, 64, 851–853.

Majumder PL, Sen RC. Moscatilin, a bibenzyl derivative from the orchid *Dendrobium moscatum*. Phytochemistry. 1987, 26, 2121–2124.

Matsuda H, Morikawa T, Toguchida I, Yoshikawa M. Structural requirements of flavonoids and related compounds for aldose reductase inhibitory activity. Chem. Pharm. Bull. 2002, 50, 788–795.

Mbah JA, Tane P, Ngadjui BT, Connolly J.D, Okunji CC, Iwu MM, Schuster BM. Antiplasmodial agents from the leaves of *Glossocalyx brevipe*s. Planta Med. 2004, 70, 437–440.

Morais SKR, Teixeira AF, Torres ZES, Nunomura SM, Yamashiro-Kanashiro EH, Lindoso JAL, Yoshida M. Biological activities of lignoids from Amazon Myristicaceae species: *Virola michelii*, *V. mollissima*, *V. pavonis* and *Iryanthera juruensis*. J. Braz. Chem. Soc. 2009, 20, 1110–1118.

Paulo A, Jimeno ML, Gomes ET, Houghton PJ. Steroidal alkaloids from *Cryptolepis obtuse*. Phytochemistry. 2000, 53, 417–422.

Potier M, Mameli L, Bélisle M, Dallaire L, Melancon SB. Fluorometric assay of neuraminidase with a sodium (4-methylumbelliferyl-α-D-Nacetylneuraminate) substrate. Anal. Biochem. 1979, 94, 287–96.

Sachdev K, Kulshreshtha DK. Phenolic constituents of *Coelogyne ovalis*. Phytochemistry. 1986, 25, 499–502.

Slimestad R, Fossen T, Vergeul MJ. The flavonoids of tomatoes. J. Agric. Food Chem. 2008, 56, 2436–2441.

Sakushima A, Coşkun M, Maoka T, Hydroxybenzoic acids from *Boreavaorientalis*. Phytochemistry. 1995, 40, 257–261.

Sritularak B, Likhitwitayawuid K. New bisbibenzyls from *Dendrobium falconer*i Helv. Chim. Act. 2009, 92, 740–744.

Sawasdee K, Chaowasku T, Likhitwitayawuid K. New neolignans and a phenylpropanoid glycoside from twigs of *Miliusa mollis*. Molecules 2010, 15, 639–648.

Sun J, Jiang Y, Wei X, Shi J, You Y, Liu H, Kakuda Y, Zhao M. Identification of (−)-epicatechin as the direct substrate for polyphenol oxidase isolated from litchi pericarp. Food Res. Int. 2006, 39, 864–870.

Supudompol B, Likhitwitayawuid K, Houghton PJ. Phloroglucinol derivatives from *Mallotus pallidus*. Phytochemistry 2004, 65, 2589–-2594.

Ulubelen A, Topcu G, Olçal S, Rearranged abietane diterpenes from *Teucrium divaricatum* subsp. *Villosum*. Phytochemistry. 1994, 37, 1371–1375.

Vasconcelos JMJ, Silva AMS, Cavaleiro JAS. Chromones and flavanones from *Artemisia campestris* subsp. *maritima*. Phytochemistry, 1998, 49, 1421–1424.

Wang Y, Hamburger M, Gueho J. Hostettmann K, Antimicrobial flavonoids from Psiadia trinervia and their methylated and acetylated derivatives. Phytochemistry. 1989, 28, 2323–2327.

Wang GC, Liang JP, Wang Y, Li Q, Ye W-C. Chemical constituents from *Flueggea viros*. Chin. J. Nat. Med. 2008, 6, 251–253.

Wang D, Zhu H-T, Zhang Y-J, Yang CR. A carbon–carbon-coupled dimeric bergenin derivative biotransformed by *Pleurotus ostreatus.* Bioorg. Med. Chem. Lett. 2005, 15, 4073–5075.

Yang, X. W.; Huang, X.; Ahmat, MMT. New neolignan from seed of *Myristica fragrans*. Chin. J. Chin. Mater. Med. 2008, 33, 397–402.

Zhang H-J, Ma C, Hung NV, Cuong NM, Tan GT, Santarsiero BD, Mesecar AD, Soejarto DD, Pezzuto JM, Fong HHS. Miliusanes, a class of cytotoxic agents from *Miliusa sinensis*. J. Med. Chem. 2006, 49, 693–708.

Zhang X, Xu JK, Wang, NL, Kurihara H, Yao XS. Antioxidant phenanthrenes and lignans from *Dendrobium nobile*. J. Chin. Pharm. Sci. 2008, 17, 314–318.